Lithofacies Characteristics, Reservoir Properties, and Ichnology of the Upper
Montney Member (Spathian)

by

Chenyang Feng

A thesis submitted in partial fulfillment of the requirements for the degree of

Doctor of Philosophy

Department of Earth and Atmospheric Sciences
University of Alberta

ABSTRACT

The Lower Triassic Montney Formation in west-central Alberta and northeastern British Columbia has become one of the most productive reservoirs in Western Canada over the past 15 years. It is projected that it will play a leading role in satisfying Canada's energy requirements over the next 20 years. This study focuses on the Upper Montney Member (UMM), which is interpreted to represent the deposition within a wave- to storm-influenced, low-gradient, predominantly siliciclastic ramp setting. The lithology is dominated by the interbedding or interlamination of dolomitic, medium- to coarse-grained siltstone and bituminous, fine- to medium-grained siltstone, with subordinate dolomitic, very fine-grained sandstone locally occurring towards the UMM top. Seven lithofacies are identified in the UMM, comprising a conformable, shoaling-upward (coarsening-upward) sequence. Along with the measured porosity-permeability data, analyses of high-resolution scanning electron microscopy (SEM) and thin-section based petrography are conducted to evaluate reservoir qualities of different lithofacies. Notably, the shoreface successions of the Upper Montney are classified by the lithofacies-dependent reservoir properties using Winland porosity-permeability plots. In addition, integrating the mineralogical analyses by X-ray-diffraction (XRD) and the measured values of total organic carbon (TOC), the origin of the bitumen is investigated and the Upper Montney is inferred to be a self-sourcing reservoir system.

This work also considers some ichnological attributes of the UMM to refine an understanding of environmental conditions during reservoir deposition. To do this, the ichnology of the eastern UMM, in Alberta, is compared to more distal positions in the western UMM, in British Columbia. In Alberta, trace fossils identified mainly include *Phycosiphon*, *Teichichnus*, *Planolites*, *Cylindrichnus* and *Skolithos* and are consistent with somewhat impoverished trace fossil assemblages associated with proximal offshore and lower shoreface settings. In British Columbia, lack of idiomorphic ichnogenera is observed in bioturbated siltstones: this is owing in part to a lack of grainsize variabilities of the host strata. To deal with these ichnotaxonomic problem, five ichnofossil types (Type a, b, c, d and e) are designated and interpreted ethologically. In order to investigate the ichnological variability of the shoreface successions within the Upper Montney Member in different areas, process ichnology data (bioturbation intensity, burrow diameter,

bioturbation diversity, and size-diversity index) are collected and analyzed. The distinct hydrodynamic conditions and the oxygen deficiency are interpreted to be the most significant physico-chemical stresses leading to the ichnological distributions and variability.

PREFACE

This dissertation is original work by Chenyang Feng. The dissertation contains material that has been submitted for publication and has involved collaboration with other researchers. The research project was designed by myself, with the assistances of my supervisors, M.K. Gingras, and supervisorial committee, J-P. Zonneveld and O. Catuneanu.

Chapters within this dissertation within this thesis have either been published within peer-reviewed journals or been submitted for publication, and include:

-Chapter 2 has been published as Feng, C.Y., Melnyk, S., Ross, C., Shanley, K., Zonneveld, J-P. and Gingras, M.K., "Lithofacies-dependent pore-throat radii and reservoir properties in the Lower Triassic Montney Formation, Puskwaskau Field, Alberta" in the Marine and Petroleum Geology (2021, Volume 131, Article 105157). Core logging, facies analysis, sample preparation and identification of thin-sections and SEM, data analysis, and manuscript composition were the responsibility of myself. Co-authors provided discussion of research, editorial guidance and feedback.

-Chapter 3 is submitted as Feng, C.Y., Melnyk, S., Baniak, G.M., Medina, S.H., Harris, N.B., Zonneveld, J-P. and Gingras, M.K., "Lithofacies characteristics and reservoir properties of the Upper Montney (Spathian) Formation in the Shell Monias Field, northeastern British Columbia" to the Bulletin of Canadian Petroleum Geology. Core logging, facies analysis, sample preparation and identification of thin-sections and SEM, data analysis, and manuscript composition were the responsibility of myself. Co-authors provided discussion of research, editorial guidance and feedback.

-Chapter 4 will be submitted as Feng, C.Y., Melnyk, S. and Gingras, M.K., "Ichnology of the Upper Montney Member in west-central Alberta" to the Bulletin of Canadian Petroleum Geology. Core logging, facies analysis, process ichnological analysis, and manuscript composition were the responsibility of myself. Co-authors provided discussion of research, editorial guidance and feedback.

- Chapter 5 will be submitted as Feng, C.Y., Melnyk, S. and Gingras, M.K., "Interpreting the cryptic ichnotaxa in core: Upper Montney Member, northeastern British Columbia" to the Ichnos. Core logging, facies analysis, process ichnological analysis, and manuscript composition were the

responsibility of myself. Co-authors provided discussion of research, editorial guidance, and feedback.

DEDICATION

This dissertation is dedicated to my parents: Lan Li, and Guangli Feng. Words cannot capture the love, support, and encouragement you have provided me throughout my life and through the journey I have taken to get where I am today.

ACKNOWLEDGMENTS

Four years ago, due to my concerns regarding the progress and project, I decided to switch to the Department of Earth Atmospheric Science and have Murray K. Gingras as my supervisor. To be frank, at that moment, I did not realize that this would be one of the best decisions in my life. Today, when I recall my past four years full of fond memories, I must acknowledge that decision has led me to an amazing, joyful and meaningful journey in Alberta, Canada.

Firstly, I am endlessly thankful for my supervisor, Murray K. Gingras, accepting me as a member of the Ichnology Research Group (IRG) at my difficult and uncertain time. What's more, I also appreciate his guidance on my study and research. For the past four more years, under the supervision of Dr. Gingras, I had the opportunity to work on my favourite research area- Sedimentology and begin my exploration in Ichnology, a truly new research field to me. More importantly, whether in daily life or in each extraordinary IRG activity, Dr. Gingras has shown me how to be a good supervisor, a good team leader and a good person, which will have a profound influence upon my life.

In addition, I would like to express my gratitude to Dr. John-Paul Zonneveld, Dr. Octavian Catuneanu, Dr. Ben Rostron, Dr. Keith Shanley, Dr. Greg Baniak, Dr. Nicholas Harris, and Dr. Jeffrey Kavanaugh. Thank you for your great support on my research.

Thank you to many people that have been a part of the Ichnology Research Group (IRG) during the time of this project. We have shared many hours of work, discussion, and laughter within the lab. I have been very lucky to have spent such a long time in the lab and have gained many lifelong friendships along the way. Thank you: Scott Melnyk, Qi Chen, Maya LaGrange Rao, Chundi Shan, Brette Harris, Cole Ross, Scott Botterill, Arzu Acikelli, Jiahui Gao, Waqar Ahmad, Cody Lazowski, Anders Cowper, Riley Morton, Carolyn Marie Furlong, Skye Lybbert, Daniel Baker, Sara Biddle, and Sheridan Sigstad.

Finally, I would like to thank the scholarship provided by the China Scholarship Council (CSC). Without this generous funding, my overseas study and life would not have been possible. Thank you to all people associated with the Graduate Students' Association (GSA) during 2017-2018. I will treasure every bit of that year and thank you for helping me firstly open the door to a whole new world.

TABLE OF CONTENTS

LIST OF TABLES

LIST OF FIGURES

CHAPTER 1: INTRODUCTION

GENERAL OVERIEW

The Lower Triassic Montney Formation is in the Western Canada Sedimentary Basin, extending across approximately 130,000 km^2 of northeastern British Columbia and west-central Alberta, Canada (National Energy Board, 2013). The Montney Formation has a maximum thickness of around 350 m. It is thickest in the west and pinches out beneath a series of unconformities to the east (National Energy Board, 2013). The depth of the top of the Montney Formation increases from northeast to southwest, ranging from approximately 500 to 4500 m (BC Oil and Gas Commission, 2012; Energy Resources Conservation Board, 2012).
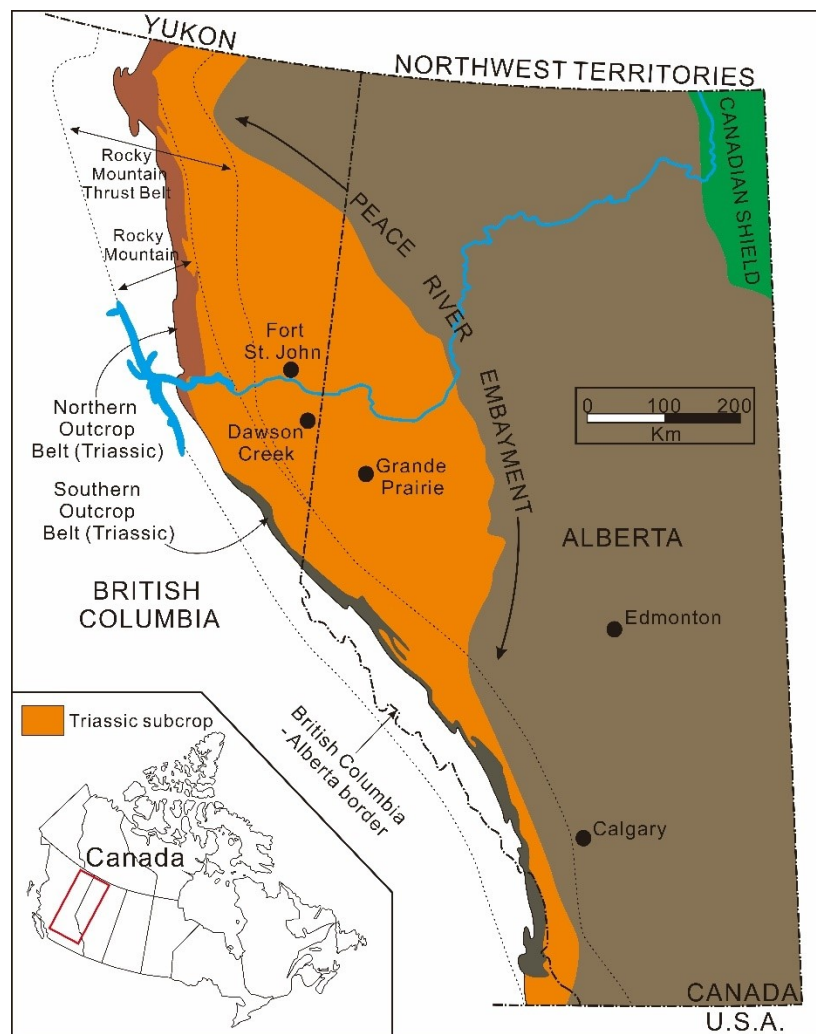
Figure 1.1-Regional map of Alberta and British Columbia showing the extent of Triassic strata (subcrop and outcrop). Note the location of the Peace River Embayment where the Montney Formation was deposited.

The Montney Formation was named by Armitage in 1962 from the Texaco NFA Buick Creek 6-26-87-21W6 (between 1714.5 and 1981.5 m), approximately 40 km northwest of Fort St. John, British Columbia. As the well was not cored, the Montney Formation was identified and described on basis of well logs and cuttings as grading from dark grey shale upwards into dark grey, argillaceous siltstone and interbedded shale (Armitage, 1962). The Montney Formation rests unconformably on Permian Belloy Formation and is sharply overlain by Middle Triassic Doig Formation (Armitage, 1962). Based on the later availability of nearly complete core coverage through the Montney interval, Zonneveld and Moslow (2018) proposed that the well 100/16-17-83-25W6M (between 2257.0 and 2528.0 m) and Progress Graham c-065-F/094-B-08 (between 2203.0 and 2574.3 m) be designated as reference sections for the Montney Formation (Zonneveld and Moslow, 2018).

The Montney Formation contains approximately 12,719 billion m^3 of marketable natural gas, 2,308 million m^3 (14,521 million barrels) of marketable natural gas liquids (NGLs), and 179 million m^3 (1,125 million barrels) of marketable oil (National Energy Board, 2013). It is projected that production of the Montney Formation will lead to the majority of Canadian natural gas production growth over the next 20 years, increasing from 6.6 Bcf/d in 2020 to 13.6 Bcf/d in 2040 (Canada Energy Regulator, 2020).

Starting in the 1950s, exploration and extraction efforts within the Montney Formation were primarily focused on conventional reservoirs (i.e., wells completed vertically) that consisted of very fine-grained sandstone-dominated turbidite successions and shoreline-associated dolomitic bioclastic grainstone, and fine-grained sandstone beds (Zonneveld et al., 2010a; Davies et al., 2018). Significant technological advances in the previous 20 years allow unconventional reservoirs mainly consisting of thick, laterally extensive bituminous siltstone successions to become increasingly exploited (Zonneveld et al., 2010a; Davies et al., 2018; Zonneveld and Moslow, 2018). Specifically, the development and refinement of horizontal drilling practices and multi-stage hydraulic fracturing have improved hydrocarbon recovery (Davies et al., 2018; Prenoslo et al., 2018; Zonneveld and Moslow, 2018).

PALAEOGEOGRAPHIC SETTING

The Western Canada Sedimentary Basin is a thin, northeastward-tapering wedge of Phanerozoic strata above Precambrian crystalline basement and the thickness of this wedge increases gradually southwestward, over a distance ranging from 600 to 1200 km, from a zero-edge in the northeast along the margin of the Canadian Shield to between 3 and 5 km at the northeastern margin of the foreland thrust and fold belt (Price, 1994). The deposition of the Triassic strata of western Canada occurred in one large, arcuate sub-basin designated the Peace River Embayment (more than 900 km long in NNW-SSE trend and at least 350 km wide from east to west) on the western margin of the supercontinent Pangea, at approximately 32-34° north latitude, facing the open ocean (Panthalassa) (Habicht, 1979; Barclay et al., 1990; Wilson et al., 1991; Davies, 1997a, 1997b; Zonneveld, 1999; Golonka, 2007; Zonneveld and Moslow, 2018).
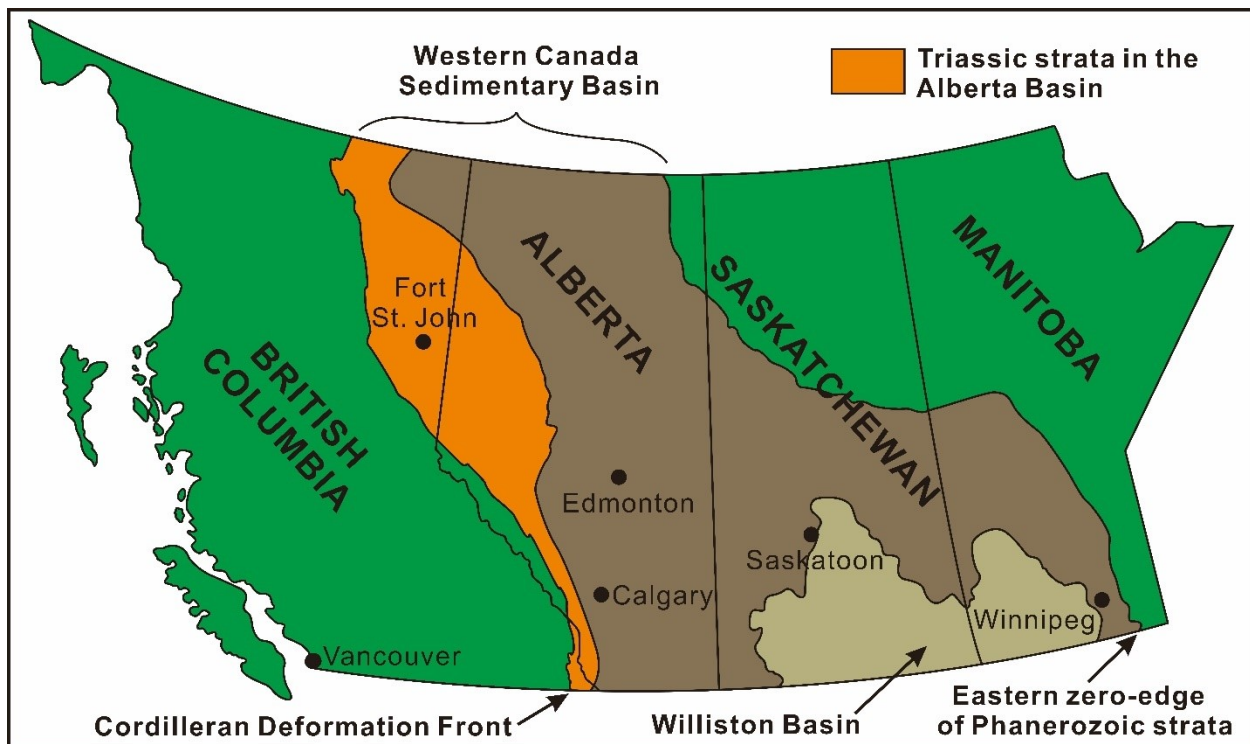
Figure 1.2-Map of Western Canada Sedimentary Basin and boundaries of Triassic strata in British Columbia, Saskatchewan, and Manitoba. The orange area shows the distribution of Triassic strata within the Western Canada Sedimentary Basin. Modified from Edwards et al. (1994).

Historically, this sub-basin was interpreted to be a passive margin basin, promoting the development of a marine ramp setting during Triassic (Dickison, 1977; Monger and Price, 1979; Coney et al., 1980; Gibson and Barclay, 1989; Edwards et al., 1994; Price, 1994; Dixson, 2009a, 2009b). Recent work has shown that under the effect of the Klondike Orogeny (Beranek and Mortensen, 2007; Colpron et al., 2007; Beranek and Mortensen, 2011), the transition of the Western Canada Sedimentary Basin from a passive margin basin to a more active tectonic setting was initiated much earlier than the late Jurassic (Beranek and Mortensen, 2007; Ferri and Zonneveld, 2008; Beranek and Mortensen, 2011; Rohais et al., 2016, 2018; Zonneveld and Moslow, 2018). As a result, the Triassic successions may be interpreted to record deposition in an evolving back-arc to foreland basin (Ferri and Zonneveld, 2008; Miall and Blakey, 2008; Zonneveld et al., 2010a; Schiarizza, 2013; Morris et al., 2014; Golding et al., 2016). Provenance analyses indicate that the Triassic sediments were dominated by the reworked Devonian rocks of the Laurentian continent to the east (Ross et al., 1997; Utting et al., 2005; Beranek et al., 2010; Morris et al., 2014), with small amounts possibly contributed by the western volcanic arc settings (Morris et al., 2014; Golding et al., 2016).

During Triassic, the Peace River Embayment played the role as the main depocenter, which was formed mainly by the progressive subsidence of the Dawson Creek Graben Complex (Douglas, 1970; Gibson and Edwards, 1990; O'Connell et al., 1990; Davies, 1997a). Recent study has suggested that the deposition of Triassic strata was profoundly impacted by tectonic and structural factors including both terrane accretion on the western margin of the supercontinent and reactivation of older tectonic elements (Davies, 1997a, 1997b; Davies et al., 2018; Zonneveld and Moslow, 2018).

BIOSTRATIGRAPHIC FRAMEWORK

There are many studies establishing biostratigraphic age dates to provide a biostratigraphic framework of the Triassic intervals, especially the Montney Formation, within the Western Canada Sedimentary Basin (Orchard and Tozer, 1997; Orchard and Zonneveld, 2009; Golding et al., 2014a, 2014b, 2015; Henderson and Schoepfer, 2017; Henderson et al., 2018). The Montney Formation approximately spans 4.8 million years, recording the deposition from the latest Permain to the Lower Triassic (Henderson, 1997; Davies et al., 2018; Henderson et al., 2018; Moslow et al., 2018;

4

Zonneveld and Moslow, 2018). It can be divided into two global stages (Induan and Olenekian) and four regional substages (Griesbachian, Dienerian, Smithian and Spathian) (Zonneveld and Moslow, 2018). Five basin-scale, roughly synchronous intra- and extra-formational unconformities are identified to separate the Montney Formation into three subdivisions, Lower (Griesbachian-Dienerian), Middle (Smithian) and Upper (Spathian) members.
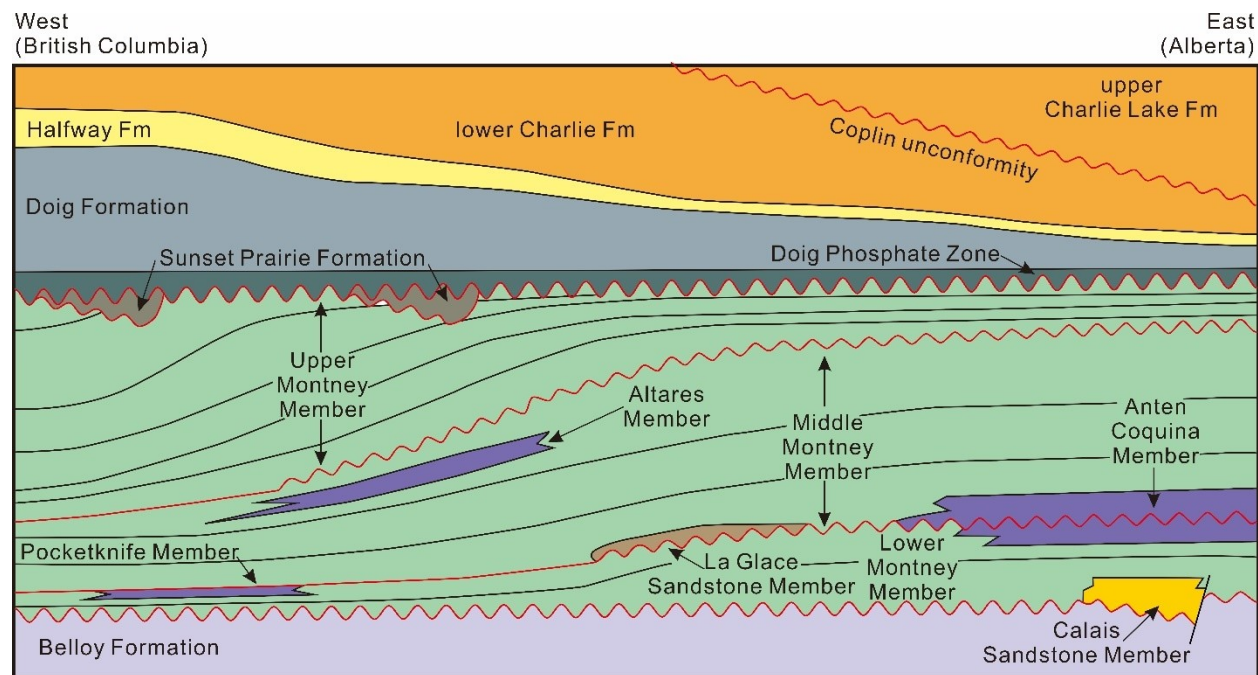
Figure 1.3-Schematic west-east cross-section displaying Montney stratigraphy, British Columbia to Alberta. The Montney Formation is divided into three members (Lower Montney Member, Middle Montney Member and Upper Montney Member) by five intra- and extra-formational unconformities (after Zonneveld and Moslow, 2018).

(Zonneveld and Moslow, 2018). Given their regular presence in Triassic-aged marine strata, conodonts are commonly used to date the Montney Formation and its outcrop equivalents (Henderson, 1997; Orchard and Tozer, 1997; Orchard and Zonneveld, 2009; Wilson et al., 2012; Golding et al., 2014a, 2015; Moslow et al., 2018; Henderson et al., 2018). The three stratigraphic depositional sequences of the Montney Formation (the Lower, Middle and Upper Montney) can be correlated with around 20 uppermost Permian to upper Lower Triassic conodont zones, potentially providing a basis for correlation of chronostratigraphic units within the Montney

Formation (Henderson et al., 2018). Palynomorphs are also used to determine the age of the Lower Triassic, and this is applied mostly the lowermost Triassic (Janonius, 1962; Utting et al., 2005). However, as there are inadequate non-degraded samples and long-ranging taxa identified from the Montney Formation, palynomorphs are not commonly used (Zonneveld and Moslow, 2018).

PALAEOENVIRONMENTAL SETTING

The deposition of the Montney Formation was significantly affected by the end-Permian mass extinction event at ~250 Ma. It is the most severe extinction that the Earth has experienced, leading to the demise of 90% to 95% of skeletonized marine species (Erwin, 1994; Benton and Twitchett, 2003; Alroy et al., 2008; Algeo et al., 2011). This catastrophe is inferred to be attributed to oxygen depletion in marine associated with climate warming (Isozaki, 1994, 1997; Hays et al., 2007; Penn et al., 2018) and ocean acidification generated by the outgassing of CO_2 from the Siberian Traps (Knoll et al., 2007; Clarkson et al., 2015; Penn et al., 2018). The prolonged, regionally extensive marine anoxic conditions extended into the Middle Triassic in many areas, postponing the faunal recovery (Wignall and Twitchett, 1996, 2002; Zonneveld et al., 2010b).

As a result, diverse palaeontological and ichnological assemblages are largely absent in the Lower Triassic Montney Formation. In terms of palaeontological assemblages, there are ammonoid and bivalve impressions commonly presenting on the bedding planes, with all shell material being eliminated (Woods and Bottjer, 2000; Rampino and Caldeira, 2005; Zonneveld et al., 2011; Zonneveld and Moslow, 2018). However, both whole and fragmentary shell material (bivalves, ammonoids, brachiopods, gastropods) are well preserved in isolated horizons within the Montney Formation, mainly including the Pocketknife Member (Dienerian in age), Anten Coquina Member (late Dienerian to early Smithian in age) and Altares Member (latest Smithian in age) (Mederos, 1995; Davies et al., 1997b; Markhasin, 1997; Sanders et al., 2018; Zonneveld and Moslow, 2018). Most Lower Triassic Montney intervals are characterized by low-diversity/low-abundance trace fossil assemblages (Beatty et al., 2008; Zonneveld et al., 2010a, 2010b; Furlong et al., 2018; Zonneveld and Moslow, 2018). Isolated areas exhibiting ichnological assemblages that are of high trace-fossil diversity, such as the Pedigree-Ring-Kahntah area and Kawaka and Karr fields, are interpreted to represent the refugia where well-oxygenated marine water facilitated

bioturbation in wave-agitated shallow-marine areas (Beatty et al., 2008; Zonneveld et al., 2010a, 2010b; Zonneveld and Moslow, 2018).

STUDY AREA AND DATASET

This thesis focuses on reservoir and ichnological characteristics of two cored areas of the Montney Formation to gain some perspective of the Upper Montney Member regional variation. The study areas are situated in the west-central Alberta and northeastern British Columbia. Five vertical wells were logged for lithofacies description and interpretation: this small number of wells is a result of the detailed level of analyses required for reservoir-property evaluation. Fifty thin sections and forty-four SEM samples from three wells (16-14-073-26W5; 14-33-073-26W5; 04-11-081-21W6 respectively) were prepared, aiding in the reservoir characterization of each lithofacies. Porosity and permeability of 296 samples from the same three wells were measured through steady-state porosimeter and permeameter. Pore-throat radius of the samples from the well 16-14-073-26W5 and 14-33-073-26W5 were estimated using Winland's equation (Kolodzie, 1980). The Winland porosity-permeability plot was utilized to show the correlation between lithofacies and pore-throat radius. 26 samples (taken from every 5 m) from the well 04-11-081-21W6 were investigated using X-ray-diffraction (XRD) and carbon analyzer to quantify the mineralogical composition and total organic carbon (TOC). Four cores were used to characterize process ichnological trends of the Upper Montney shoreface successions.

	Well ID	Well Name
1	100/16-14-073-26W5/00	BARRIC PUSKWA 16-14-73-26
2	100/14-33-073-26W5/00	BARRIC PUSKWA 14-33-73-26
3	100/04-11-081-21W6/00	SHELL MONIAS 04-11-081-21
4	100/04-09-084-22W6/00	ARCRES ATTACHIE 04-09-084-22
5	100/16-06-081-17W6/00	OVV HZ TOWER c16-06-081-17

Table 1.1-Summary of wells with Montney Formation drill core, which were logged in this thesis.

ORGANIZATION OF DISSERTATION

This thesis is divided into 6 chapters (including the introduction and conclusion), which mainly investigate the sedimentology and ichnology of the Upper Montney Member from the two cored study areas. As the paper-based format was chosen for this dissertation, some replication of figures and data are inevitably present in order to provide the essential background for each chapter. The subject and content of each chapter is outlined below.

Chapter 2 demonstrates that the pore-throat radii and reservoir qualities of the Montney Formation in the Puskwaskau Field are generally lithofacies-dependent. Four lithofacies are divided on basis of sedimentological, ichnological analyses. Lithofacies 1 (L-1) is composed of interlaminated bituminous very fine- to medium-grained siltstone and dolomitic medium- to coarse-grained siltstone. Lithofacies 2 (L-2) consists of interbedded dolomitic medium- to coarse-grained siltstone and bituminous very fine- to medium-grained siltstone. Lithofacies 3 (L-3) is dominated by bitumen-stained dolomitic medium- to coarse-grained siltstone. Lithofacies 4 (L-4) is characterized by dense, dolomitic coarse-grained siltstone to very fine-grained sandstone. Sediments within the study area are interpreted to have been deposited within a wave- to storm-influenced shoreface and offshore transition zone, comprising conformable progradational successions. The reservoir quality of these deposits is evaluated by comparing reservoir characteristics of each lithofacies. Analyzed properties include porosity, permeability, pore-throat radius, clay content and cementation. Winland plots are used to show the predicted pore-throat diameters of lithofacies based on measured porosity and permeability. The range of values observed within each lithofacies effectively constrains the reservoir characteristics and demonstrate the correspondence of lithofacies classification to reservoir quality in this producing field.

Chapter 3 describes the lithofacies of the Montney Formation in a low-gradient, predominantly siliciclastic ramp setting, corresponding to offshore transition to offshore environments. Lithofacies 1 represents the deposition within the upper ramp (offshore transition), with rare to intermittent interferences by storm waves, mostly consisting of interlamination of wavy parallel to planar laminated medium- to coarse-grained siltstone and bituminous fine- to medium-grained siltstone. Lithofacies 2 and 3 are interpreted to be deposited within the lower ramp setting (offshore), subject to linear-sourced turbidity currents initiated by mass wasting. On

basis of the degree of impacts by the low-density turbidity currents, the lower ramp can be subdivided into distal and proximal lower ramp settings. Lithofacies 2 generally includes interlamination of bituminous fine- to medium-grained siltstone and wavy parallel to lenticular bedded medium- to coarse-grained siltstone, recording the deposition in the distal lower ramp (distal to the site of mass wasting). Whereas, lithofacies 3 is interpreted to be deposited in the proximal lower ramp (proximal to the site of mass wasting) on account of the common presence of relatively thick dolomitic medium- to coarse-grained siltstone beds representing turbidites. Combined with mineralogical data from X-ray-diffraction (XRD) and analyses of high-resolution scanning electron microscopy (SEM) and thin-section petrography, it is concluded that the lithological similarities lead to comparably predictable and less heterogeneous reservoir properties of these three lithofacies. Nevertheless, the reservoir qualities of the three lithofacies are poor: all three lithofacies show very similar porosity and permeability values, ranging from 6.43 to 6.75% and 2.53×10^{-6} to 1.42×10^{-5} mD, respectively.

Chapter 4 and 5 investigates the ichnological characteristics of the shoreface successions within the Upper Montney Member in west-central Alberta and northeastern British Columbia through process ichnological analysis. The process ichnology was introduced by Gingras et al. (2011) and integrates the ichnogenera characteristics and physical sedimentology to interpret the physico-chemical stresses affecting sedimentary environment at the time of deposition. One of the advantages of this approach is several process ichnology proxies are semi-quantitative variables that can be analyzed statistically (Timmer et al., 2016a, 2016b). So far, this method was mainly applied to conduct the analysis of the marginal marine setting and rarely used within a fully marine system (Hubbard et al., 2004; Hauck et al., 2009; Gingras et al., 2011; Botterill, 2015; Timmer et al., 2016a, 2016b). Four wells located in the northeastern British Columbia and west-central Alberta are selected to do the process ichnological analysis. The primary ichnological data collected are comprised of bioturbation intensity (BI) (Reineck, 1963, 1967; Droser and Bottjer, 1986; Taylor and Golding, 1993), maximum burrow diameter, ichnofossil diversity and size-diversity index (SDI) (Hauck et al., 2009; Gingras et al., 2011; Botterill, 2015; Timmer et al., 2016a, 2016b). The difference associated with depositional environments between the shoreface successions in northeastern British Columbia and west-central Alberta are indicated. And the discrepancies of hydrodynamic conditions and dissolved oxygen levels are interpreted to lead to the ichnological variability of the shoreface successions within the Upper Montney Member.

CHAPTER 2: LITHOFACIES-DEPENDENT PORE-THROAT RADII AND RESERVOIR PROPERTIES IN THE LOWER TRIASSIC MONTNEY FORMATION, PUSKWASKAU FIELD, ALBERTA

INTRODUCTION

The Lower Triassic Montney Formation in west-central Alberta and northeastern British Columbia is an exceptional hydrocarbon reservoir. The Montney Formation contains approximately 12,719 billion m^3 of marketable natural gas, 2,308 million m^3 (14,521 million barrels) of marketable natural gas liquids (NGLs), and 179 million m^3 (1,125 million barrels) of marketable oil (National Energy Board, 2013). It is projected that production of the Montney Formation will lead to the majority of Canadian natural gas production growth over the next 20 years, increasing from 6.6 Bcf/d in 2020 to 13.6 Bcf/d in 2040 (Canada Energy Regulator, 2020). Starting in the 1950s, exploration and extraction efforts were primarily focused on conventional reservoirs (i.e., wells completed vertically) that consisted of very fine-grained sandstone-dominated turbidite successions and shoreline-associated dolomitic bioclastic grainstone, and fine-grained sandstone beds (Zonneveld et al., 2010a; Davies et al., 2018). Significant technological advances in recent years have allowed unconventional reservoirs to become increasingly exploited (Zonneveld et al., 2010a; Davies et al., 2018). Specifically, the development and refinement of horizontal drilling practices and multi-stage hydraulic fracturing have improved hydrocarbon recovery (Davies et al., 2018; Prenoslo et al., 2018; Zonneveld and Moslow, 2018).
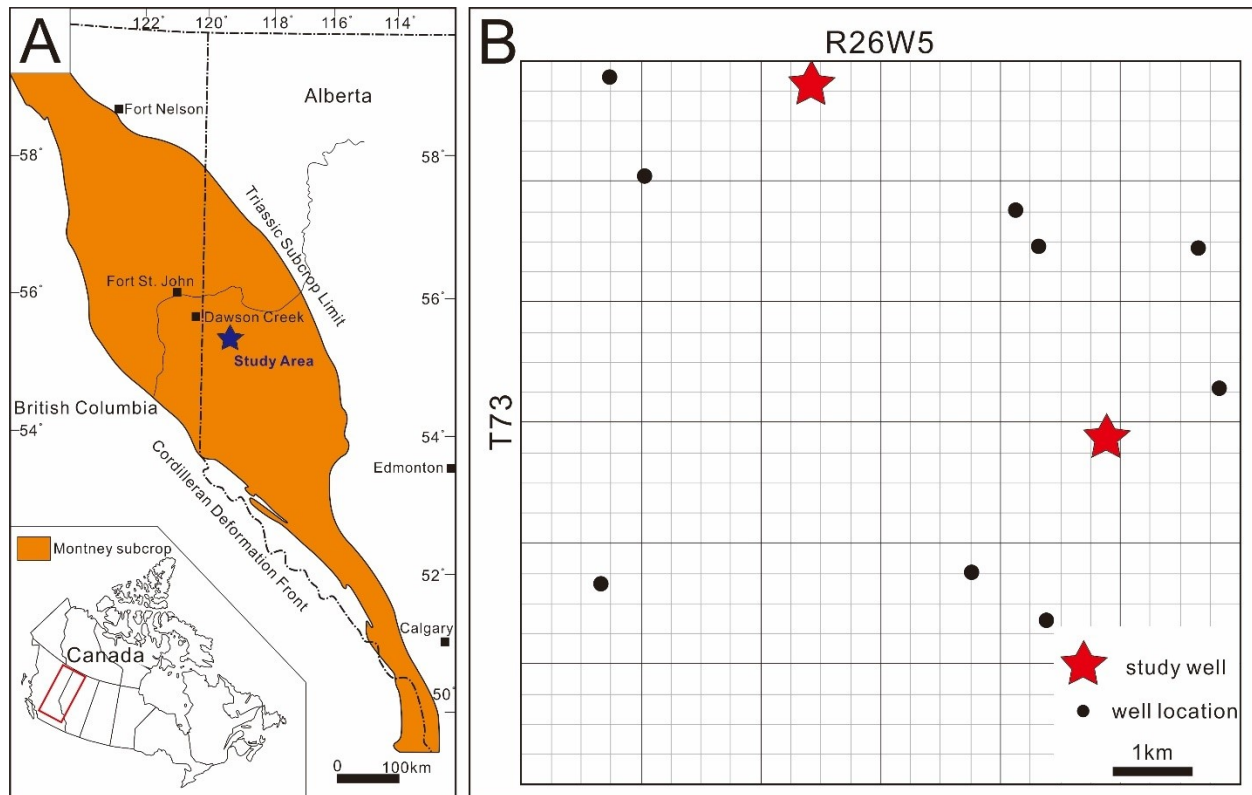
Figure 2.1-Location map of the Puskwaskau Field (A) and study wells (B) (after Wood et al., 2018).

Several basin-scale stratigraphic analyses have recently been proposed for the Montney Formation (Davies et al., 2018; Rohais at al., 2018; Zonneveld and Moslow, 2018). However, detailed analyses of field and well reservoir quality are limited to a few areas. The focus of this study is to determine the reservoir characteristics of lithofacies observed within core from the Puskwaskau Field and evaluate the factors contributing to the reservoir quality (Fig. 2.1).

Geological Background

The Montney Formation is situated in the Western Canada Sedimentary Basin which was formed by terrane accretion during the late Mesozoic (Aitken, 1993). Tectonism generally has exerted a strong influence on the deposition of the Montney Formation (Zonneveld et al., 2010a),

particularly subsidence of the Peace River Arch and movement of its constituent structural elements (Sturrock and Dawson, 1991; Davies, 1997; Davies et al., 1997; Zonneveld et al., 2010a).

The distribution of the Lower Triassic Montney Formation is widespread, extending across approximately 130,000 km^2 of British Columbia and Alberta, Canada. The Montney has a maximum thickness of approximately 350 m. It is thickest in the west pinching out beneath a series of unconformities to the east (National Energy Board, 2013). The depth to the top of the Montney Formation increases from northeast to southwest (ranging from about 500 to 4500 m), resulting in an overall increase in reservoir pressure towards the west/southwest (BC Oil and Gas Commission, 2012; Energy Resources Conservation Board, 2012).
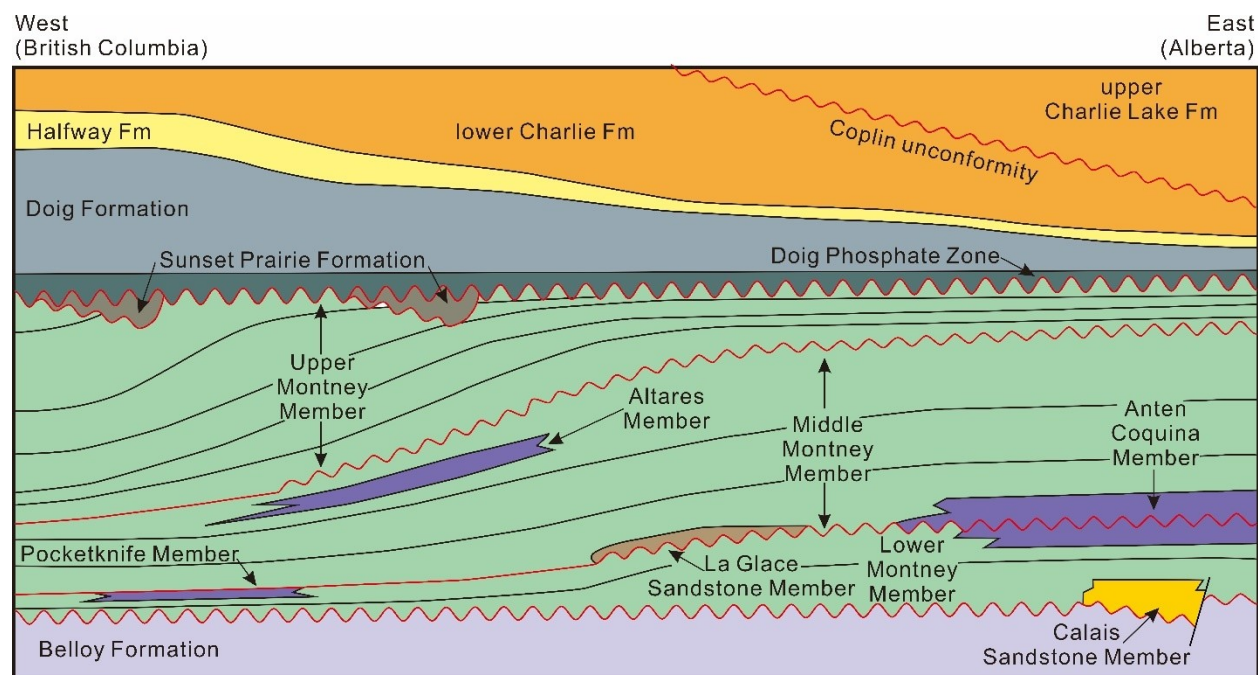
Figure 2.2-Schematic diagram of the Montney stratigraphy, British Columbia to Alberta, exhibiting three unconformity-bounded third-order depositional sequences (Lower, Middle and Upper member) (after Zonneveld and Moslow, 2018).

The Montney Formation is divided into three unconformity-bounded third-order depositional sequences (Embry, 1997; Henderson et al., 2018; Zonneveld and Moslow, 2018) (Fig. 2.2). These units are referred to as the Lower, Middle and Upper Montney members, and correspond to the

Induan (Griesbachian-Dienerian), Lower Olenekian (Smithian) and upper Olenekian (Spathian) stages (Golding et al., 2014; Davies et al., 2018; Henderson et al., 2018; Zonneveld and Moslow, 2018) (Fig. 2.2). The Montney Formation unconformably overlies sandstone, bioclastic packstone /grainstone and spicule-rich chert (spiculite) units of the Permian Belloy Formation (Henderson et al., 2018), and is overlain unconformably by a diachronous Lower Anisian sandstone wedge (Furlong et al., 2018) and Anisian Doig Phosphate Zone (Golding et al., 2015). Deposition of the Montney Formation occurred over an interval of approximately 4.8 Ma (Golding et al., 2014; Henderson et al., 2018).

Zonneveld and Moslow (2018) subdivided the Montney Formation into eight formal members including three mixed-siliciclastic-bioclastic members (Pocketknife Member, Altares Member and Anten Coquina Member), two sandstone-dominated units (La Glace Sandstone Member and Calais Sandstone Member) and three siltstone-dominated members (Lower, Middle and Upper Montney members) (Fig. 2.2).

STUDY AREA AND METHODS

This study focuses on the Upper Member of the Montney Formation in the Puskwaskau Field Township 73, Range 26W5M. Cores from two wells (16-14-73-26W5M and 14-33-73-26W5M) were analyzed to assess the relationship between pore throats and lithofacies.

Lithofacies were subdivided based on distinct lithological, sedimentological and ichnological criteria. Thin section analyses and scanning electron microscopy (SEM) aided in the reservoir characterization of each lithofacies. Parameters affecting the overall reservoir quality include grain size, grain sorting, composition of grains and cement, pore-throat radius, and the interconnectivity of pores.

Thin sections (30 μm thick) were stained with alizarin red S and potassium ferricyanide. With alizarin red S calcite will obtain pale pink to red stain whereas dolomite will take on no color. With potassium ferricyanide, ferroan dolomite stains pale to deep turquoise and ferroan calcite is stained mauve, purple or royal blue (Dickson, 1966). High-resolution SEM images were taken using a Zeiss Sigma 300 VP-FESEM owned by the University of Alberta to identify the morphology of minerals, mineral composition and assess the interconnectivity of pores.

Bulk volumes and grain volumes of samples were obtained through nitrogen porosimetry by the Core Laboratories Canada Ltd located in Calgary. Porosity values were calculated using the following equation:

$$\Phi = \frac{V_b - V_g}{V_b} * 100\%$$

where Φ is porosity (%), V_b and V_g represent bulk volume (cm³) and grain volume (cm³) of a sample. A steady-state gas permeameter was employed to obtain permeability values from slabbed core samples based on Darcy's Law. Pore-throat radius values were estimated using Winland's equation (published by Kolodzie, 1980):

$$\log R_{35} = 0.732 + 0.588 \log K - 0.864 \log \Phi$$

where R_{35} represents pore-throat radii (μm) corresponding to the 35th percentile of mercury saturation from a mercury injection capillary pressure test, K is air permeability (mD) and Φ is porosity (%). This empirical relationship between pore-throat radius, porosity and permeability was established by H. D. Winland (Amoco Production Company), who conducted regression analyses for multiple mercury saturations on 322 samples containing both sandstone and carbonate (Pittman, 1992). His results show that the best correlation was obtained at a mercury saturation of 35%. Pittman (1989, 1992) subsequently reported that the 35th percentile of mercury saturation generally corresponds to pore-throat radius values that result in the effective interconnectivity of pores, which is directly related to reservoir quality (Swanson, 1977, 1981; Hartmann and Coalson, 1990). Winland R_{35} pore-throat radii are subdivided into 5 categories: (1) megapores with R_{35} values greater than 10 μm; (2) macropores with R_{35} values between 2 and 10 μm; (3) mesopores with R_{35} ranging between 0.5 and 2.0 μm; (4) micropores with R_{35} values ranging from 0.1 to 0.5 μm; (5) nanopores with R_{35} values greater than 0.01 μm and less than 0.1 μm (Martin et al., 1997; Aguilera, 2002). As pore-throat radius is subject to depositional processes and diagenesis, varying R_{35} values can represent the distribution of porosity and permeability for different lithofacies. Differences in R_{35} of the two wells (16-14-73-26W5M and 14-33-73-26W5M) are illustrated by Winland plots and are used to classify rock types and lithofacies that display similar pore-throat radius values. (Martin et al., 1997).

14

LITHOFACIES DESCRIPTIONS AND INTERPRETATIONS

Four lithofacies were identified in the study area (Table 2.1). Lithofacies were subdivided based on sedimentological and ichnological characteristics (Figs. 2.3 and 2.4). Each lithofacies is discussed in detail below. A notable decrease in relative clay content is observed from Lithofacies 1 to 4.

FACIES	LITHOLOGY	BEDDING	PHYSICAL SEDIMENTARY STRUCTURE	ICHNOLOGICAL ASSEMBLAGE	DEP. ENVIRONMENT
L-1	Interlaminated bituminous very fine- to medium-grained siltstone and dolomitic medium- to coarse-grained siltstone	Sharp based; normal graded; mm-scale interlamination	Planar lamination; lenticular bedding; unidirectional flow ripple; oscillation flow ripples; convolute bedding; microfault; water-escape structure	Scattered *Skolithos*; thin intensely bioturbated beds comprising *Phycosiphon* and *Cylindrichnus*	Offshore transition
L-2	Interbedded dolomitic medium- to coarse-grained siltstone and bituminous very fine- to medium-grained siltstone	Sharp base; normal grading; 1-30 cm for beds	Hummocky cross-stratification; combined flow ripples; oscillation flow ripples; wavy lamination; low angle cross-stratification; planar-lamination; flame structure; load cast; syneresis crack	Diminutive and concentrated *Phycosiphon;* isolated *Teichichnus* and *Skolithos*	Lower shoreface
L-3	Bitumen-stained, dolomitic medium- to coarse-grained siltstone with few bituminous very fine- to medium-grained siltstone laminae or beds	Sharp based; normal grading; 18-82 cm for beds	Massive bedding; hummocky cross-stratification; wavy lamination; rippled lamination; planar-lamination; load cast; subaqueous cracking and sand dykes	None-observed	Middle shoreface
L-4	Dolomitic, coarse-grained siltstone to very fine-grained sandstone	Sharp based; ungraded; 52 cm in thickness totally	Fuzzy bedding resulted from bioturbation	Intense bioturbation with indiscernible traces	Upper shoreface

Table 2.1-Summary of sedimentary lithofacies characteristics of the Montney Formation in the Puskwaskau Field, Alberta.
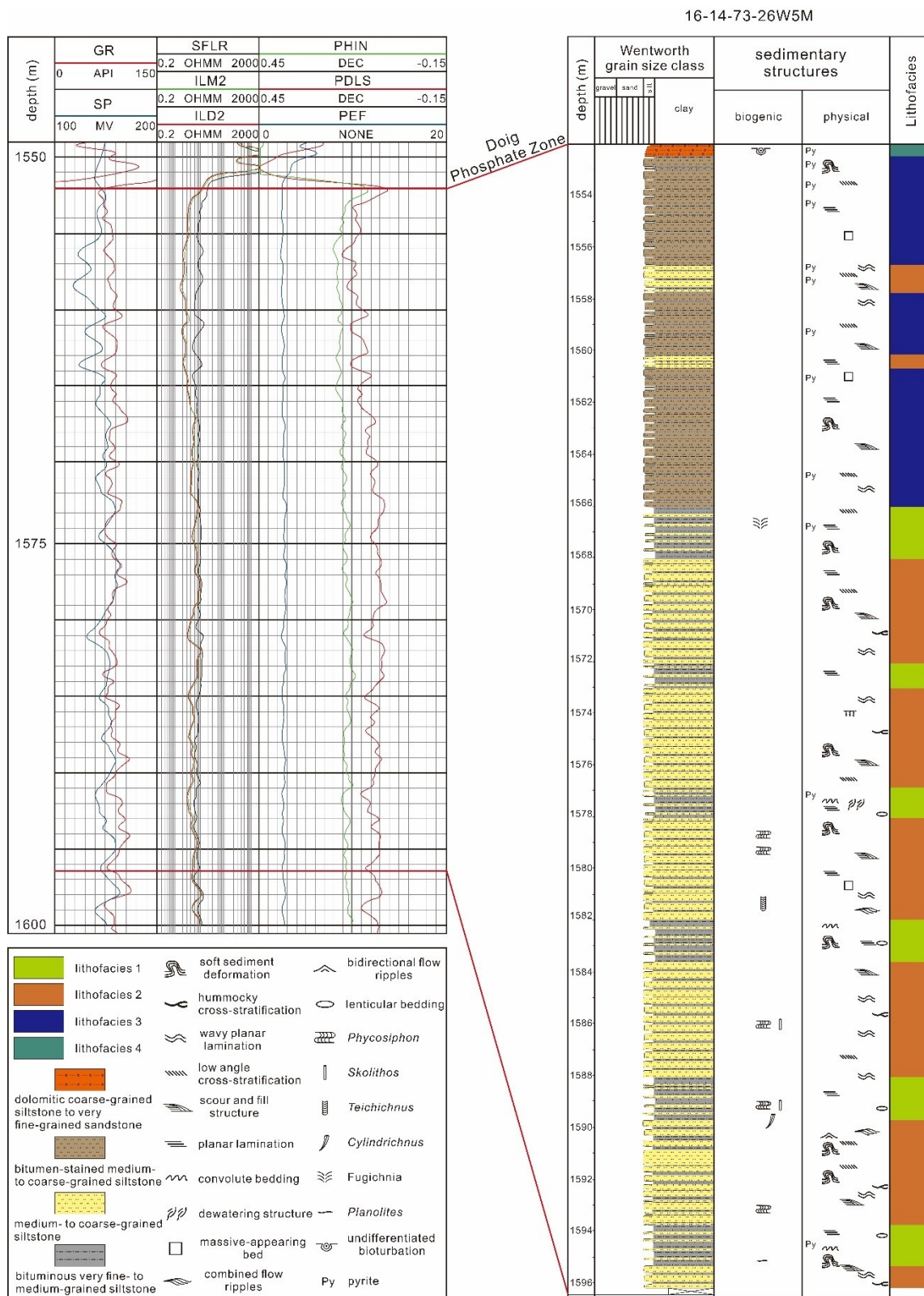
Figure 2.3-Gamma Ray, Spontaneous Potential, Resistivity, Neutron Porosity, Density Porosity and Photoelectic Effect logs and core description for the 16-14-73-26W5M (1552.01-1596.46 m).
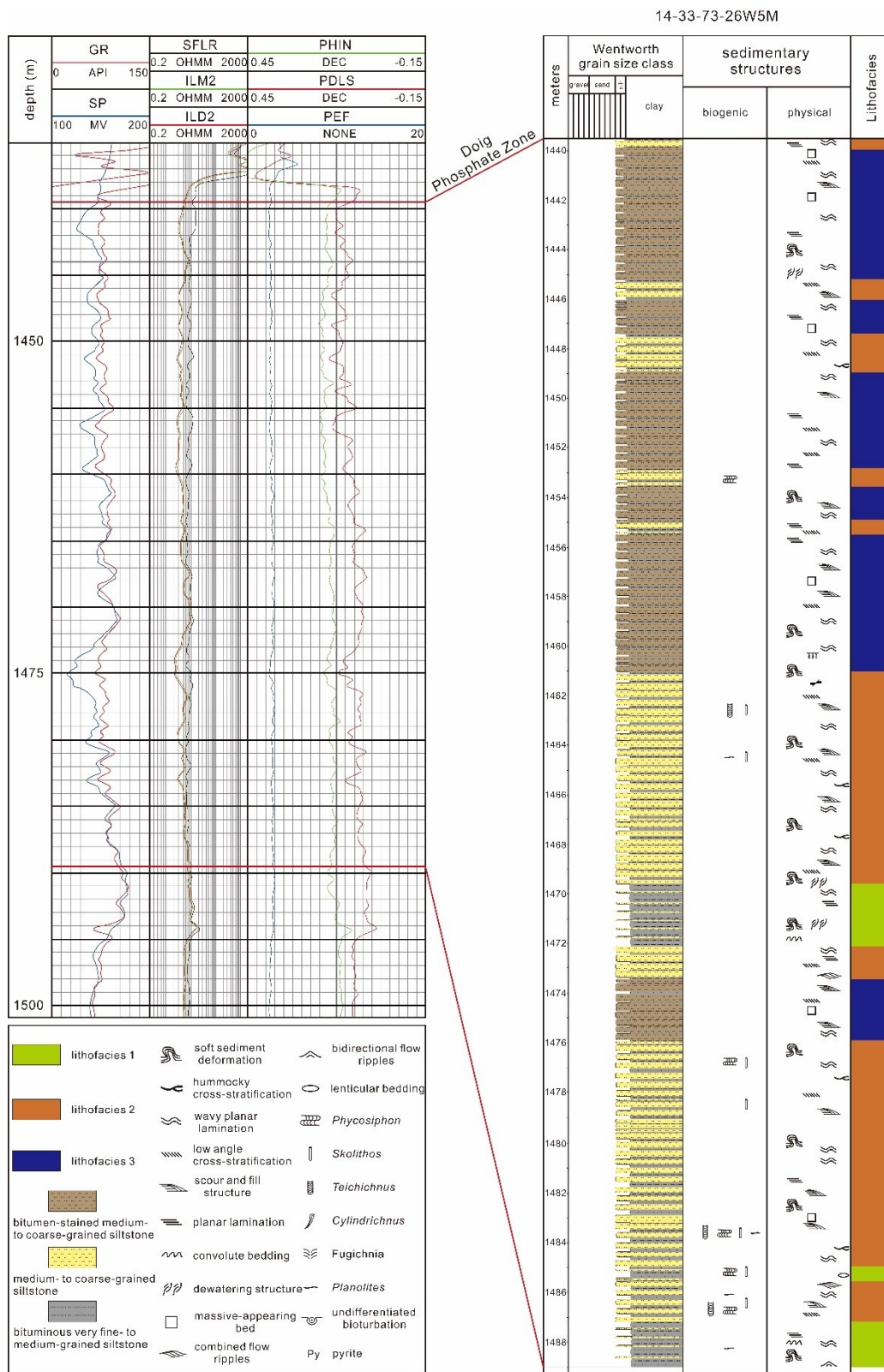
Figure 2.4-Gamma Ray, Spontaneous Potential, Resistivity, Neutron Porosity, Density Porosity and Photoelectic Effect logs and core description for the 14-33-73-26W5M (1439.49-1489.49 m).
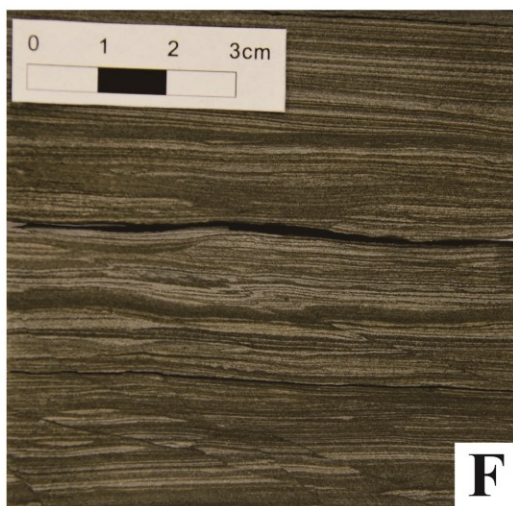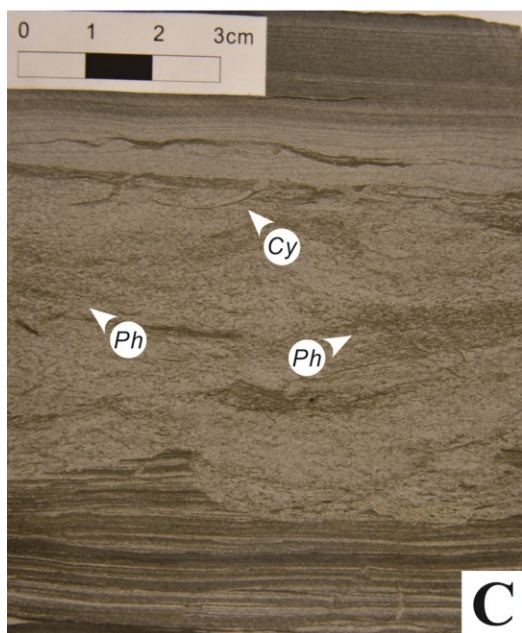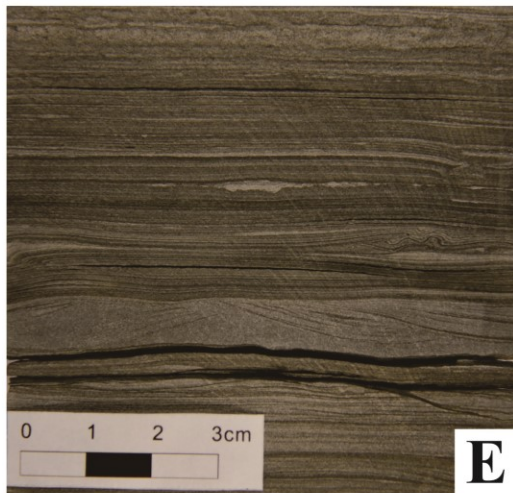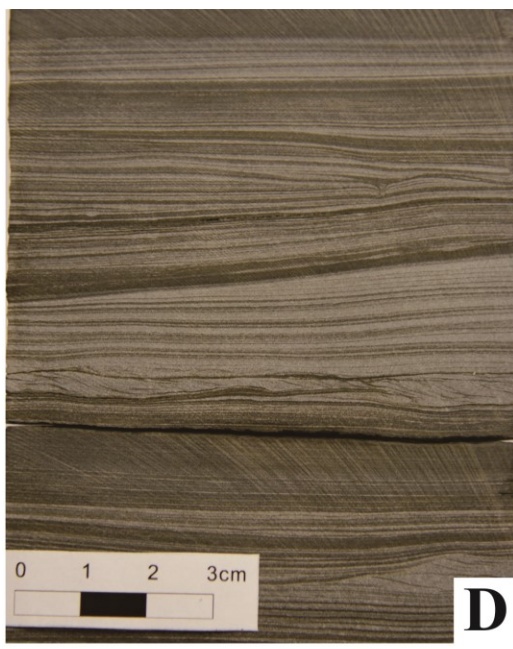
Figure 2.5-Core photographs of Lithofacies 1. **A**. Lenticular bedded bituminous very fine- to medium-grained siltstone and medium- to coarse-grained siltstone. 14-33-73-26W5M; 1485.29 m. **B**. Wavy parallel interlaminated bituminous very fine- to medium-grained siltstone and medium- to coarse-grained siltstone. 16-14-73-26W5M; 1594.45 m. **C**. Intensely bioturbated layer. Ichnogenera include *Phycosiphon* (*Ph*) and subordinate *Cylindrichnus* (*Cy*). 16-14-73-26W5M; 1589.15 m. **D**. Wavy parallel lamination and small-scale combined flow ripples. 16-14-73-26W5M; 1575.72 m. **E**. Locally occurring oscillation flow ripples and convolute bedding. 14-33-73-26W5M; 1487.79 m. **F**. Microfaulting within a parallel laminated interval; 16-14-73-26W5M; 1594 m.

Lithofacies 1

Description

Lithofacies 1 (L-1; Fig. 2.5) is composed of interlaminated bituminous very fine- to medium-grained siltstone and dolomitic medium- to coarse-grained siltstone. Coarser laminae are typically sharp based and grade upwards into finer laminae (Fig. 2.5B). Interlaminae are mm scale in thickness. L-1 is characterized by heterolithic stratification; planar- to wavy- parallel lamination predominates with less common lenticular bedding (Fig. 2.5A). Oscillation and combined flow ripples occur locally (Figs. 2.5D and E). Convolute bedding, water-escape structures and microfaults are also present (Figs. 2.5E and F). Some intervals are cemented by dolomite or ferroan dolomite. Pyrite occurs in varying proportions as framboids and grain coatings. Bioturbation is typically confined to rare escape structures (fugichnia), however thin (cm scale) layers of heavily bioturbated (BI=4-5) very fine- to medium-grained siltstone are present locally. In these zones, identification of ichnogenera is difficult due to limited grain size variability and extensive biogenic reworking, although abundant *Phycosiphon* and subordinate *Cylindrichnus* and *Planolites* have been identified (Fig. 2.5C).

Interpretation

Lithofacies 1 is interpreted to have been deposited in the offshore transition zone dominated by weak storm-wave reworking and offshore sediment transport. The heterolithic nature of L-1 is interpreted to represent storm-associated sedimentation from suspension (Reineck and Singh, 1971;

Zonneveld et al., 2010a). During storm events, large quantities of fine-grained sediment were transported subaqueously in suspension from the coast to the offshore transition zone. Following storm events, hydraulic energy gradually decreased, resulting in the successive deposition of silt and clay. The abundance of fine-grained materials and planar lamination suggests that deposition occurred under low energy conditions. Low energy conditions were punctuated by periods of increased storm influence, indicating that deposition occurred above storm-wave base (Basilici et al., 2012). Lenticular bedding is interpreted to represent waning storm influence whereby coarser laminae were deposited as lenses which were then overlain by post-storm very fine- to medium-grained siltstone laminae (Reineck and Wunderlich, 1968; Dalrymple, 2010; Baas et al., 2015). Periods of rapid sedimentation are indicated by the presence of synsedimentary structures such as convolute bedding and water-escape structures. Thin, intensely bioturbated layers record post-storm opportunistic colonization by a low-diversity trace fossil suite dominated by *Phycosiphon* with subordinate *Cylindrichnus* (MacEachern et al., 2009a; Zonneveld et al., 2010b; Davies et al., 2018). Low trace fossil diversity has been implicated in regional oxygen-stressed conditions during earliest Montney deposition (Zonneveld et al., 2010a, 2010b).
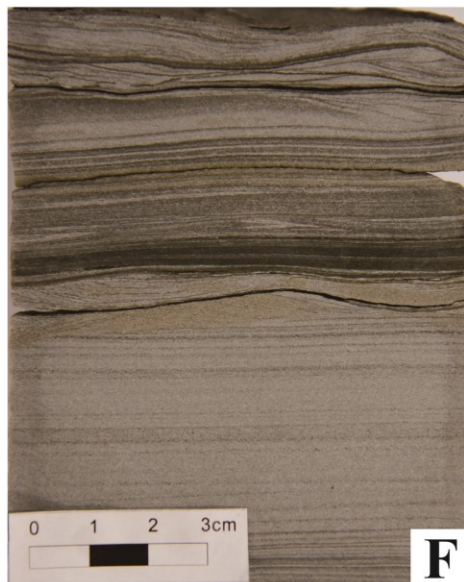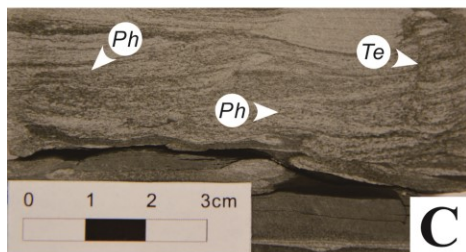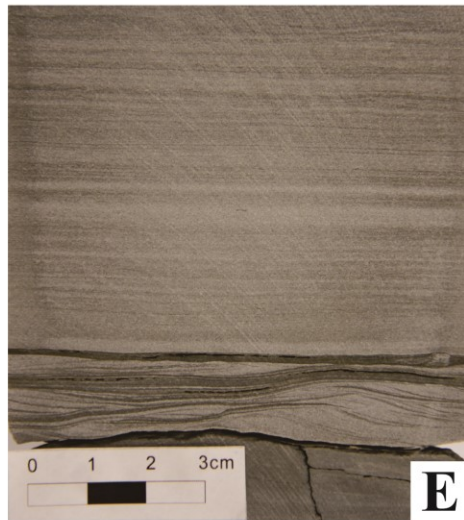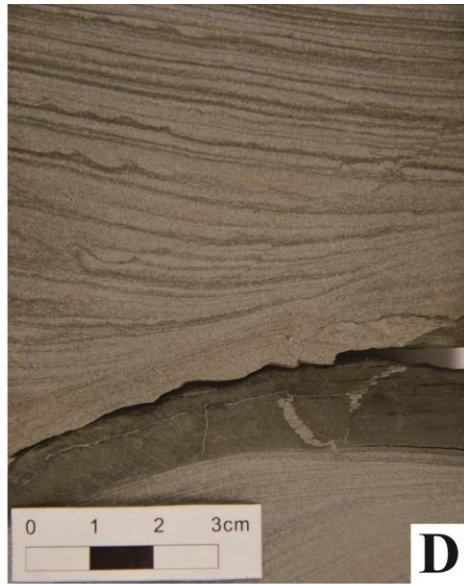
Figure 2.6-Core photographs of lithofacies 2. **A**. Hummocky cross-stratified medium- to coarse-grained siltstone. 16-14-73-26W5M; 1596 m. **B**. Low angle to hummocky cross-stratified medium- to coarse-grained siltstone interbedded with fissile, massive-appearing, bituminous very fine- to medium-grained siltstone. 16-14-73-26W5M; 1571.09 m. **C**. Heavily bioturbated layer consisting of *Phycosiphon* (*Ph*), and subordinate *Teichichnus* (*Te*). 14-33-73-26W5M; 1483.32 m. **D**. Deformed medium- to coarse-grained siltstone with abundant flame structures and rare syneresis cracks occurring within a bituminous very fine- to medium-grained siltstone bed. 16-14-73-26W5M; 1574.45 m. **E**. Isolated combined flow ripples; 14-33-73-26W5M; 1473.24m. **F**. Interval containing oscillation and combined flow ripples; 16-14-73-26W5M; 1589.91 m.

Lithofacies 2

Description

Lithofacies 2 (L-2; Fig. 2.6) consists of interbedded, sharp-based, dolomitic medium- to coarse-grained siltstone and fissile, bituminous very fine- to medium-grained siltstone. Normally graded coarse to very fine siltstone couplets range from 1 to 30 cm in thickness. Individual beds are commonly truncated. An array of physical structures occur within the medium- to coarse-grained siltstone beds, including hummocky, low-angle and planar cross-stratification, planar- to wavy-lamination and combined flow ripples. Rare, contorted bedding is present within low-angle planar cross-stratified beds, displaying abundant microflame structures (Fig. 2.6D). Dolomite cementation is common within the medium- to coarse-grained siltstone beds. Very fine- to medium-grained siltstone beds, which account for approximately ~15-20% of L-2, are massive appearing to faintly laminated. These beds contain abundant pyrite framboids and grain coatings. Rare synaeresis cracks are also present in the very fine- to medium-grained siltstone beds (Fig. 2.6D). Moderately to heavily bioturbated very fine- to medium-grained siltstone beds mainly contain *Phycosiphon* and isolated *Skolithos*, *Teichichnus* and *Planolites* (Fig. 2.6C).

Interpretation

Lithofacies 2 is interpreted to represent the deposition on the lower shoreface, recording the rising and waning stages of storm deposits. Sharp-based basal contacts of the medium- to coarse-grained siltstone and local truncation of bedding represent an erosional contact with the underlying

23

very fine- to medium-grained siltstone beds. These contacts likely represent increased storm influence. Rapid, episodic sedimentation is further evidenced by the occurrence of microflame structures within the low angle cross-stratified coarser siltstone beds. Planar to wavy lamination commonly occurs at the base of the coarser siltstone beds and is interpreted to represent deposition in an upper flow regime (Cheel, 1991; Cheel and Leckie, 1993). The middle portions of these beds display low angle and hummocky cross-stratification associated with persistent storm activity. The upper portions display oscillation flow ripples, which represent waning storm influence followed by fair-weather conditions (Cheel, 1991; Cheel and Leckie, 1993; Plint, 2010). Unidirectional flow resulting from coastal setup, together with storm waves, gives rise to the formation of locally occurring combined flow ripples (Swift et al., 1986). Although combined flow ripples may be present throughout the shoreface, well preserved hummocky cross-stratification is commonly attributed to deposition within the lower shoreface to proximal offshore transition (Hamblin and Walker, 1979; Harms, 1979). Storm-associated siltstone beds are mantled by fissile, very fine- to medium-grained siltstone beds, recording post-storm deposition under lower energy conditions. The abundance of these finer beds suggests that deposition of L-2 was dominated by fair-weather conditions. The majority of these very fine- to medium-grained siltstone beds are unburrowed, owing to the oxygen-stressed conditions during deposition (MacEachern et al., 2009b). However, the presence of thin, moderately to highly bioturbated beds may record periods of favourable physico-chemical conditions (i.e., comparably well-oxygenated and lowered sedimentation stress) that promoted opportunistic colonization (Howard and Frey, 1975; MacEachern and Pemberton, 1992; Botterill et al., 2015).
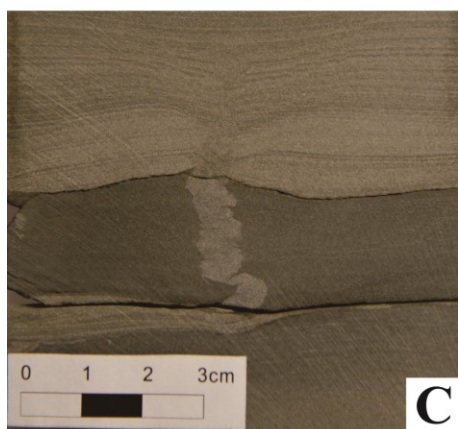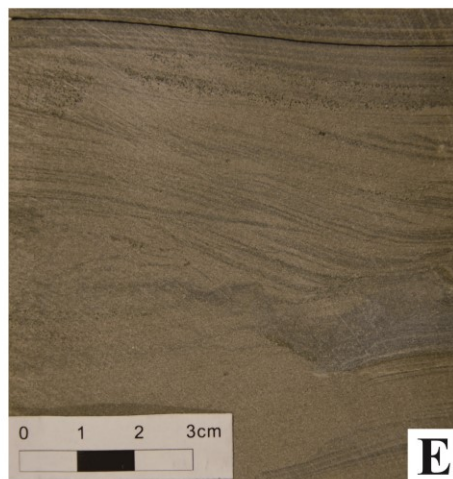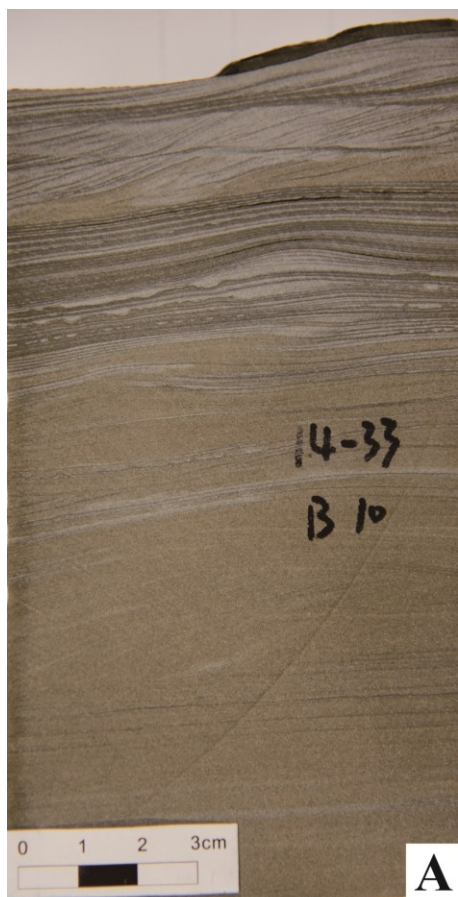
Figure 2.7-Core photographs of lithofacies 3. **A**. Interval displaying planar and ripple lamination, and oscillation and current ripples. Load casts are also observed. 14-33-73-26W5M; 1458.08 m. **B**. Micro-hummocky cross-stratified, bitumen-stained medium- to coarse-grained siltstone. 14-33-73-26W5M; 1448.26 m. **C**. Subaqueous cracking and sand dykes induced by rapid sediment loading and dewatering; 14-33-73-26W5M; 1444.90m. **D**. Low angle cross-stratification. 16-14-73-26W5M; 1563.58 m. **E**. Deformed ripple-laminated, bitumen-stained medium- to coarse-grained siltstone. 16-14-73-26W5M; 1552.87 m. **F**. Massive appearing siltstone grading into wavy-laminated siltstone; 14-33-73-26W5M; 1446.49 m.

Lithofacies 3

Description

Lithofacies 3 (L-3; Fig. 2.7) consists of bitumen-stained, commonly sharp-based, dolomitic medium- to coarse-grained siltstone with few bituminous very fine- to medium-grained siltstone laminae or beds. Individual interbeds range in thickness from 18 to 82 cm. Sedimentary structures within the amalgamated bitumen-stained medium- to coarse-grained siltstone beds include low angle and hummocky cross-stratification, planar to wavy lamination and current ripples. Massive appearing bedding is common (Fig. 2.7F). Rare sand dykes are present (Fig. 2.7C). Medium- to coarse-grained siltstone beds are commonly cemented by dolomite or ferroan dolomite. Massive appearing to planar laminated very fine- to medium-grained siltstone beds comprise approximately 6% of L-3. Pyrite occurs as both discontinuous laminae and nodules. Bioturbation is markedly absent.

Interpretation

Lithofacies 3 is interpreted to represent deposition within the middle shoreface (Reinson, 1984; MacEachern and Bann, 2008). Similar to L-2, medium- to coarse-grained siltstone occurs as well-developed storm beds (Fig. 2.7A), with typical successions grading from planar lamination and hummocky cross-stratification into wavy and ripple lamination, recording the rising and waning stages of storms. L-3 is characterized by persistent wave action and thus above the fair-weather wave base. This is owing to the overall lack of bioturbation and decrease in the abundance of very fine- to medium-grained siltstone beds (MacEachern and Pemberton, 1992). This is further

supported by abundant scour and fill structures, indicating frequent and intense storm-wave activity. Current ripples associated with unidirectional flow are interpreted to result from periods of significant coastal setup following storms (Swift et al., 1986). Penecontemporaneous deformation such as internal load casts and sand dykes suggests rapid deposition over a hydroplastic less-dense layer (Dzulynski and Kotlarcczyk, 1962; Van Loon and Wiggers, 1976; Prenoslo et al., 2018). The absence of trace fossils in Lithofacies 3 is attributed to persistent and energetic hydrodynamic conditions that were unfavorable to infaunal colonization (MacEachern and Pemberton, 1992; Plint, 2010; Wesolowski et al., 2018).
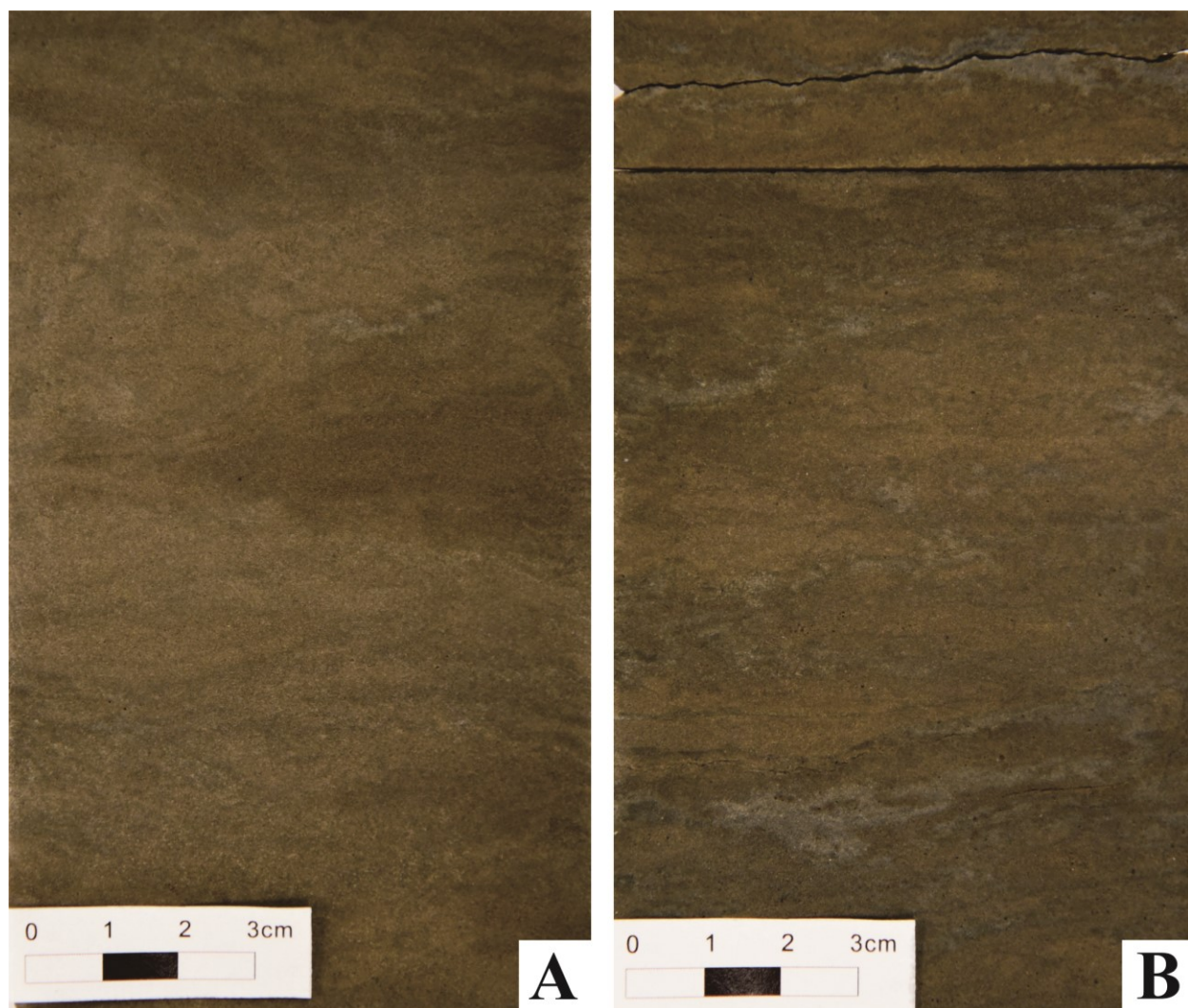
Figure 2.8-Core photographs of lithofacies 4. **A**. Pervasively bioturbated dolomitic coarse-grained

siltstone and very fine-grained sandstone. 16-14-73-26W5M; 1552.25 m. **B**. Interval with apparent interbedding owing to a slight decrease in bioturbation. 16-14-73-26W5M; 1552.43 m.

Lithofacies 4

Description

Lithofacies 4 (L-4; Fig. 2.8) is composed of dense, sharp-based, dolomitic, coarse-grained siltstone to very fine-grained sandstone. The occurrence of L-4 is limited at the uppermost part of the Montney Formation in well 16-14-73-26W5M, overlain by Doig Phosphate Zone (Fig. 2.3). The interval is 52 cm thick and is intensely bioturbated, precluding the identification of ichnogenera (Figs. 2.8A and B). Approximately 50% of L-4 is cemented by dolomite. Local calcite cementation is also present.

Interpretation

Lithofacies 4 is interpreted to represent deposition on the upper shoreface/foreshore, specifically, the longshore trough positioned landward of the subaqueous longshore bar (Fig. 2.9). This interpretation is made on account of remarkable increase in grain size in contrast to lithofacies 1-3 and more critically, thorough bioturbation. Under non-barred coastal system, the upper shoreface and foreshore are generally high energy depositional settings because of the integrated effect of storms and shoaling waves. The existence of a subaqueous longshore bar, separated from the beach by a trough, can protect the longshore trough against strong wave and storm energies seaward of the bar (Hunter et al., 1979; Leckie and Walker, 1982; Reading and Collinson, 1996; Herbers et al., 2016). The lack of pyrite framboids suggests that the upper shoreface/foreshore environment was well oxygenated. Settings characterized by high dissolved oxygen concentrations, lowered hydraulic energy and slow sediment accumulation rates can lead to intense bioturbation whereby the sediment is reworked beyond the recognition of individual trace fossils (Gingras et al., 2011; Botterill et al., 2015).

Sedimentary Environment

Deposition within the study area is interpreted to represent a continuously wave- to storm-influenced shallow siliciclastic ramp in an arid coastal margin. Sediments are interpreted to be sourced from onshore settings and delivered to the system by two transport mechanisms: aeolian and ephemeral fluvial processes (Zonneveld and Moslow, 2014, 2018). From coastal settings, very fine- to fine-grained silt (smaller than 0.020 mm) can be suspended and carried by wind for several kilometres offshore (Nickling and Neumann, 2009). In addition, medium- to coarse-grained silt and very fine-grained sand (0.020-0.125 mm) may be transported to the coast by wind-driven saltation (Nickling and Neumann, 2009). Ephemeral streams flushed large quantities of sediment from arid coastal regions into the ocean, reducing the effects of subaqueous chemical weathering within the fluvial systems (Zonneveld and Moslow, 2018). Sediments delivered to the shoreface by wind and ephemeral streams might be transported by longshore drift, although storm reworking was the dominant transport mechanism.
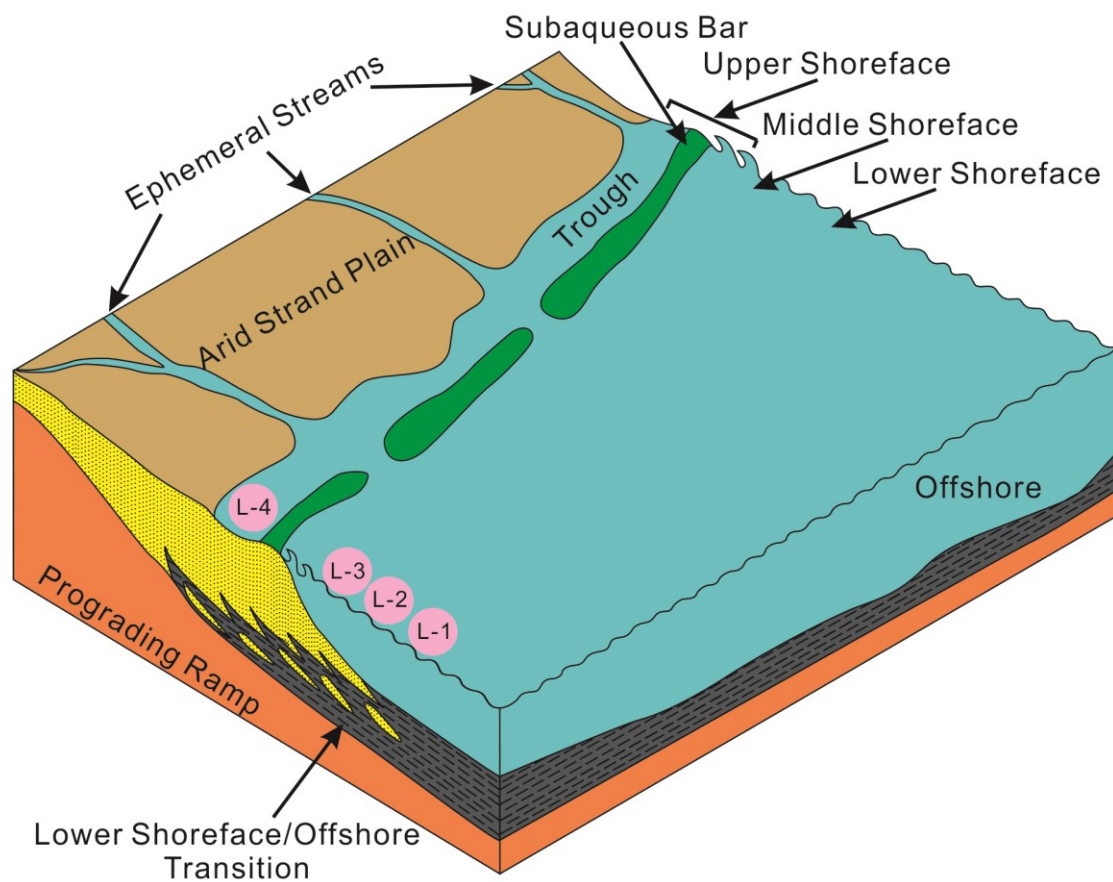
Figure 2.9-Schematic depositional model of a storm-influenced prograding shoreface with the development of longshore subaqueous bars under arid climatic conditions. The locations of the four lithofacies identified in this study are shown (from Deutsh, 1992; Herbers et al., 2016; Moslow et al., 2018).

Based on the two wells, the Montney Formation is characterized as progradational as evidenced by an upwards increase in bed thickness and grain size. The textural maturity of siltstone and sandstone units is ascribed to persistent storm reworking and wind activity within this depositional ramp (Tucker, 2001). Well-developed hummocky cross-stratified intervals commonly occur and are interpreted to be tempestites (Ager, 1973; Dattilo et al., 2012; Yao et al., 2016). The significant upwards increase in thickness of storm beds (from occasional thin tempestites within the offshore transition to thick amalgamated hummocky cross-stratified storm beds of the middle shoreface) suggests that storm influence was heightened at shallower depths. However, the presence of longshore subaqueous bars effectively sheltered the upper shoreface/foreshore from the effects of storm-related wave reworking, resulting in lower energy conditions (Herbers et al., 2016) (Fig. 2.9). Reduced storm influence and an increase in oxygen levels in these settings gave rise to the abundant bioturbation observed in the upper shoreface/foreshore deposits of L-4. Although the middle shoreface was likely well-oxygenated, the bioturbation within the middle shoreface (Lithofacies 3) was suppressed as a result of persistent wave reworking (MacEachern et al., 2009b). The lower shoreface (Lithofacies 2) and offshore transition (Lithofacies 1) were generally characterized by oxygen stress, supported by impoverished ichnofossil assemblages, and the presence of pyrite framboids and coatings. The occasional thin, moderately to highly bioturbated beds suggest that intervals of increased dissolved oxygen concentrations, potentially associated with storm-associated mixing of the shallow waters or seasonal variations in O_2 productivity (Howard and Frey, 1975; MacEachern and Pemberton, 1992; Botterill et al., 2015).

PETROGRAPHY RESULTS
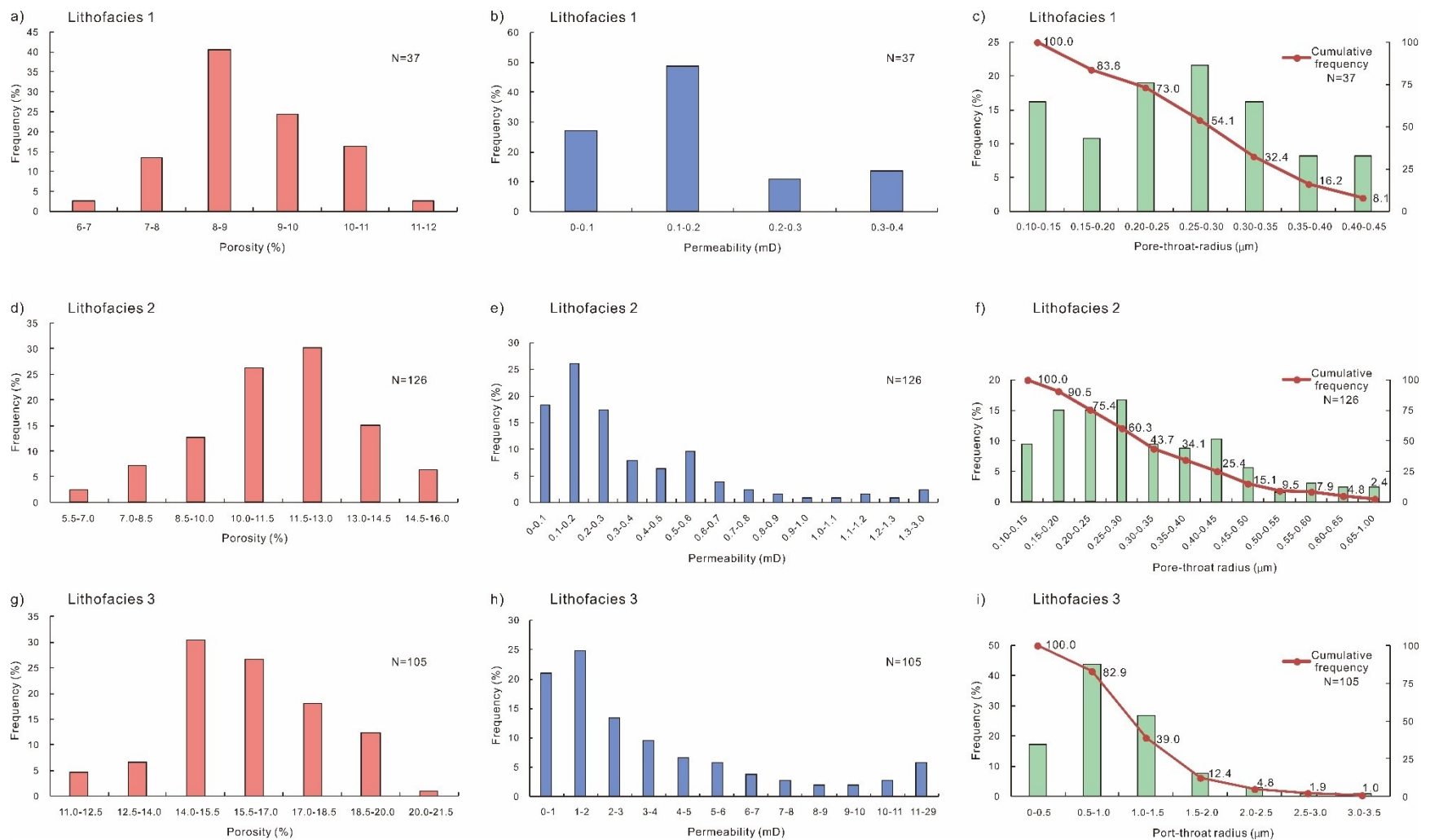
Figure 2.10-Distribution of porosity, permeability and pore-throat radius values for lithofacies 1, 2 and 3.

Each lithofacies was analyzed using SEM images and thin sections to assess their reservoir quality. The data are described below, and the reservoir quality of each lithofacies is discussed. It is noted that the estimation of pore-throat radii is derived by using Winland R_{35} equation and the interconnectivity of pore throats is mainly based on observation of SEM photographs.
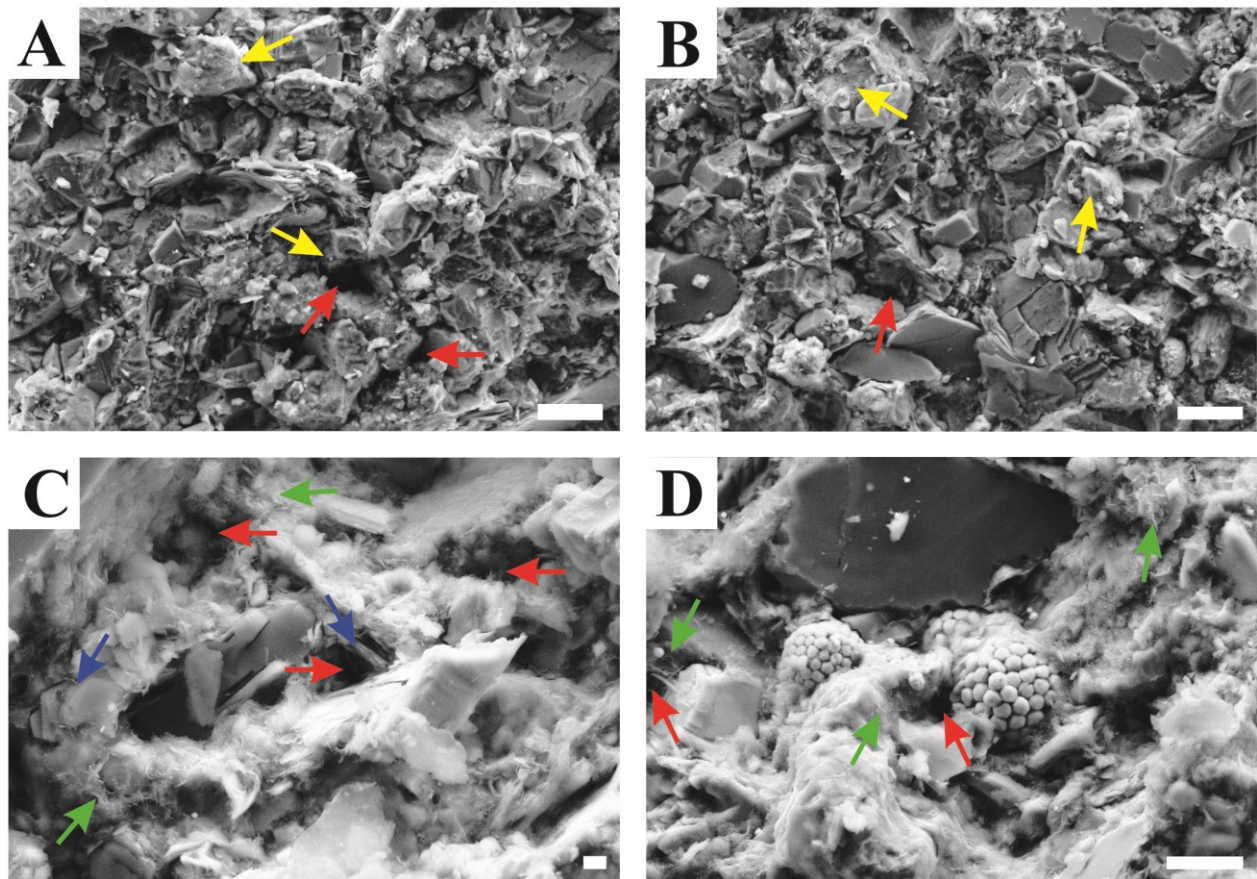
Figure 2.11-SEM images of lithofacies 1. **A**. Clay minerals (yellow arrows) and isolated pores throats (red arrows). Scale bar is 20 μm. **B**. Clay minerals (yellow arrows) and isolated pores (red arrows). Scale bar is 20 μm. **C**. Pores (red arrows) surrounded or blocked by euhedral kaolinite booklets (blue arrows) and fibrous illite (green arrows). Scale bar is 2 μm. **D**. Pores (red arrows) surrounded or blocked by pyrite framboids and fibrous illite (green arrows). Scale bar is 2 μm.
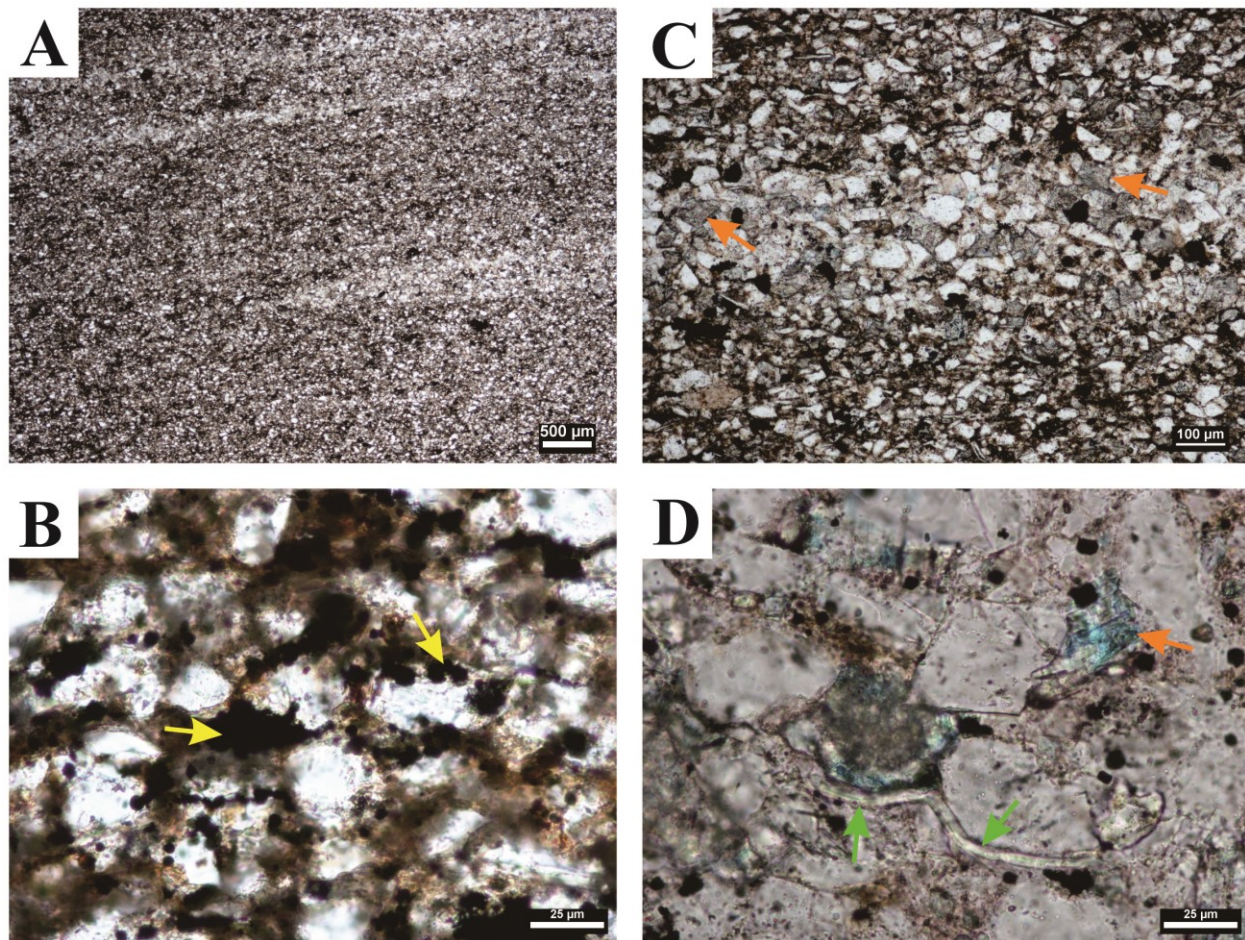
Figure 2.12-Thin section photomicrographs of lithofacies 1. **A.** Typical expression with few clean coarser siltstone laminae. PPL image; 14-33-73-26W5M; 1470.89 m. **B.** Abundant bitumen and pyrite (yellow arrows). PPL image; 14-33-73-26W5M; 1470.89 m. **C.** Clean coarser siltstone lamina containing detrital and authigenic dolomite and ferroan dolomite (orange arrows) within bituminous very fine- to medium-grained siltstone unit. PPL image; 14-33-73-26W5M; 1470.89 m. **D.** High magnification view of clean coarser siltstone containing few bitumen, pyrite and ferroan dolomite (orange arrow). The deformed muscovite (green arrows) indicates strong compaction. PPL image; 14-33-73-26W5M; 1485.08 m.

Lithofacies 1

Lithofacies 1 (L-1; Figs. 2.11 and 2.12) contains interlaminated, poorly sorted, bituminous very fine- to medium-grained siltstone and texturally mature dolomitic medium- to coarse-grained

siltstone. Thinner "clean" siltstone laminae display a range of grain sizes from 0.016 to 0.063 mm with an average of 0.036 mm. These beds are preferentially cemented by dolomite and ferroan dolomite. By contrast, grain sizes within the thicker very fine- to medium-grained siltstone range from 0.003 to 0.030 mm, with an average grain size of 0.017 mm. Very fine- to medium-grained siltstone of L-1 are characterized by a relatively larger amount of clay minerals (predominantly kaolinite and illite), muscovite and authigenic pyrite, compared with L-2, L-3 and L-4.

Porosity values of L-1 range from 6.4% to 11.1% with an average of 8.9%. Over 80% of porosity values occur between 8% and 11% (Fig. 2.10a). Permeability values range from 0.03 to 0.36 mD (0.15 mD on average), with more than 75% of the values being less than 0.20 mD (Fig. 2.10b). Overall, porosity and permeability values show a positive correlation (Figs. 2.19 and 2.20). Pore-throat radii are classified as micropores and range from 0.10 to 0.45 μm. Over 80% of analyzed pore throats in L-1 have a radius of less than 0.35 μm (Fig. 2.10c). Pore throats are largely isolated and thus have poor interconnectivity. The sole pore-filling clay within L-1 is euhedral kaolinite booklets. Pore-lining illite is less common and occasionally extend into the pore-bridging category. Abundant pyrite microcrystals (including framboids) of various sizes also occur as both aggregates and in isolation and represent very early diagenesis (Davies, 1997). Abundant microscopic flake-like muscovite grains are present along bedding planes, contributing to a significant reduction in vertical permeability. Although well-sorted medium- to coarse-grained siltstone laminae are largely devoid of clay, pyrite and muscovite, these intervals are heavily cemented by dolomite and ferroan dolomite, resulting in significant loss of porosity and permeability. Additionally, L-1 has been subjected to significant compaction, which is evidenced by the tight-fitting arrangement of grains, the interpenetration of grains and distorted muscovite flakes. Taken together, these factors contribute to the poor reservoir quality that characterizes L-1.
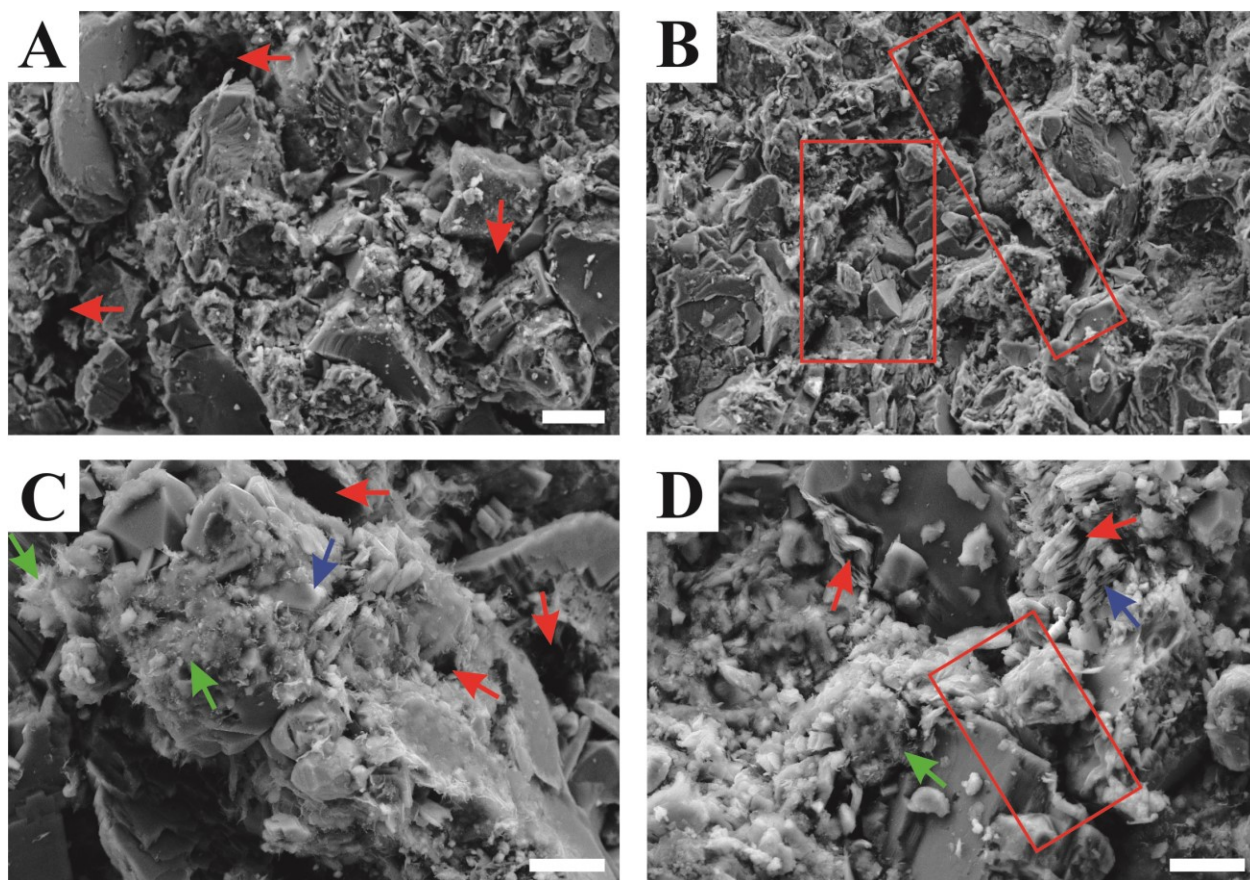
Figure 2.13-SEM images of lithofacies 2. **A**. Isolated pore throats (red arrows) with small amounts of clay. Scale bar is 20 μm. **B**. Interconnected pore throats (red boxes) with small amounts of clay. Scale bar is 10 μm. **C**. Isolated pores (red arrows) are surrounded or blocked by kaolinite (blue arrow) and illite (green arrows). Scale bar is 10 μm. **D**. Pore throat system (red box) restricted by illite coatings and fibres. Micropores (red arrows) are associated with illite (green arrow) and kaolinite (blue arrow). Scale bar is 10 μm.
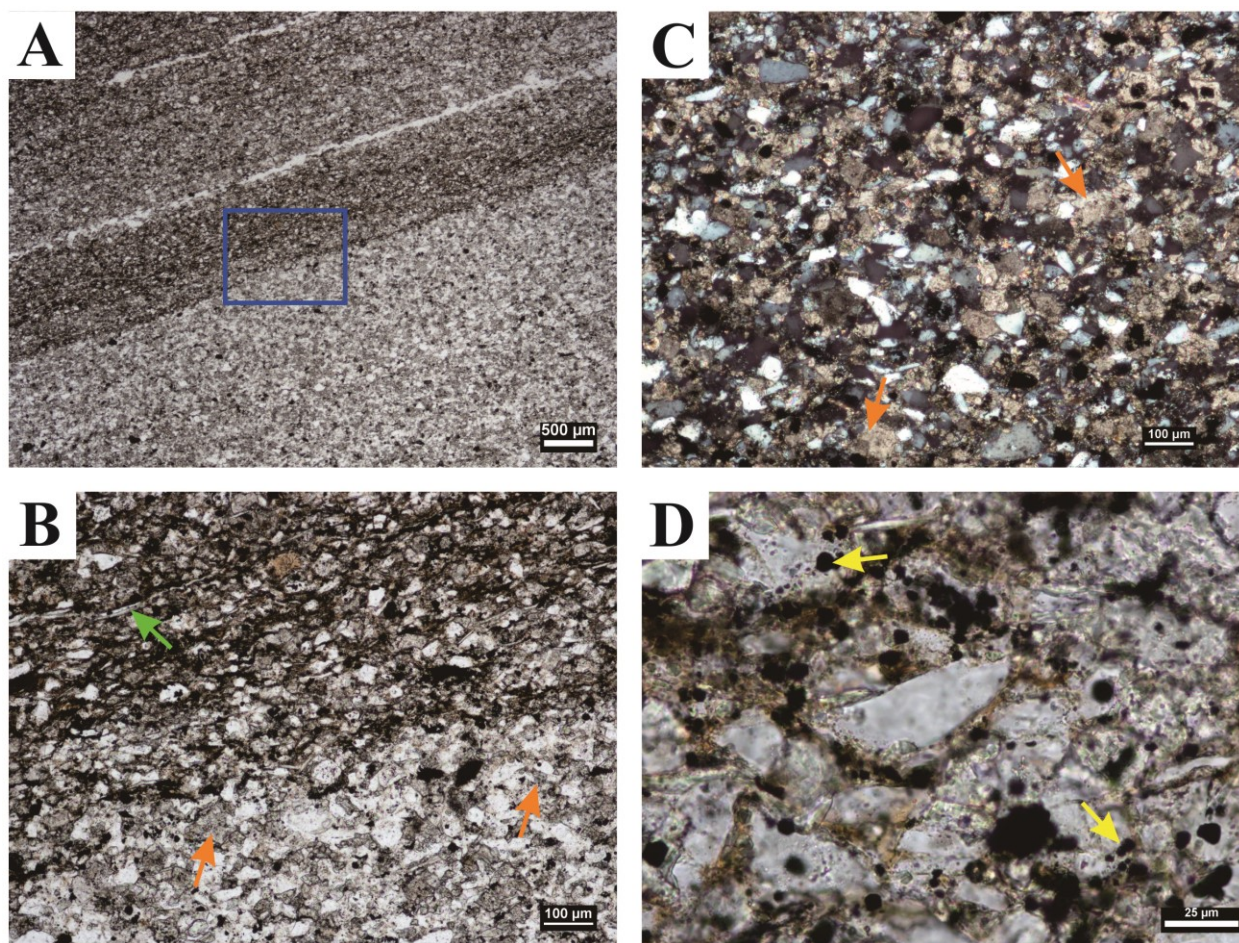
Figure 2.14-Thin section photomicrographs of lithofacies 2. **A**. Typical expression of interlaminated medium- to coarse-grained siltstone and bituminous very fine- to medium-grained siltstone. PPL image; 16-14-73-26W5M; 1572.77 m. **B**. Magnified view of A (blue box). Interlaminated medium- to coarse-grained siltstone and bituminous very fine- to medium-grained siltstone. Finer siltstone contains abundant bitumen, muscovite (green arrow) and pyrite. Clean coarser siltstone contains abundant detrital and authigenic dolomites and ferroan dolomites (orange arrows). PPL image; 16-14-73-26W5M; 1572.77 m. **C**. Medium- to coarse-grained siltstone with abundant dolomites and ferroan dolomites present as both euhedral rhombic crystals (orange arrows) and micro- to cryptocrystalline clusters; XPL image; 16-14-73-26W5M; 1572.77 m. **D**. Very fine- to medium-grained siltstone with abundant brown bitumen and pyrite (yellow arrows) occurring as detrital grain coatings or clusters. PPL image; 16-14-73-26W5M; 1572.77 m.

Lithofacies 2

Lithofacies 2 (L-2; Figs. 2.13 and 2.14) consists of interbedded dolomitic medium- to coarse-grained siltstone and texturally immature, bituminous very fine- to medium-grained siltstone. Thicker medium- to coarse-grained siltstone beds are moderately sorted and contain a range of grain sizes from 0.014 to 0.059 mm (0.036 mm on average). Abundant dolomite and ferroan dolomite cements and small amounts of clay and pyrite are present within the medium- to coarse-grained siltstone beds. The grain size of the thinner very fine- to medium-grained siltstone ranges from 0.004 to 0.027 mm, with an average grain size of 0.017 mm. Similar to L-1, these beds contain relatively higher amount of clay minerals (kaolinite and illite), muscovite and pyrite.

Porosity values of lithofacies 2 range from 5.8% to 15.2% with an average of 11.4% with over 70% of samples falling between 10% and 14.5% (Fig. 2.10d). Permeability values range from 0.04 to 2.75 mD (0.35 mD on average). Whereas over 60% of the measured values are less than 0.30 mD, values greater than 1.00 mD account for over 6% (Fig. 2.10e). Like L-1, L-2 displays a positive correlation between porosity and permeability (Figs. 2.19 and 2.20). Pore-throat radii within L-2 range from 0.11 to 0.94 μm with an average of 0.31 μm. As such, L-2 includes both micropores and mesopores, with mesopores accounting for 15.1% of the sample size (Fig. 2.10f). Interconnectivity of porosity is observed in greater abundance within L-2 however reservoir quality is restricted as a result of clay and dolomite. In contrast to L-1, clay content consists predominantly of kaolinite booklets with decreased amounts of illite present as pore-lining elements. In addition to clays, pyrite framboids and muscovite flakes within the silty mudstone decrease reservoir quality by reducing pore throats. The porosity and permeability of the siltstone is also significantly reduced by abundant dolomite and ferroan dolomite cementation.

Compared with L-1, there is a marked increase in porosity and permeability as a result of an increase in grain size and greater interconnectivity of pores. The compaction of L-2 is subdued in comparison to L-1, owing to the moderate sorting of the siltstone beds. Moderate sorting permits fair reservoir conditions although the inhibiting factors present in L-2 (and L-1) restrict the overall reservoir quality.
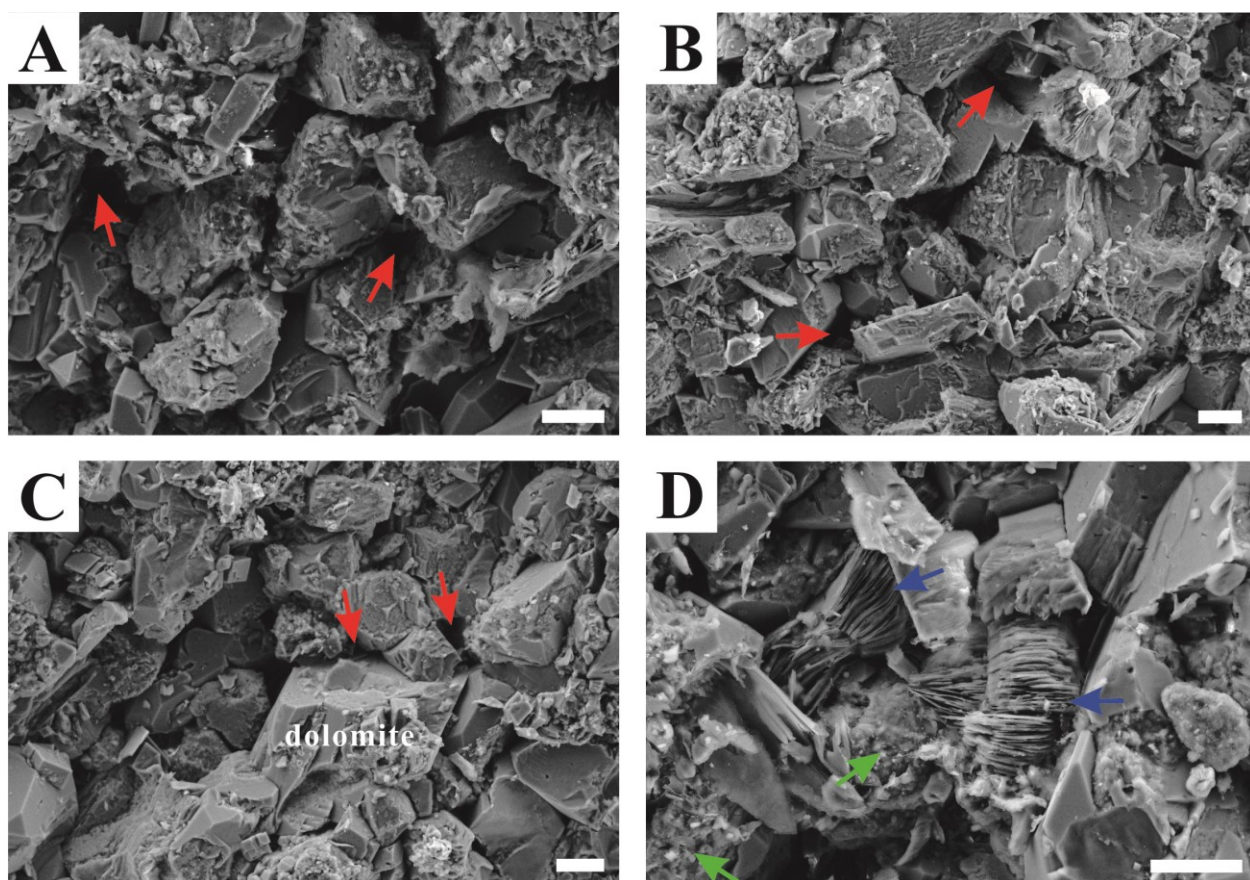
Figure 2.15-SEM images of lithofacies 3. **A**, **B**. Interconnected pores throats (red arrows) with very few clay minerals. Scale bar is 20 μm. **C**. Dolomite grains and abundant pore throats (red arrows). Scale bar is 20 μm. **D**. Abundant clay minerals including kaolinite booklets (blue arrows) and fibrous illite (green arrows). Intergranular micropores associated with kaolinite and illite are also present. Scale bar is 20 μm.
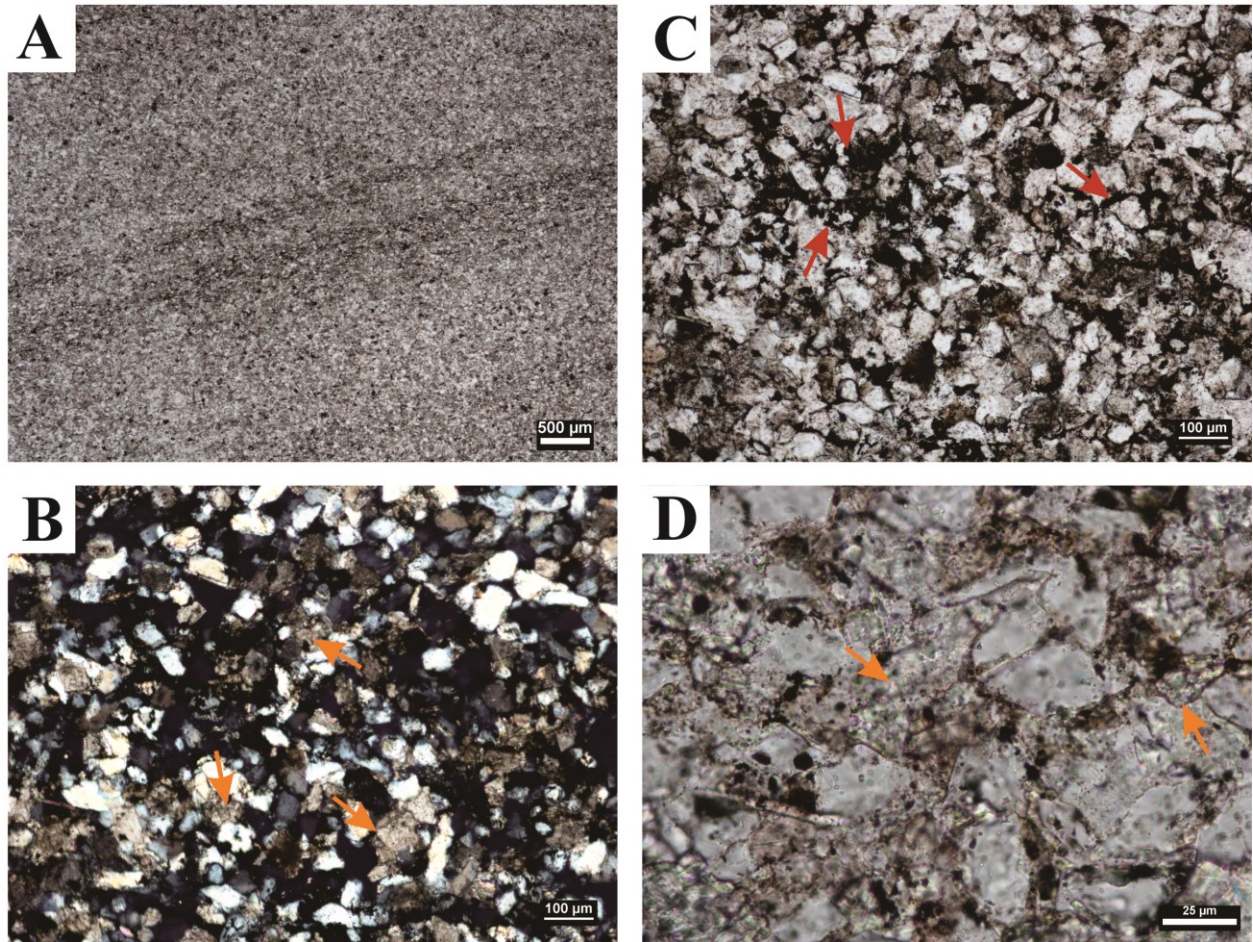
Figure 2.16-Thin section photomicrographs of lithofacies 3. **A.** Medium- to coarse-grained siltstone with very few very fine- to medium-grained laminae. PPL image; 14-33-73-26W5M; 1440.55 m. **B.** Medium- to coarse-grained siltstone with abundant dolomite and ferroan dolomite present mainly as euhedral rhombic crystals (orange arrows). XPL image; 16-14-73-26W5M; 1561.23 m. **C.** Bitumen-stained (brown arrows) medium- to coarse-grained siltstone. PPL image; 16-14-73-26W5M; 1561.23 m. **D.** Clean medium- to coarse-grained siltstone with abundant dolomite (orange arrows) and few bitumen and pyrite. PPL image; 14-33-73-26W5M; 1440.55 m.

Lithofacies 3

Lithofacies 3 (L-3; Figs. 2.15 and 2.16) mainly consists of well-sorted, texturally mature, bitumen-stained, dolomitic medium- to coarse-grained siltstone, with few bituminous very fine- to medium-grained siltstone. Grain sizes range from 0.019 to 0.065 mm, averaging 0.045 mm. L-3

displays a marked decrease in clay content and other pore reducing elements, with only small amounts of kaolinite, illite, muscovite and pyrite observed. However, dolomite and ferroan dolomite occur sporadically as both cement and detrital grains.

Porosity of L-3 ranges from 11.3% to 20.6% with an average of 16.1%. More than 85% of samples have porosity of larger than 14%, and over 75% of porosity values are between 14% and 18.5% (Fig. 2.10g). Permeability of lithofacies 3 ranges from 0.23 to 28.70 mD (4.04 mD on average). Almost 90% of samples have permeability of larger than 1.00 mD and approximately 9% of the permeability values are over 10.00 mD (Fig. 2.10h). Pore-throat radii range from 0.20 to 3.01 μm, comprising micropores (17%), mesopores (75%) and macropores (8%) (Fig. 2.10i). Siltstone beds are well sorted within L-3. As a result, the interconnectivity of pores is high and the effects of compaction significantly reduced, giving rise to the higher permeability values of L-3. Reservoir damage is restricted to locally abundant clay and sporadic dolomite and ferroan dolomite cementation. As such, L-3 is considered to have a good reservoir potential.
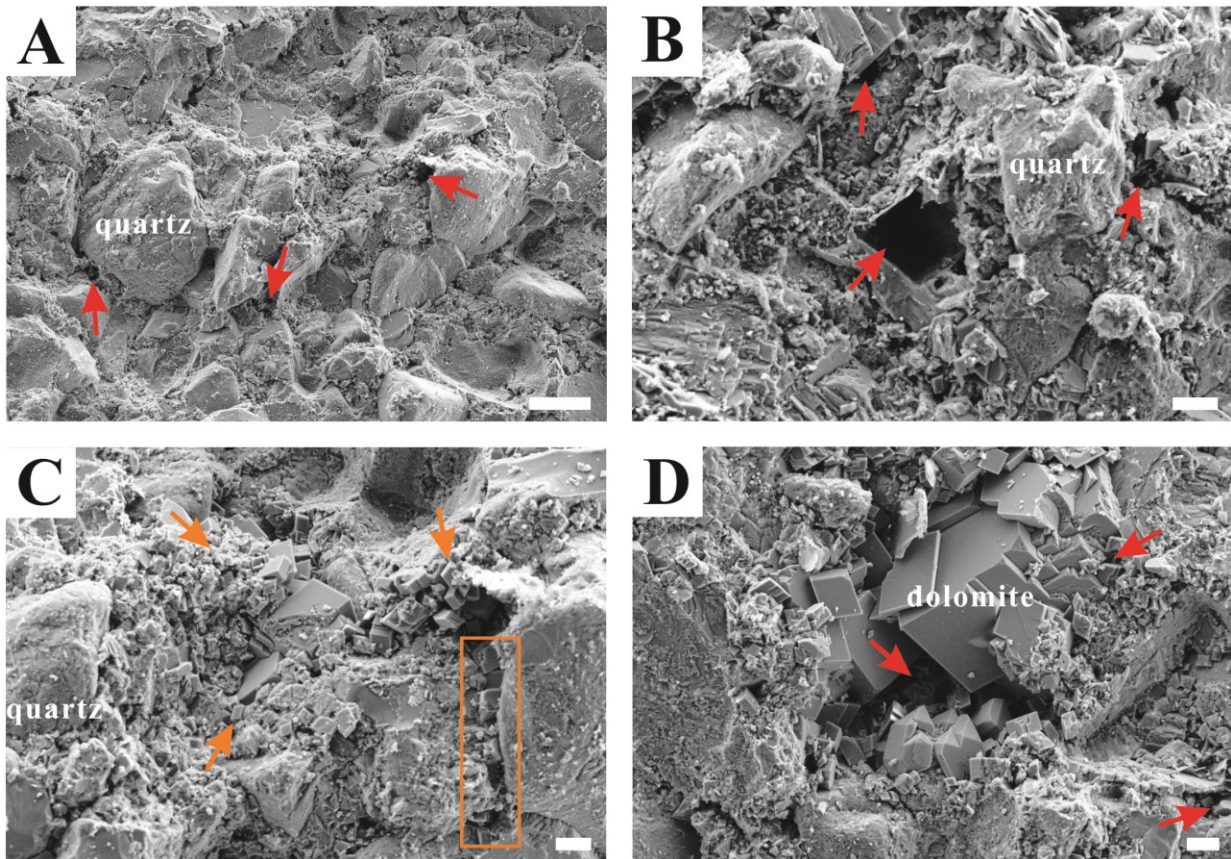
Figure 2.17-SEM images of lithofacies 4. **A**, **B**. Isolated pore throats (red arrows) with very few clay minerals. Scale bar is 100 μm. **C**. Abundant rhombohedral dolomite cement (orange arrows). Intercrystalline pore throat is filled by dolomite rhombs (orange box). Scale bar is 20 μm. **D**. Intercrystalline pores (red arrows) between abundant dolomite rhombs. Scale bar is 20 μm.
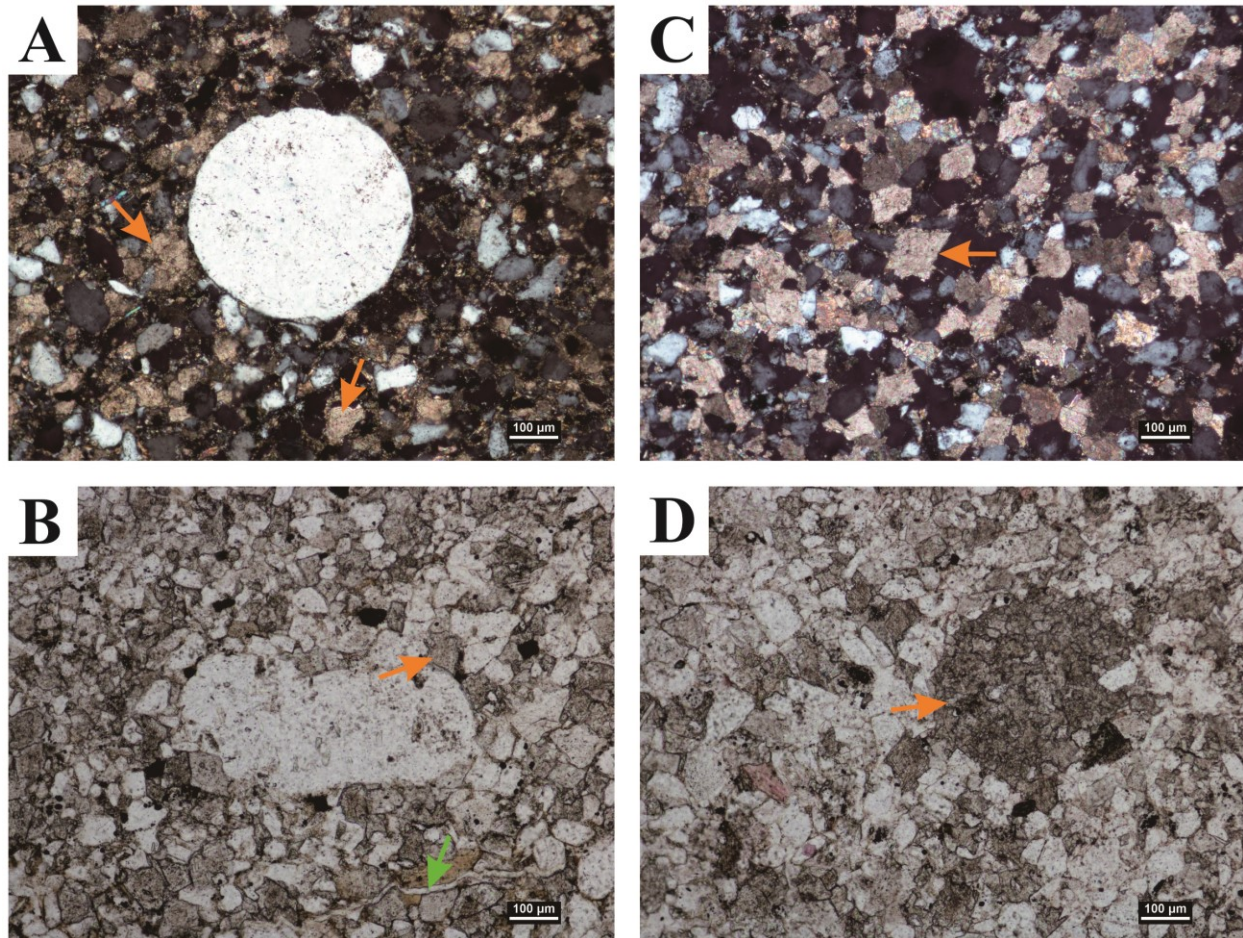
Figure 2.18-Thin section photomicrographs of lithofacies 4. **A**. Abundant detrital and authigenic dolomites and ferroan dolomites (orange arrows) with calcisphere. XPL image; 16-14-73-26W5M; 1552.52 m. **B**. Tightly arranged grains with abundant dolomite (orange arrow) and a deformed muscovite flake (green arrow) indicative of strong compaction. PPL image; 16-14-73-26W5M; 1552.52 m. **C**. Very fine-grained sandstone with abundant euhedral dolomite and ferroan dolomite (orange arrow). Concavo-convex contact recording strong compaction. XPL image; 16-14-73-26W5M; 1552.52 m. **D**. Cluster composed of micro- to cryptocrystalline dolomite and ferroan dolomite (orange arrow). PPL image; 16-14-73-26W5M; 1552.52 m.

Lithofacies 4

Lithofacies 4 (L-4; Figs. 2.17 and 2.18) is composed of moderately sorted, dolomitic coarse-grained siltstone to very fine-grained sandstone. Grain sizes range from 0.033 to 0.073 mm with an average of 0.055 mm. L-4 has a characteristically high abundance of dolomite and ferroan dolomite cements and detrital grains. Reservoir characteristics cannot be confidently determined due to the restricted occurrence of L-4, however limited data show that the porosity and permeability have average values of 6.0% and 0.06 mD, respectively. In addition, pore-throat radii range from 0.17 to 0.25 μm (micropores). SEM images (Fig. 2.17) show that pores are isolated and rare. Significant compaction of L-4 is evidenced by the tight arrangement of grains and deformation of muscovite flakes. The reservoir quality of L-4 is considered very low due to the effects of compaction as well as pervasive cementation.

DISCUSSION

Relationship Between Bioturbation and Reservoir Qualities

In general, the porosity and permeability of the reservoir rocks are always influenced by the presence of bioturbation. This can lead to either the enhancement or diminishment of the reservoir quality (Pemberton and Gingras, 2005; Gingras et al., 2009). However, the thin (cm scale) layers that are moderately to heavily bioturbated, mostly recorded in Lithofacies 1 and 2, exhibit porosity and permeability values which are very similar to the mean values of these two lithofacies. In other words, the impact of the bioturbation on reservoir quality in Lithofacies 1 and 2 is difficult to determine. This may be owing to the combined effects of the homogeneous distributions of grain size and cement. Moreover lithofacies 1 and 2 are predominantly well sorted siltstone, and so the bioturbation has little impact on the overall pore-throat distributions (Gingras et al., 2009). Similarly, the poor reservoir quality of Lithofacies 4, which is characterized by intense bioturbation, is primarily ascribed to the presence of abundant dolomite and ferroan dolomite cements. So, it is interpreted that the role of the bioturbation with respect to porosity, permeability

and reservoir qualities of the Montney Formation in the Puskwaskau Field are subordinate to the importance of the unimodal (i.e., well sorted) grain size distribution and cement.
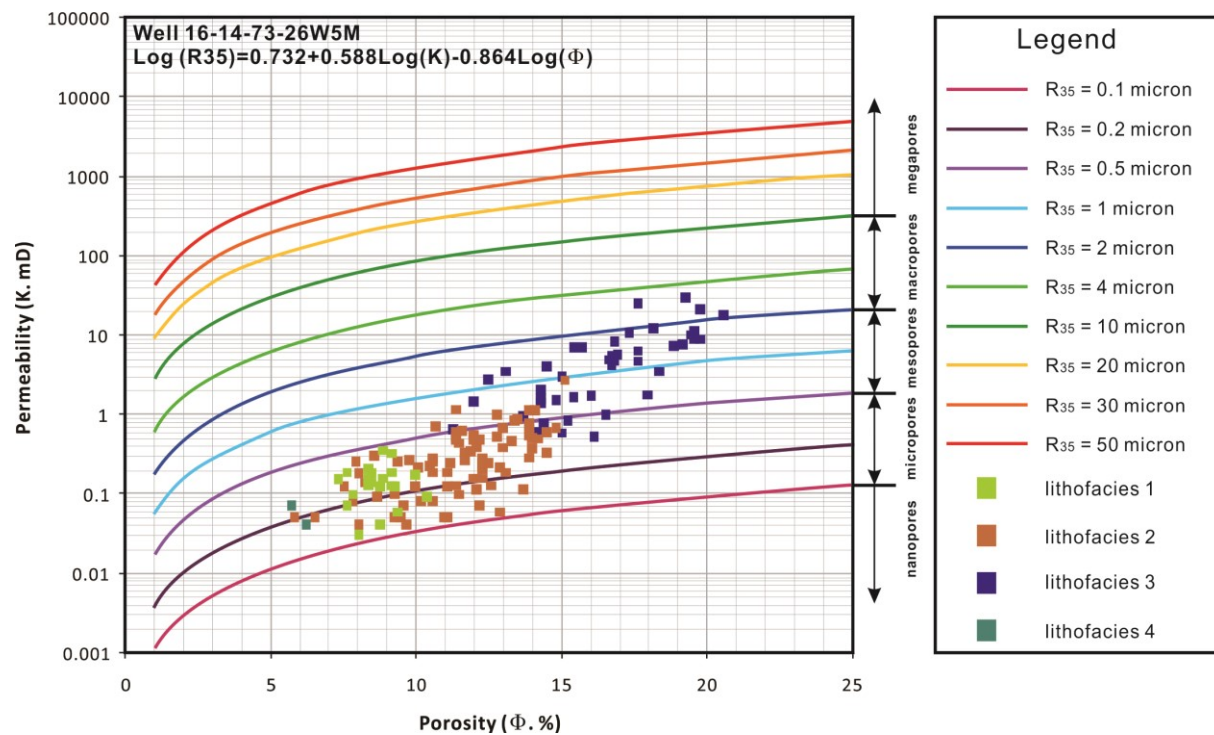
Figure 2.19-Winland porosity-permeability plot showing the correlation between porosity and permeability through the distribution of pore-throat radii for the different lithofacies of the Montney Formation within well 16-14-73-26W5M.
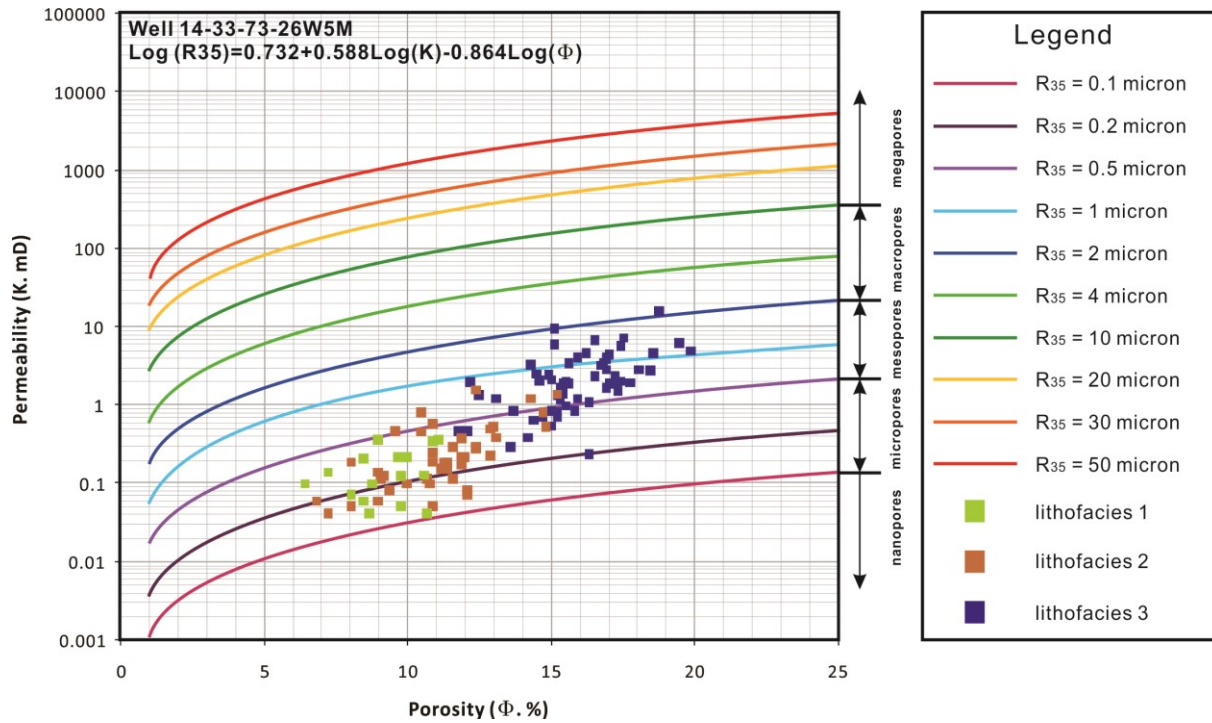
Figure 2.20-Winland porosity-permeability plot showing the correlation between porosity and permeability through the distribution of pore-throat radius for the different lithofacies of the Montney Formation within well 14-33-73-26W5M.

Lithofacies-Dependent Pore-Throat Size Distribution

For conventional reservoirs, Winland's equation is a practical way to estimate pore-throat radius (Pittman, 1992; Chatellier et al., 2018). Lithofacies-dependent pore-throat radius distributions of the two wells studied in the Puskwaskau Field are displayed in Winland porosity-permeability plots (Figs.2.19 and 2.20). In both wells, the lithofacies distributions and their pore-throat radius distributions are similar. Winland's equation can be reorganized as:

$$R_{35} = 10^{0.732} \frac{K^{0.588}}{\Phi^{0.864}}$$

The estimated R_{35} is proportional to permeability and inversely proportional to porosity. R_{35} interpolation lines representing different inferred pore-throat radii show that because the range of permeability values is greater than that of the porosity, permeability variation has a greater

influence on estimated pore-throat radius compared to porosity. In our dataset, L-3 (middle shoreface) has better flow-media characteristics than L-2 (lower shoreface), L-1 (offshore transition) and L-4 (upper shoreface / foreshore) respectively. This relationship of lithofacies to reservoir quality is an intuitive outcome of hydraulic sorting and winnowing proportional to sedimentary energies inherent in those sub environments, but it does evidence the validity of detailed facies analyses in the context of reservoir analyses. That is not to say that each lithofacies has entirely predictable reservoir character. For example, the pore-throat sizes and permeability of L-2 are generally more favorable than those of L-1, but L-1 and L-2 overlap substantially in permeability and porosity space, an observation that may in part be explained by gradational transitions within and between Facies Associations.

CONCLUSIONS

The Montney Formation in the Puskwaskau Field represents deposition on a wave- and storm-dominated siliciclastic ramp. It consists of multicyclic, coarsening upwards successions of bituminous very fine- to medium-grained siltstone, medium- to coarse-grained siltstone and very fine-grained sandstone. There are four lithofacies identified in the study area comprising a conformable shoaling-upwards sequence from offshore transition to upper shoreface/foreshore. In general, reservoir quality increases from L-1 to L-3 owing to an increase in grain size and sorting and decrease in the amount of clay, muscovite and pyrite. The reservoir quality of L-4 is significantly reduced by authigenic pore-filling dolomite cement. Dolomite and ferroan dolomite of both detrital and authigenic origin are ubiquitous in the study area and occur in various morphologies such as idiomorphic crystals, amorphous crystals and micro- to cryptocrystalline clusters. The dolomite is present dominantly within the cleaner, coarser laminae or beds, significantly reducing the porosity. Winland plots of these two study wells show that lithofacies are well correlated with pore-throat radii, porosity and permeability distributions, demonstrating that lithofacies can be used to reliably estimate pore-throat radii and reservoir properties.

CHAPTER 3: LITHOFACIES CHARACTERISTICS AND RESERVOIR PROPERTIES OF THE UPPER MONTNEY MEMBER (SPATHIAN) IN THE SHELL MONIAS FIELD, NORTHEASTERN BRITISH COLUMBIA

INTRODUCTION

The Lower Triassic Montney Formation covers an area of approximately 130,000 km^2, extending from northeast British Columbia to west-central Alberta (National Energy Board, 2013). It has become one of the most commercially viable unconventional prospects globally. The increase in development followed the advent of horizontal drilling and advancements in multistage horizontal fracturing techniques. It is projected that production of the Montney Formation will be responsible for most Canadian natural gas production growth over the next 20 years, increasing from 6.6 Bcf/d in 2020 to 13.6 Bcf/d in 2040 (Canada Energy Regulator, 2020).

The Montney Formation was deposited during the Induan and Olenekian stages of the Lower Triassic within the Western Canada Sedimentary Basin. Basin-scale unconformities and basinward correlative conformities divide the Montney Formation into three main sequences that correspond roughly to the Lower (Induan), Middle (Smithian substage of the Olenekian) and Upper (Spathian substage of the Olenekian) members (Moslow et al., 2018; Zonneveld and Moslow, 2018). Lithologically, the Montney Formation mainly consists of a westward-thickening succession of interbedded or interlaminated bioclastic packstone/grainstone, siliciclastic sandstone, and fine to coarse siltstone (Furlong et al., 2018; Wust et al., 2018; Zonneveld and Moslow, 2018).

The Montney Formation is interpreted to record a low-gradient, mixed siliciclastic-carbonate ramp succession deposited in an arid coastal setting, which is supported by the low proportion of clay minerals, pervasive, early diagenetic dolomite and locally concentrated anhydrite cements (Davies et al., 1997; Zonneveld et al., 2011; Moslow et al., 2016; Gegolick, 2017; Wust et al., 2018; Zonneveld and Moslow, 2018).

This study focuses on the Upper Montney Member (Spathian), which is characterized by interbedding of highly bituminous fine- to medium-grained siltstone and dolomitic, medium- to

coarse-grained siltstone (Golding et al., 2014; Zonneveld and Moslow, 2018). The Upper Montney Member is unconformably overlain by the Doig Phosphate Zone or the Sunset Prairie Formation (Golding et al., 2014, 2015; Crombez et al., 2016; Furlong et al., 2018; Zonneveld and Moslow, 2018). Throughout most areas of northeastern British Columbia, the Upper Montney Member sharply overlies the Middle Montney Member, which consists of bioclastic packstone and grainstone interbedded with bituminous dolomitic siltstone. The contact approximates the Smithian-Spathian (mid-Olenekian) boundary (Zonneveld and Moslow, 2018). The Upper Montney Member exhibits thinning towards the east and is largely absent in Alberta (Zonneveld and Moslow, 2018). For lithofacies division and interpretation, the ramp setting wherein the Upper Montney was deposited is divided in this study into upper and lower ramp. The upper ramp setting corresponds to the offshore transition, which lies above mean storm wave base and below mean fair-weather wave base (Reading and Collinson, 1996), and was subjected to occasional storm influences. The lower ramp is positioned below mean storm wave base and is dominated by deposition out of suspension. It bears noting that the lower ramp setting may be commonly interfered by turbidity currents associated with mass wasting. Thus, the lower ramp setting can be further subdivided into proximal lower ramp and distal lower ramp depending on the degree of impact by turbidity currents. Generally, proximal lower ramp setting is characterized by relatively abundant, thick turbidites, implying it is adjacent to the site of mass wasting and the turbidity currents are relatively frequent and strong. In contrast, the proportion of turbidites within the distal lower ramp is much lower, commonly occurred as thin beds, laminae, or even small lenses, representing that the deposition position is far away from the site of mass wasting and the activities of turbidity currents are rare and weak.

The primary objective of this paper is to identify characteristic facies associations of Upper Montney reservoir units in a northeastern British Columbia natural gas play and establish primary reservoir characteristics that are associated with the different lithological units. Although there are a number of detailed studies on the Upper Montney, they have primarily focused on sedimentological, ichnological and (or) stratigraphic aspects of the Member (e.g., Playter, 2013; Egbobawaye, 2016; Gegolich, 2017; Zonneveld and Moslow, 2018). In the context of those earlier works this paper assesses and summarizes reservoir properties of the Upper Montney Member in the Monias Field in a framework of detailed sedimentological analyses and discusses the main factors that determine the reservoir properties. In addition, the integration of mineralogical and

sedimentological data with total organic carbon (TOC) distributions provides insight into the origin of the bitumen pervasively present within the Upper Montney strata.

STUDY AREA AND METHODS

The aim of this paper is to provide a geological context for the composition and porosity distributions of an offshore Upper Montney (Spathian) succession. The core used (128.2m total length), is the Shell Monias 04-11-81-21W6, located in northeastern British Columbia, about 35 km southwest of Fort St. John (Fig. 3.1).

Lithofacies were divided on basis of lithology, primary physical sedimentary structures, fossil assemblages and trace fossil assemblages. In order to investigate grain size, mineralogy, diagenesis, proportion and origin of clay minerals, pore features of different lithofacies, high-resolution photographs of thin sections and scanning electron microscopy (SEM) were taken. Thin sections (20 microns in thickness) impregnated with blue epoxy were prepared by Wagner Petrographic in Lindon, Utah. Thin sections were also impregnated with alizarin red S and potassium ferricyanide to aid the identification of distinct carbonate minerals. The instrument Zeiss Sigma 300 VP-FESEM from the University of Alberta was used to aquire high-resolution SEM images from which the morphology of minerals, morphology and size of pores can be documented. According to the classification put forward by the International Union of Pure and Applied Chemistry (IUPAC), pores are subdivided into three categories based on the width of the pore: macropores (>50 nm), mesopores (2-50 nm) and micropores (<2 nm) (Rouquérol et al., 1994; Xu et al., 2018).

Twenty-six samples, taken from every 5 meters, were analyzed using X-ray-diffraction (XRD) to discern and quantify the mineralogical composition. Lab analyses were carried out by CBM Solutions in Calgary, Alberta. The samples were ground to homogenous particles (2 microns in size) with a micronizing mill. Using ethanol as the transfer medium, smear slides of the samples were prepared and dried. X-ray diffraction was carried out between 3 to 70° 2Theta via a Cu X-ray tube with a Siemens D500 Kristalloflex apparatus. The results were analyzed using the PDF-4 Minerals database 2009 and mineral identification was completed by reference to the International Center for Diffraction Data database. The mineral phases identified from XRD data were quantified using Jade 9 software on basis of Rietveld theory. It should be noted that the clay

content derived from XRD data represents the sum of muscovite and illite because they are similar in crystalline structure, although muscovite generally occurs in higher abundance.
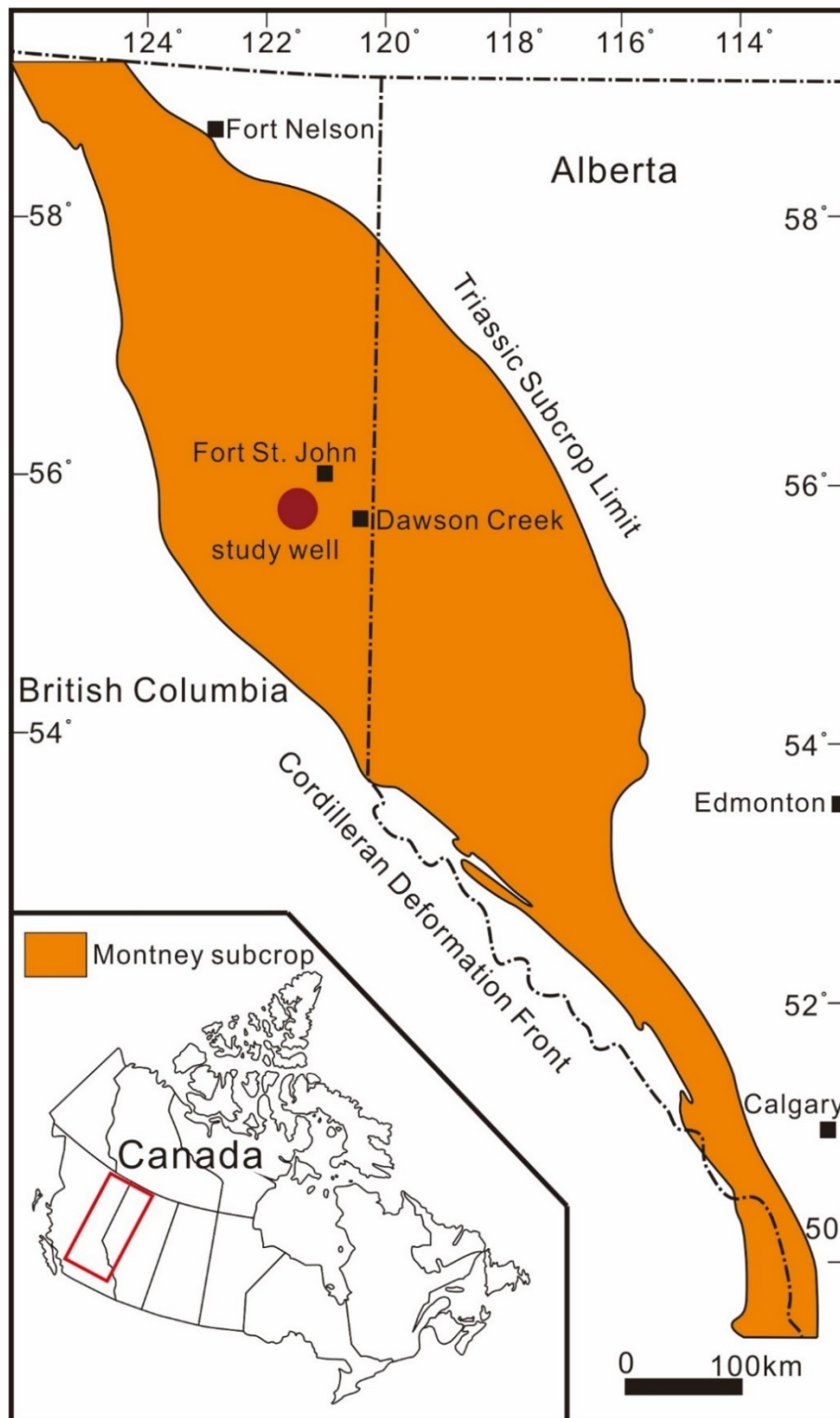
Figure 3.1-Overview map of the study area in western Canada showing the Montney Formation and the location of the study well (after Wood et al., 2018).

Twenty-six samples (different from the samples for XRD measurements) taken from approximately every 5 meters were prepared to assess porosity and permeability. Analyses were conducted at The Weatherford Laboratories Core Analysis Division in Houston, Texas. The grain volume of the core plugs was measured by helium injection and determined using Boyle's Law. The helium pore volume was then quantified for the designated net confining stress of ambient pressure. Hydrostatic pressure was applied via Frank Jones steady-state Porosimeter. Porosity was calculated using the following equation:

$$\emptyset = \frac{V_p}{V_g + V_p} \cdot 100\%$$

Where $\emptyset$ is porosity (%) and V_p and V_g represent pore volume (cm^3) and grain volume (cm^3) of a sample, respectively. On basis of the Darcy's Law, helium permeability of the core plugs was determined using a steady-state gas permeameter.

Total organic carbon (TOC) of this well was also evaluated because the overwhelming majority of siltstone successions in the Montney Formation are bituminous, and correlation between TOC and porosity or different mineral phases may be established to reveal the origin of the bitumen. Twenty-six samples taken from the same depths as those prepared for XRD analysis were ground into particles less than 0.25 mm. Next, 0.1g of ground sample was treated with concentrated hydrochloric acid to remove carbonates. Two hours later, the acid was removed using a filtration device with a glass microfiber filter. A LECO® crucible was used to dry the sample at 110° for one hour. The dried sample was then examined by the LECO® 600 Carbon Analyzer to obtain its TOC content (wt. %).

RESULTS

Table 1 presents the permeability, porosity and TOC between 2085.5 to 2210.5 m. A general negative correlation can be seen between porosity and TOC. Table 3.2 summarizes the observed

lithofacies characteristics as 3 lithofacies. Although the 3 lithofacies are similar in grain-size and lithology and their porosity and permeability distributions are similar, there are differences in TOC among the 3 lithofacies, with lithofacies 3 having the highest abundance. The lithofacies distributions are shown as Figure 3.2 as a detailed litholog. The key petrophysical logs (Gamma Ray, Resistivity, Neutron Porosity and Density logs) are presented as Figure 3.3.

Measured Reservoir Properties and Lithofacies Characteristics

Depth (m)	Permeability (mD)	Porosity (%)	TOC (%)
2085.5	8.71×10^{-6}	5.71	3.14
2090.5	9.97×10^{-6}	6.83	1.95
2094.9	3.49×10^{-6}	7.29	1.95
2100.0	1.23×10^{-6}	3.76	0.52
2104.9	5.46×10^{-6}	7.68	1.74
2109.9	1.43×10^{-5}	7.31	2.23
2115.4	2.58×10^{-5}	6.50	1.98
2119.8	4.46×10^{-5}	6.38	2.37
2124.8	1.86×10^{-6}	5.41	2.39
2130.4	1.86×10^{-6}	6.08	3.67
2134.8	2.75×10^{-6}	6.70	2.07
2140.5	3.82×10^{-6}	7.60	1.88
2144.9	1.50×10^{-6}	5.79	1.99
2150.6	2.88×10^{-6}	7.37	1.62
2155.0	1.02×10^{-6}	5.99	1.62
2159.9	1.45×10^{-6}	6.81	1.69
2164.9	6.86×10^{-7}	6.20	3.14
2169.9	4.03×10^{-6}	8.23	1.51
2174.9	1.35×10^{-6}	7.41	1.43
2180.4	2.52×10^{-6}	6.59	1.18
2185.0	4.14×10^{-7}	5.32	0.89
2190.0	1.55×10^{-6}	7.02	1.43
2195.5	8.33×10^{-6}	7.15	1.36
2200.5	9.04×10^{-6}	7.17	1.38
2204.9	1.53×10^{-5}	6.88	1.54
2210.5	3.89×10^{-6}	6.33	3.23

Table 3.1-Porosity, permeability and TOC of the Montney Formation within the Shell Monias 4-11-81-21W6.

FACIES	LITHOLOGY	PHYSICAL & BIOGENICSEDIMENTARY STRUCTURE	POROSITY (%)	PERMEABILITY (mD)	TOC (%)	DEP. ENVIRONMENT
L-1	Interlamination of wavy parallel to planar laminated medium- to coarse-grained siltstone and bituminous fine- to medium-grained siltstone	Wavy parallel lamination; planar lamination; low-angle planar lamination; scour and fill structure; load cast; dewatering structure; lenticular bedding; convolute bedding; soft sediment deformation; no trace fossils observed.	5.32 - 7.37 (6.61 on average)	4.14×10^{-7} to 1.53×10^{-5} (4.40×10^{-6} on average)	0.89 - 1.99 (1.47 on average)	upper ramp (offshore transition)
L-2	Interlamination of bituminous fine- to medium-grained siltstone and wavy parallel to lenticular bedded medium- to coarse-grained siltstone	Lenticular bedding; wavy parallel lamination; load cast; current ripples (some showing slight climbing feature); scour and fill structure; planar lamination; low angle cross-stratification; dewatering structure; convolute bedding.	3.76 - 7.68 (6.43 on average)	1.23×10^{-6} to 4.46×10^{-5} (1.42×10^{-5} on average)	0.52 - 3.14 (1.99 on average)	distal lower ramp (offshore, distal to the site of mass wasting)

| L-3 | Dolomitic, planar to low-angle cross-bedded, medium- to coarse-grained siltstone interbedded with bituminous, fine- to medium-grained siltstone | Planar bedding; low-angle cross bedding; load cast; ripple cross-lamination; wavy parallel bedding; soft sediment deformation. | 5.41 - 8.23 (6.75 on average) | 6.86×10^{-7} - 4.03×10^{-6} (2.53×10^{-6} on average) | 1.43 - 3.67 (2.42 on average) | proximal lower ramp (offshore, proximal to the site of mass wasting) |

Table 3.2-Summary of lithofacies characteristics, associated reservoir properties and TOC values of the Montney Formation within the Shell Monias 4-11-81-21W6.

▨ lithofacies 1	〰 wavy parallel lamination	◁ current ripples	⬭ carbonate concretion	⧚ *Phycosiphon*
▨ lithofacies 2	⧅ low angle cross stratification	▤ planar lamination	⋏ carbonate veins	⧙ *Teichichnus*
▨ lithofacies 3	▭ low angle cross beds or laminae	⬭ lenticular bedding	⋰ phosphate granules	⌐ *Planolites*
▨ bituminous fine- to medium-grained siltstone	⬚ soft sediment deformation	⏝ load casts	∂∂∂ shell debris	❘ *Skolithos*
▨ medium- to coarse-grained siltstone	℘℘ dewatering structure	⟋ scour and fill structure	Py pyrite	
▨ calcareous fine- to medium-grained siltstone	⌇ convolute bedding	➤ fault	⧛ *Zoophycos*	

54

Figure 3.2-Core description and lithofacies division of the Montney Formation within the Shell Monias 04-11-81-21W6 (2080.00-2211.50 m). Gamma ray curve is displayed at the left side of the strip log, with the scale ranging from 0 to 300 in API.
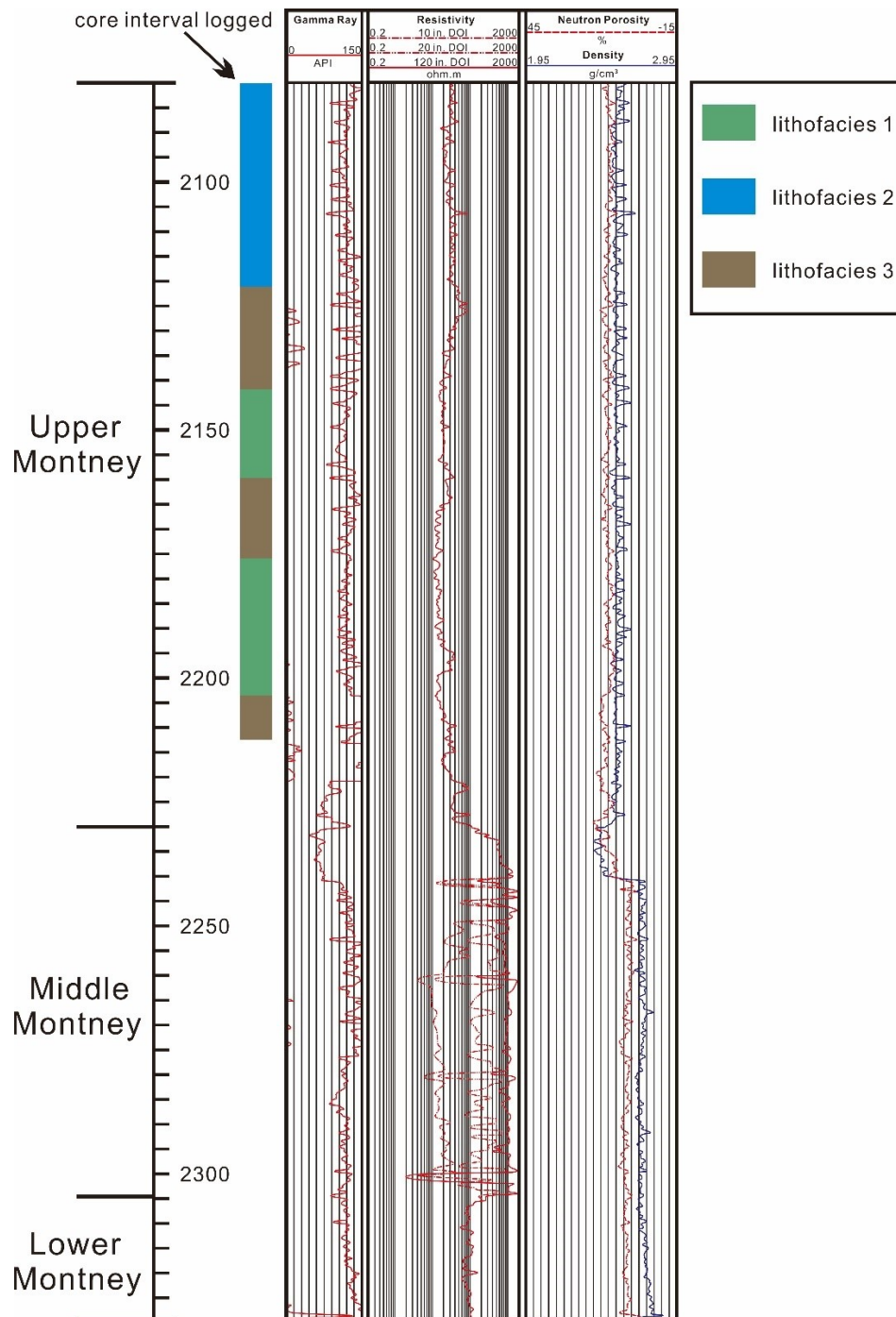
Figure 3.3-Gamma Ray, Resistivity, Neutron Porosity and Density logs and the core interval logged within the Shell Monias 04-11-81-21W6 (2080.00-2211.50 m).
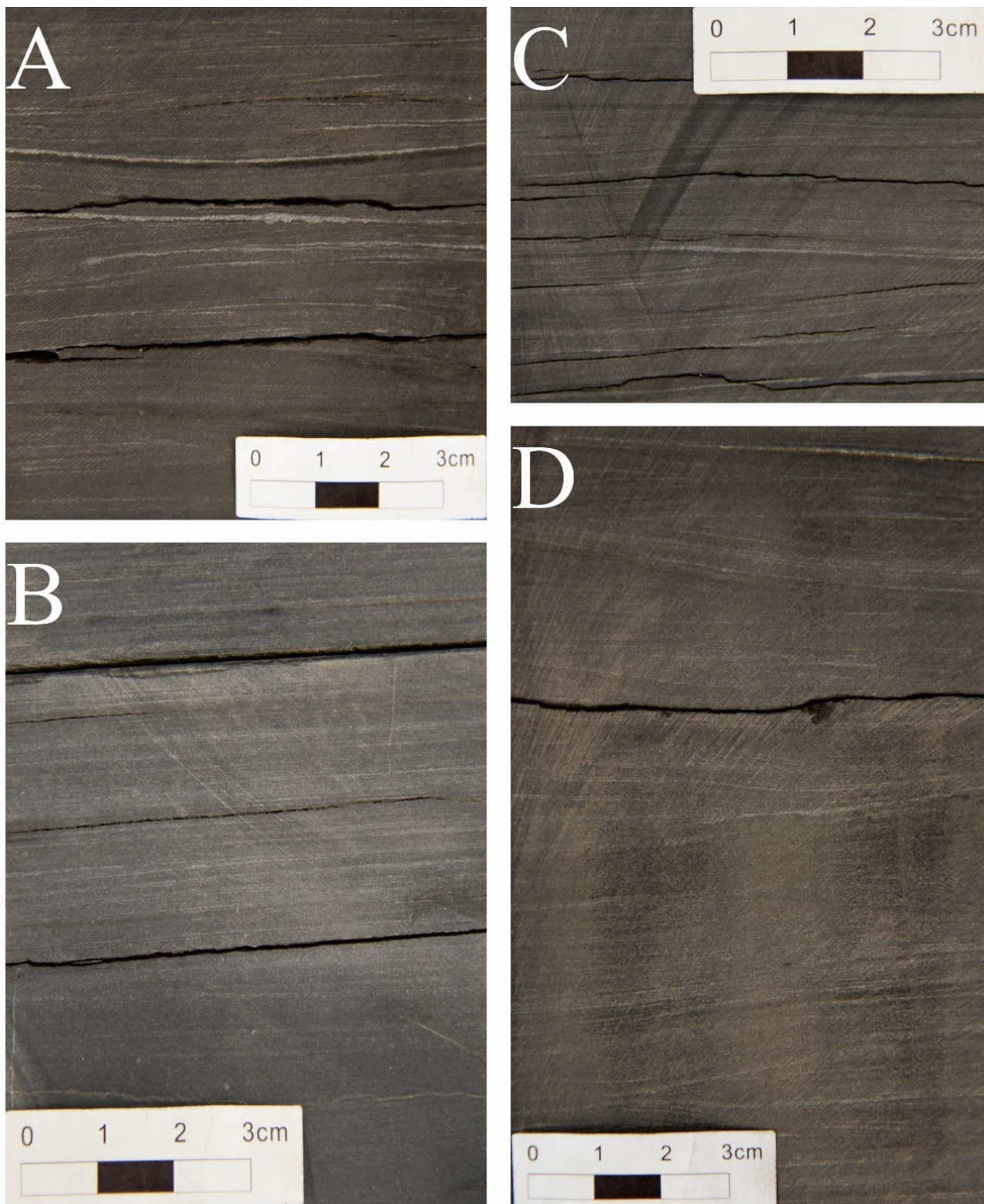
Figure 3.4-Core photographs of lithofacies 1 of the Montney Formation in well 04-11-081-21W6.
A. Wavy parallel lamination and convolute bedding. Note the sharp contact between medium- to

coarse-grained siltstone and bituminous, fine- to medium-grained siltstone. 2146.56 m. **B.** Low angle planar cross lamination (hummocky cross lamination). 2152.05 m. **C.** Sporadic thin, black mudstone truncating the underlying interlamination of fine- to medium-grained siltstone and silty mudstone. 2156.95 m. **D.** Truncation and wavy parallel lamination. 2186.83 m.

Lithofacies Descriptions and Interpretations

Three lithofacies were identified within the Montney Formation through the combination of well log and drill core analysis (Figs. 3.2, 3.3, Table 3.2).

Lithofacies 1

Description

Lithofacies 1 (Fig. 3.4) consists of interlaminated medium- to coarse-grained siltstone and bituminous, fine- to medium-grained siltstone. Finer siltstone laminae are usually dark grey to black whereas coarser siltstone laminae (ranging from 0.3 to 1.4 mm in thickness) are pale grey to white in color as a result of abundant dolomite and ferroan dolomite. Commonly, medium- to coarse-grained siltstone laminae sharply overlie bituminous, fine- to medium-grained siltstone laminae. The clay content of L-1 is notably low.

Primary sedimentary structures observed in L-1 include planar to wavy parallel lamination and low-angle planar laminae (Fig. 3.4). Few scours and fill structures are present, with some underlying layers truncated by thin (0.7 to 1.2 mm in thickness), black mudstone laminae (Fig. 3.4C). Soft-sediment deformation structures mainly include load-casts, dewatering structures, and convolute bedding. Few pyrite-rich horizons or nodules are present, but microcrystalline pyrite framboids identified from SEM photographs are quite prevalent (Fig. 3.4C). There are no biogenic sedimentary structures observed in L-1.

Interpretation

Lithofacies 1 is interpreted to represent deposition within an upper ramp setting, corresponding to the offshore transition (MacEachern and Pemberton, 1992; Reading and Richards, 1994; Prenoslo et al., 2018). Occasional low-angle planar laminated beds are interpreted as

hummocky cross stratification (Fig. 3.4B), indicating that L-1 was deposited above storm wave base and under the influence of intermittent storm-generated waves. Scour and fill structures provide evidence of discontinuous effects of storm waves. Medium- to coarse- grained siltstone lenses and laminae containing load casts are likely products of waning storm waves overlain by post-storm finer-grained siltstone units (Reineck and Wunderlich, 1968; Baas et al., 2015).

Thin, black mudstone laminae occasionally truncate the underlying layers, representing deposition by turbidity currents presumably associated with storm-generated waves (Myrow et al., 2002; Lamb et al., 2008; Stow and Smillie, 2020). The absence of trace fossils is in part the consequence of wave agitation from intermittent storms and periodic disruption by turbidity currents. Even so, anoxic/dysoxic conditions at the sea floor, as indicated by the numerous microcrystalline pyrite framboids, are interpreted to be the prime reason for the paucity of trace fossils (Berner et al., 1985).

Lithofacies 2

Description

Lithofacies 2 (Fig. 3.5) is composed of interlaminated bituminous, fine- to medium-grained siltstone and dolomitic, wavy-parallel to lenticular bedded, medium- to coarse-grained siltstone. Interlaminae are millimeter to centimeter scale whereas coarser siltstone laminae range from 0.4 to 8.5 mm in thickness. Fine- to medium-grained siltstone layers commonly have sharp upper contacts and locally exhibit scoured bases. Rare and subtle normal grading is observed (Fig. 3.10A and B). The medium- to coarse-grained siltstone lenses and laminae are highly cemented by calcite and dolomite, resulting in the distinctive color contrast between pale grey coarser siltstone units and dark grey to black bituminous finer siltstone units.
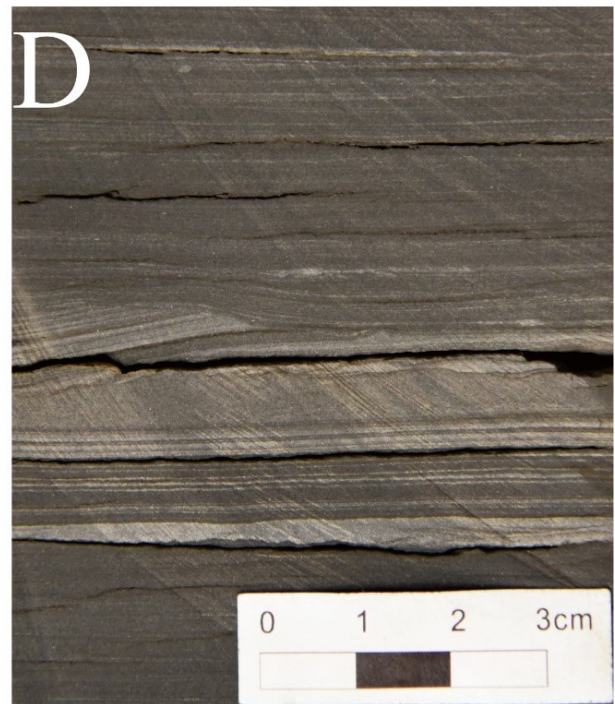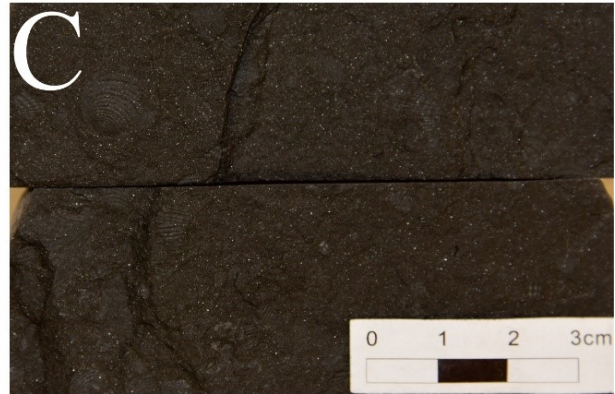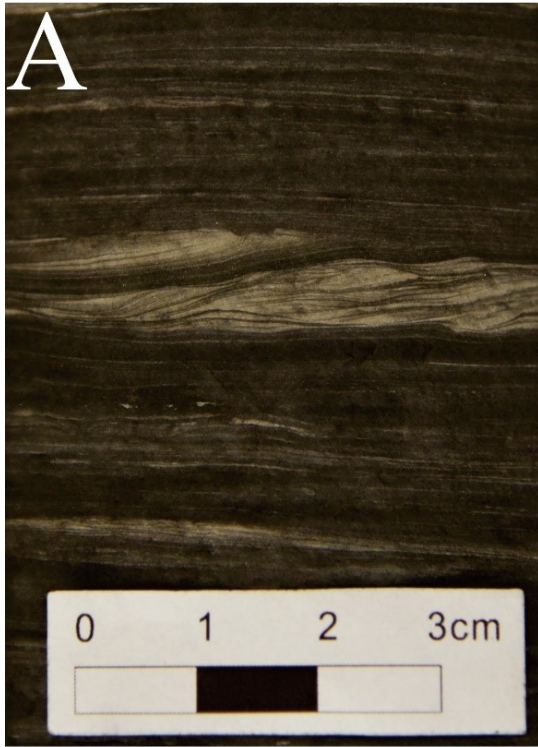
Figure 3.5-Core photographs of lithofacies 2 of the Montney Formation in the well 04-11-081-21W6. **A.** Dolomitic, medium- to coarse-grained lenses or laminae with current ripples showing slight climbing features. 2097.29 m. **B.** Dewatering structure within interlamination of bituminous, fine- to medium-grained siltstone and dolomitic, medium- to coarse-grained siltstone. 2092.11 m. **C.** *Claraia* sp. on the bedding plane. 2082.76 m. **D.** Low angle cross-stratification, current ripples and truncation. 2114.69 m. **E.** Lenticular bedding, soft sediment deformation and truncation caused by black, thin, bituminous fine- to medium-grained siltstone laminae. 2115.46 m.

This lithofacies is wavy-parallel laminated and lenticular bedded, with the coarser-grained lenses rarely exceeding 7.4 mm in thickness. Load casts are commonly observed not only on the bottom of coarser siltstone laminae but also on some of the thinner black mudstone laminae. Other penecontemporaneous deformation structures include dewatering structures and convolute bedding (Fig. 3.5B). Scour and fill structures are identified throughout L-2. Current ripples (some showing slight climbing) and low-angle cross-stratification are only associated with the coarser siltstone lenses (Fig. 3.5A and D). Occasionally, the coarser-grained beds show incomplete to complete pyritization. Scattered bivalve shells (*Claraia* sp.) are present along bedding planes, mainly occurring as disarticulated shell debris (Fig. 3.5C). There is no bioturbation present within L-2.

Interpretation

Lithofacies 2 is interpreted to represent alternating deposition of fine-grained turbidites and suspension deposition within the distal lower ramp setting (Stow and Shanmugam, 1980; Stow and Smillie, 2020). The presence of disarticulated shell fragments (*Claraia* sp.) imply that they were not found *in situ* and have most likely experienced high-energy transportation (Furlong et al., 2018). Their deposition is here interpreted to be associated with low-density turbidity currents. Abundant medium- to coarse-grained siltstone lenses and laminae are also products of low-density turbidity currents. Current ripples showing slight climbing imply that the coarser siltstone was deposited by waning currents allowing sedimentation from traction and suspension (Stow, 1979; Stow and Shanmugam, 1980; Mulder and Alexander, 2001). Pervasive load casts and occasional dewatering structures and convolute bedding indicate rapid sedimentation of siltstone over hydroplastic layers (Van Loon and Wiggers, 1976; Prenoslo et al., 2018). Planar laminated fine-

to medium-grained siltstone is probably a record of suspension deposition. It is also noted that thin, black mudstone laminae displaying sharp bases (truncation and load casts) are common, which, similar to L-1, are interpreted as mud turbidites (Stow and Smillie, 2020). These mud turbidites are much more common in L-2 owing to the lowered influence of storm-generated erosion. The absence of trace fossils is attributed to frequent disruption by turbidity currents in addition to a lack of dissolved oxygen at the sea floor.

Lithofacies 3

Description

Lithofacies 3 (L-3) consists of dolomitic, planar to low-angle cross-bedded, medium- to coarse-grained siltstone interbedded with bituminous, fine- to medium-grained siltstone. White to pale grey, dolomitic medium- to coarse-grained siltstone beds range from 0.7 to 16.2 cm in thickness and have sharp upper and lower contacts with dark grey to black, bituminous fine- to medium-grained siltstone (Fig. 36A and C). Some thick dolomitic medium- to coarse-grained siltstone beds show locally subtle normal grading (Fig. 3.6A).

Fine- to medium-grained beds are planar laminated, whereas the coarser siltstone beds are commonly planar to low-angle cross-bedded. Lenticular bedding and wavy parallel lamination are observed locally (Fig. 3.6B). Secondary structures include abundant load casts and less common dewatering structures. Fully or partially pyritized beds are quite common, and coarser siltstone laminae often contain abundant disseminated pyrite (Fig. 3.6C and D). Dolomite-filled veins ranging from 0.3 to 1.1 mm wide and up to 16.4 cm in length cross-cut siltstone beds. Lithofacies 3 is devoid of bioturbation.
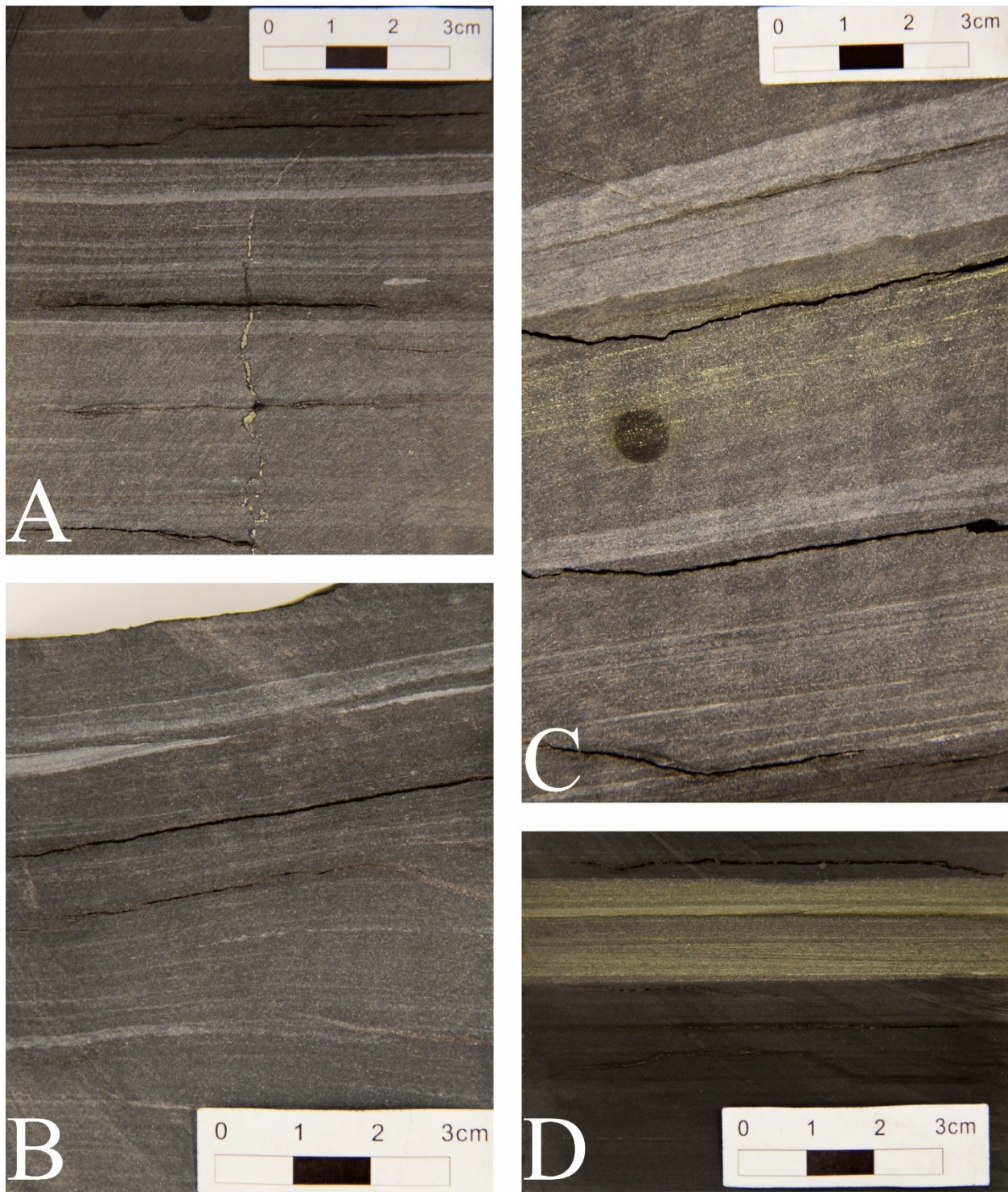
Figure 3.6-Core photographs of lithofacies 3 of the Montney Formation in the well 04-11-081-21W6. **A.** Interbedding of dolomitic, medium- to coarse-grained siltstone and bituminous, fine- to medium-grained siltstone, with coarser siltstone beds showing planar bedding and locally subtle

normal grading and finer siltstone beds exhibiting faint planar lamination. 2162.26 m. **B.** Wavy parallel lamination and medium- to coarse-grained siltstone lenses displaying ripple cross-lamination. 2141.55 m. **C.** Low angle planar cross bedding and locally abundant disseminated pyrites. 2141.68 m. **D.** Bituminous, faintly planar laminated, fine- to medium-grained siltstone beds interbedded with fully pyritized medium- to coarse-grained siltstone bed. 2122.84 m.

Interpretation

Lithofacies 3 represents alternating deposition of the fine-grained turbidites and suspension settling within the proximal lower ramp setting. This is supported by the lack of wave-generated sedimentary structures, suggesting L-3 was deposited below the mean storm wave base. The ripple cross-lamination, scoured beds, low-angle planar bedding, abundant load casts and locally subtle normal grading denote that the coarser siltstone beds were deposited by high-energy unidirectional currents which are interpreted as low-density turbidity currents. Occasional wavy-parallel lamination may have formed under upper-flow-regime conditions induced by low-density turbidity currents. In contrast to L-2, it is inferred that L-3 was deposited in an area proximal to the site of mass wasting on account of the significant increase in thickness of the coarser siltstone beds. The finer siltstone beds are probably the product of deposition from suspension. Anoxic/dysoxic conditions near the sediment-water interface is interpreted from the abundance of pyrite within L-3. As with L-1 and L-2, this, in addition to the environmental stresses associated with turbidity currents, explains the paucity of trace fossils.

Mineralogical Analyses by XRD

The mineralogical composition of the samples from the Shell Monias 4-11-81-21W6 is listed in Table 3.3. The Montney Formation is composed of quartz, feldspar, carbonate (calcite and dolomite), clay minerals (kaolinite, illite, muscovite), apatite and pyrite. Quartz contents mostly range between 33-47% with the exceptions of the samples that have high dolomite contents (i.e., 2090.25m, 2190.15 m) and thus the quartz content there is only 23-28%. The Montney samples have feldspar contents ranging between 10-25%. In terms of carbonates, the amount of dolomite (mostly 10-31%) is higher than that of calcite (5-12%). As a portion of illite detected in the XRD represents muscovite, clay minerals could be quantified include illite & muscovite, kaolinite. Illite

& muscovite are present in all samples and range from 5 to 10% while kaolinite is only detected in the deeper section (2135.15-2210.25 m), ranging between 4.4-9.2%. Apatite is either absent or present only in trace amounts throughout all samples. Few pyrites display a slight decreasing trend between 2080.25 m and 2210.25 m.

Depth (m)	Quartz	Feldspar	Calcite	Dolomite	Kaolinite	Illite & Muscovite	Apatite	Pyrite
2085.25	35.80	22.20	11.80	17.40	0.00	9.50	1.10	2.20
2090.25	28.10	14.80	11.60	37.20	0.00	5.40	1.50	1.90
2095.15	40.30	21.60	7.60	17.50	0.00	9.40	1.70	1.90
2100.15	37.80	24.90	7.00	18.80	0.00	8.00	1.70	1.70
2105.15	43.10	22.30	5.40	17.30	0.00	8.10	2.10	1.80
2110.15	39.60	25.50	5.40	17.60	0.00	8.70	1.20	2.00
2115.25	39.50	24.10	5.80	18.30	0.00	8.50	1.90	1.80
2120.15	43.70	24.80	5.40	13.70	0.00	9.00	1.60	1.80
2125.15	33.00	18.10	7.80	31.20	0.00	6.60	1.20	2.20
2130.15	33.60	23.30	6.60	22.10	0.00	9.00	2.30	3.10
2135.15	37.10	19.10	6.40	24.50	4.40	6.30	0.00	2.10
2140.25	39.90	20.70	5.40	17.30	5.50	8.70	0.70	1.80
2145.15	40.30	21.00	5.80	15.20	6.20	8.40	1.50	1.60
2150.30	40.90	17.60	9.10	16.90	6.50	7.60	0.00	1.50
2155.15	44.00	14.80	9.20	17.20	5.60	7.40	0.10	1.90
2160.15	41.10	18.90	9.40	13.70	6.10	8.40	0.60	1.80
2165.15	40.10	19.80	5.90	17.70	6.00	7.70	0.80	2.00
2170.15	33.50	14.80	5.40	31.40	5.90	6.90	0.80	1.40
2175.15	37.40	17.30	8.90	21.40	7.00	6.90	0.00	1.20
2180.25	44.60	16.70	10.20	15.80	6.10	5.40	0.00	1.10
2185.25	39.60	16.00	6.00	23.20	5.90	7.50	0.40	1.50
2190.15	23.00	10.30	4.90	50.90	4.80	5.10	0.00	1.10
2195.25	40.30	18.00	10.80	13.20	9.20	7.00	0.00	1.50
2200.25	41.70	20.70	7.90	16.60	6.30	5.10	0.00	1.70
2205.15	44.30	18.20	9.10	12.00	7.40	6.00	1.50	1.50
2210.25	47.40	16.40	7.20	9.40	7.40	10.10	0.40	1.80

Table 3.3-Mineralogy of the Montney Formation within the Shell Monias 4-11-81-21W6 by XRD.

Figure 7 shows the ternary context of 26 samples from the Shell Monias 4-11-81-21W6 core, showing the three endmembers (quartz, carbonate and clay) used to determine the lithology of 3 lithofacies. It is noticeable that three lithofacies have similar lithologies; all samples plot adjacent

to the quartz-carbonate line on the ternary diagram because of the very low abundance of clay present.
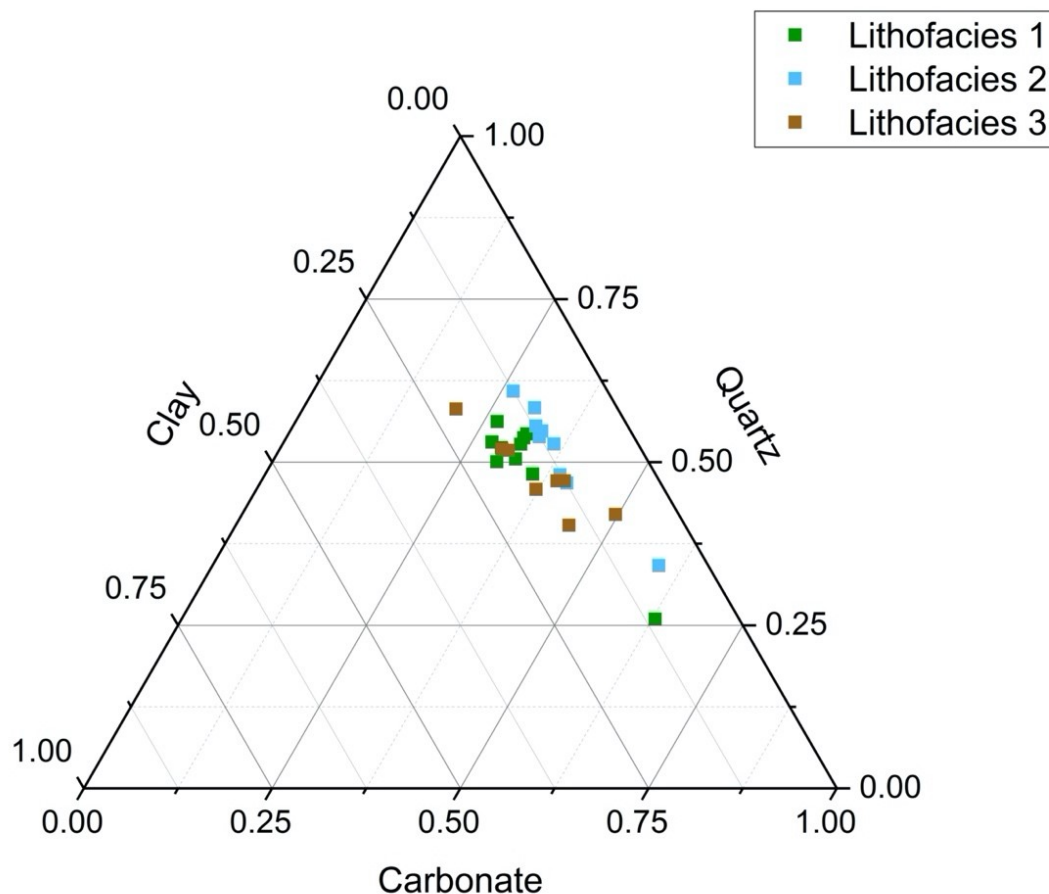
Figure 3.7-Ternary diagram of the samples from the Shell Monias 4-11-81-21W6 core showing the quartz, carbonate, and clay contents.

Scanning Electron Microscopy

Nine samples were viewed in SEM mainly for the investigation of pore types and their distribution. Overall, most pores observed are macropores and can be classified as intergranular, intragranular and intercrystalline pores on basis of their distribution/nature. In addition, mineralogical information, especially the characteristics of the dolomite, pyrite, halite and clay minerals and their effects on pore spaces, are also shown in SEM images.
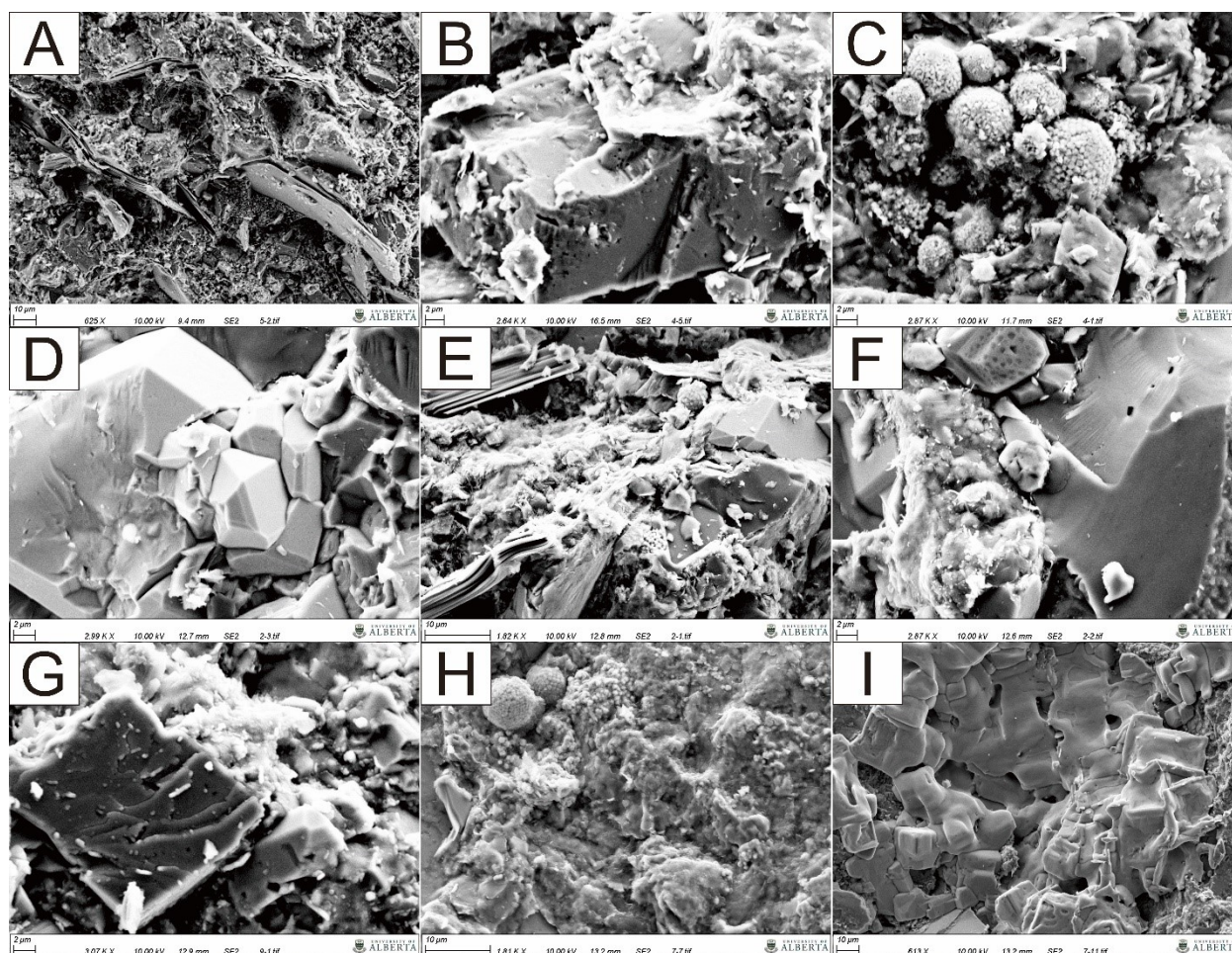
Figure 3.8-SEM images of Lithofacies 1, 2, and 3. **A.** Lithofacies 1; deformed muscovite flakes indicating compaction of relatively uncemented material. Narrow and elongated intercrystalline pores associated with muscovite flakes; 2156.54 m. **B.** Lithofacies 1; intragranular pores identified from a dolomite and irregular intercrystalline pores within illite coatings; 2186.83 m. **C.** Lithofacies 1; pore-filling, euhedral, rhombic authigenic dolomite. Microcrystalline pyrite framboids form in clusters as authigenic replacements, filling a significant portion of pore spaces. Intercrystalline pores are mostly present within clay coatings. There are some intergranular pores presenting along the boundaries of microcrystalline pyrite framboids and dolomite; 2186.83 m; **D.** Lithofacies 2; diagenetic overgrowths associated with quartz exhibit smooth, partially interlocking crystal boundaries/faces. Such overgrowth cementation contributes to the reduction of the total porosity. Intercrystalline pores occur along the boundaries of subhedral to euhedral quartz crystals; 2097.29 m. **E.** Lithofacies 2; illite coatings play a key role in decreasing the porosity through

bridging pores. Tiny euhedral, rhombic, authigenic dolomites are observed to fill the pore spaces associated with illite coatings. The replacements of scarce microcrystalline pyrite framboids lead to the occlusion of porosity. Few elongated to irregular intercrystalline pores are associated with muscovite flakes, microcrystalline pyrite framboids and illite coatings; 2097.29 m. **F.** Lithofacies 2; there are few fibrous, authigenic illites growing on the surface of illite coatings. Intragranular pores are identified from the quartz grains and intercrystalline pores are mostly associated with illite coatings; 2097.29 m. **G.** Lithofacies 3; dolomite and feldspar contribute to many intragranular pores and intercrystalline pores are identified within the illite coatings and along the boundary between dolomite and feldspar; 2162.26 m. **H.** Lithofacies 3; detrital grains and even authigenic microcrystalline pyrites are almost completely covered by illite coatings. Very small intercrystalline pores are still present within the dense illite coatings. Some pore spaces are blocked by microcrystalline pyrite framboids; 2211.55 m. **I.** Lithofacies 3; large, well-connected pores deprived from halite dissolution; 2211.55 m.

Thin Section Photomicrographs

Twenty-one thin sections were used to investigate the grain-size and microscopic features of the laminae (contacts, grading and mineralogical composition). With the assistance of staining, the abundance and distribution of dolomite, ferroan dolomite, calcite and ferroan calcite were also investigated: these are primarily concentrated in the coarser siltstone laminae and play a role as cement. Brown to black bitumen is pervasively present, filling the boundaries between grains especially in the finer siltstone units. Although impregnated with blue epoxy, there are no pores identified.
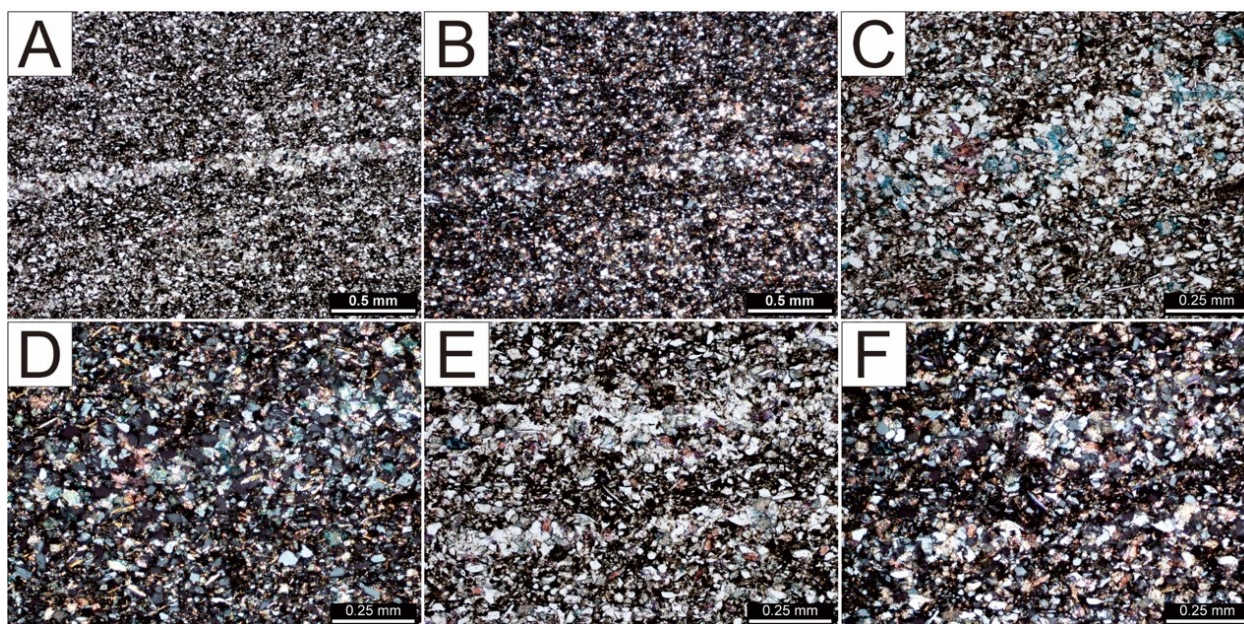
Figure 3.9-Thin section photomicrographs of Lithofacies 1. All thin section photomicrographs are present in PPL/XPL pairs. Photomicrographs A and B are taken under 5x magnification while C-F are under 10x magnification. Thin sections have been stained with Alizarin Red-S and Potassium Ferricyanide and impregnated with blue epoxy. **A-B.** Thin medium- to coarse-grained siltstone lamina displaying load casts within bituminous fine- to medium-grained siltstone units; 2195.89 m. **C-D.** Medium- to coarse-grained siltstone lamina contains more carbonates (calcite, ferroan calcite, dolomite and ferroan dolomite) and less muscovite flakes; 2146.62 m. **E-F.** Interlamination of medium- to coarse-grained siltstone laminae and bituminous fine- to medium-grained siltstone laminae, showing few disoriented muscovite flakes; 2195.89 m.
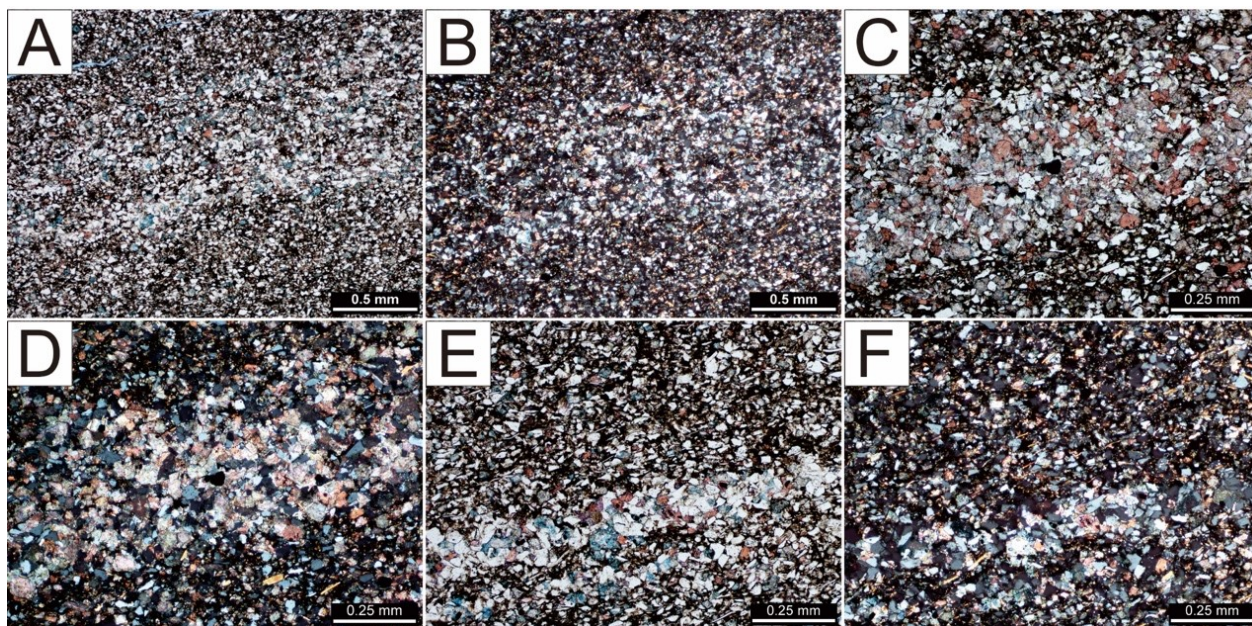
Figure 3.10-Thin section photomicrographs of Lithofacies 2. All thin section photomicrographs are present in PPL/XPL pairs. Photomicrographs A and B are taken under 5x magnification while C-F are under 10x magnification. Thin sections have been stained with Alizarin Red-S and Potassium Ferricyanide and impregnated with blue epoxy. **A-B.** Subtle normal grading is present within medium- to coarse-grained siltstone lamina; 2096.70 m. **C-D.** Intensive calcite and dolomite cementation throughout medium- to coarse-grained siltstone lens; 2088.17 m; **E-F.** Interlamination of medium- to coarse-grained siltstone laminae and bituminous fine- to medium-grained siltstone laminae, with coarser laminae showing abundant calcite, ferroan calcite, dolomite and ferroan dolomite; 2096.70 m.
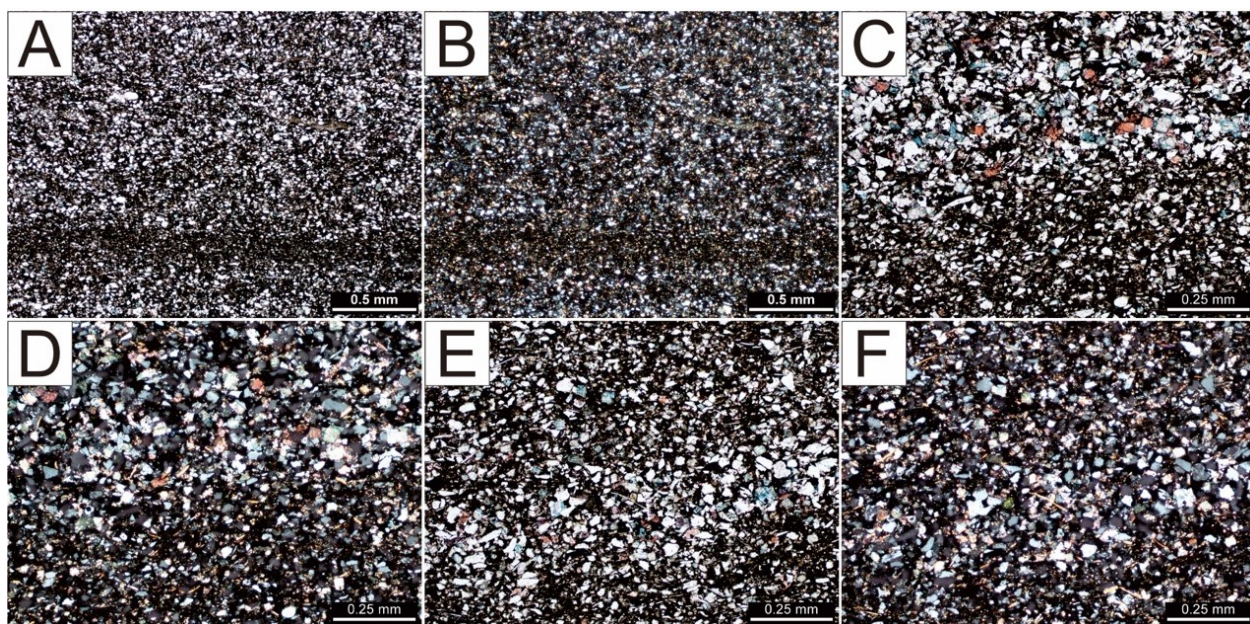
Figure 3.11-Thin section photomicrographs of Lithofacies 3. All thin section photomicrographs are present in PPL/XPL pairs. Photomicrographs A and B are taken under 5x magnification while C-F are under 10x magnification. Thin sections have been stained with Alizarin Red-S and Potassium Ferricyanide and impregnated with blue epoxy. **A-B.** Thin mudstone lamina within bituminous fine- to medium-grained siltstone units; 2133.14 m. **C-D.** Interlamination of medium- to coarse-grained siltstone laminae and bituminous fine- to medium-grained siltstone laminae, with coarser laminae showing more calcite, ferroan calcite, dolomite and ferroan dolomite; 2132.74 m. **E-F.** Medium- to coarse-grained siltstone laminae displaying load casts and features of normal grading; 2132.74 m.

Organic Matter

Four correlations associated with TOC were made. Clay, small mica minerals (illite and muscovite) and pyrite are positively correlated with TOC, with the Pearson correlation coefficient being 0.66 and 0.78, respectively (Figs. 3.12 and 3.14). Whereas, there is a negative correlation between the detrital grains (quartz and carbonate) and TOC (Pearson correlation coefficient r=-0.44) (Fig. 3.13). Porosity is also negatively correlated with TOC (Pearson correlation coefficient r=-0.58) (Fig. 3.15).
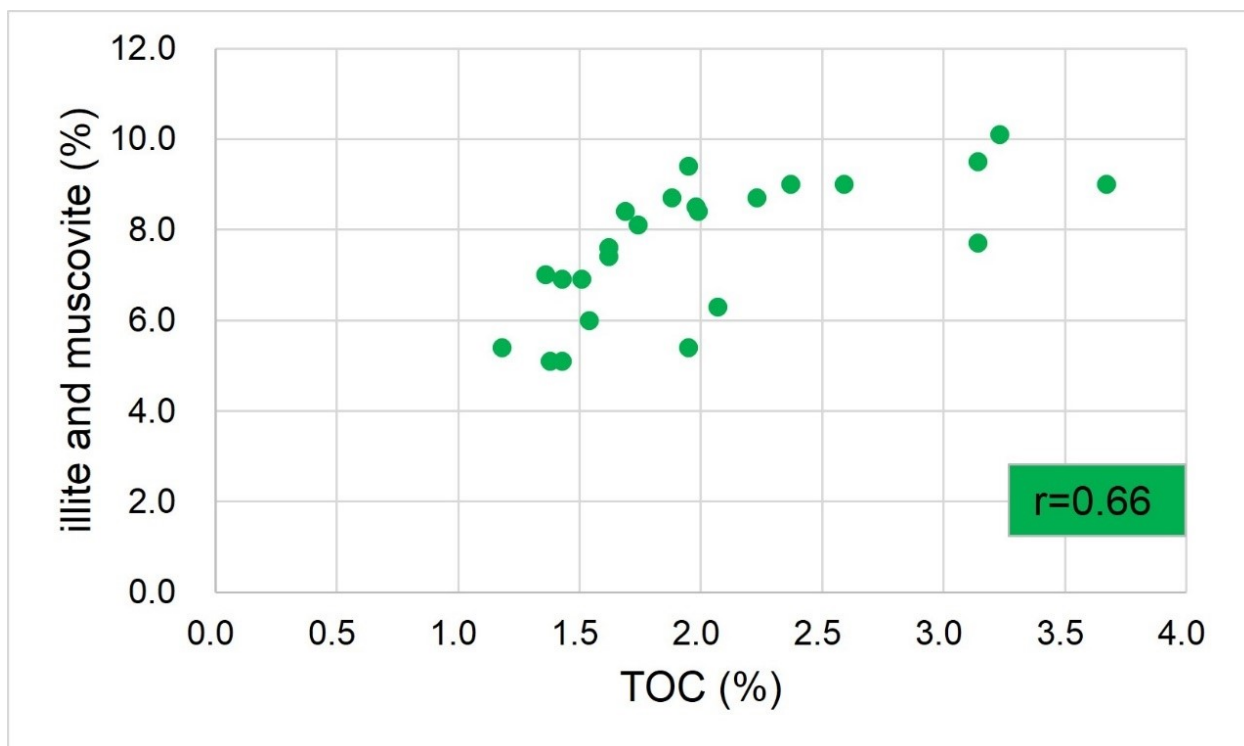
Figure 3.12-Illite, muscovite content versus TOC of the Shell Monias 4-11-81-21W6 (Pearson correlation coefficient r=0.66).
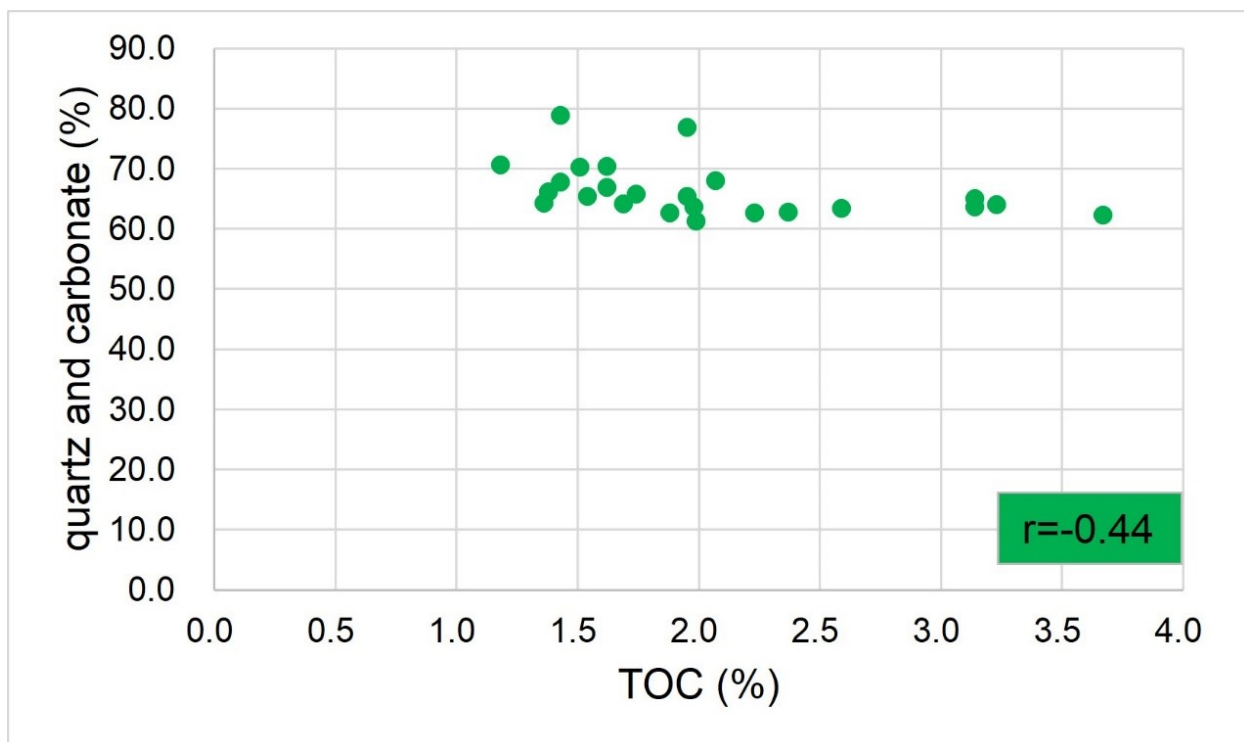
Figure 3.13-Main detrital minerals (quartz, carbonate content) versus TOC of the Shell Monias 4-11-81-21W6 (Pearson correlation coefficient r=-0.44).
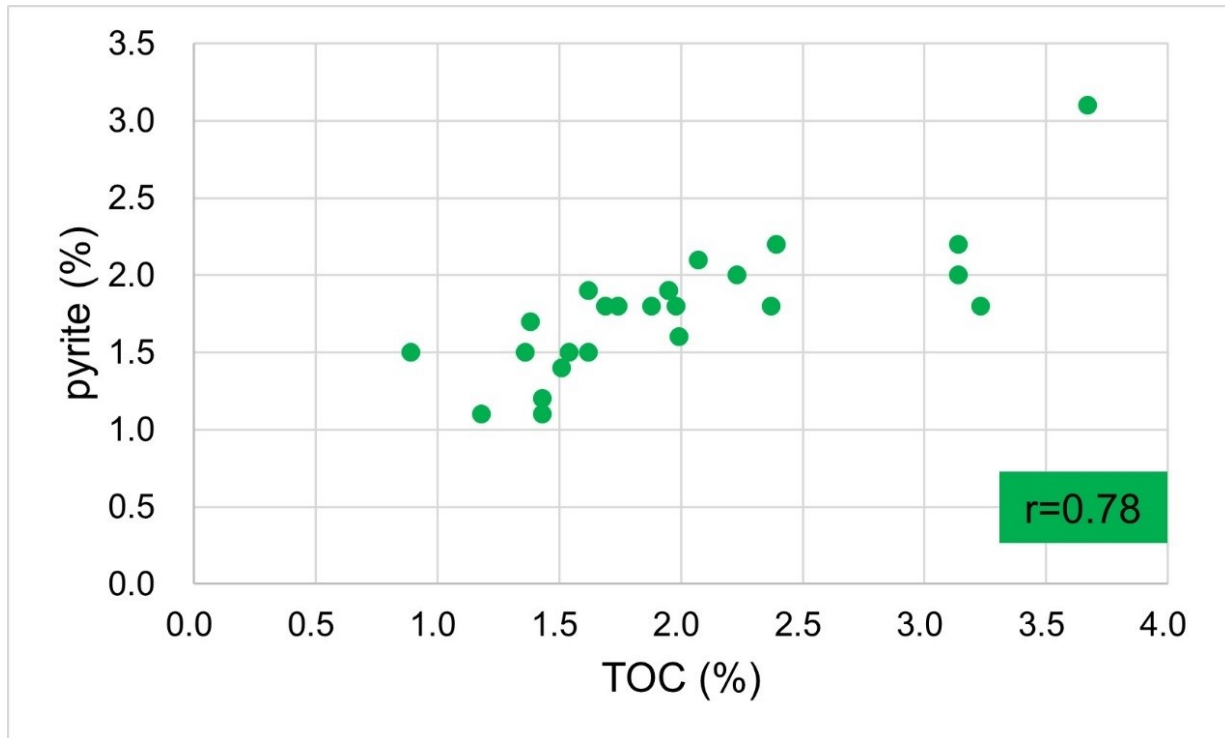
Figure 3.14-Pyrite content versus TOC of the Shell Monias 4-11-81-21W6 (Pearson correlation coefficient r=0.78).
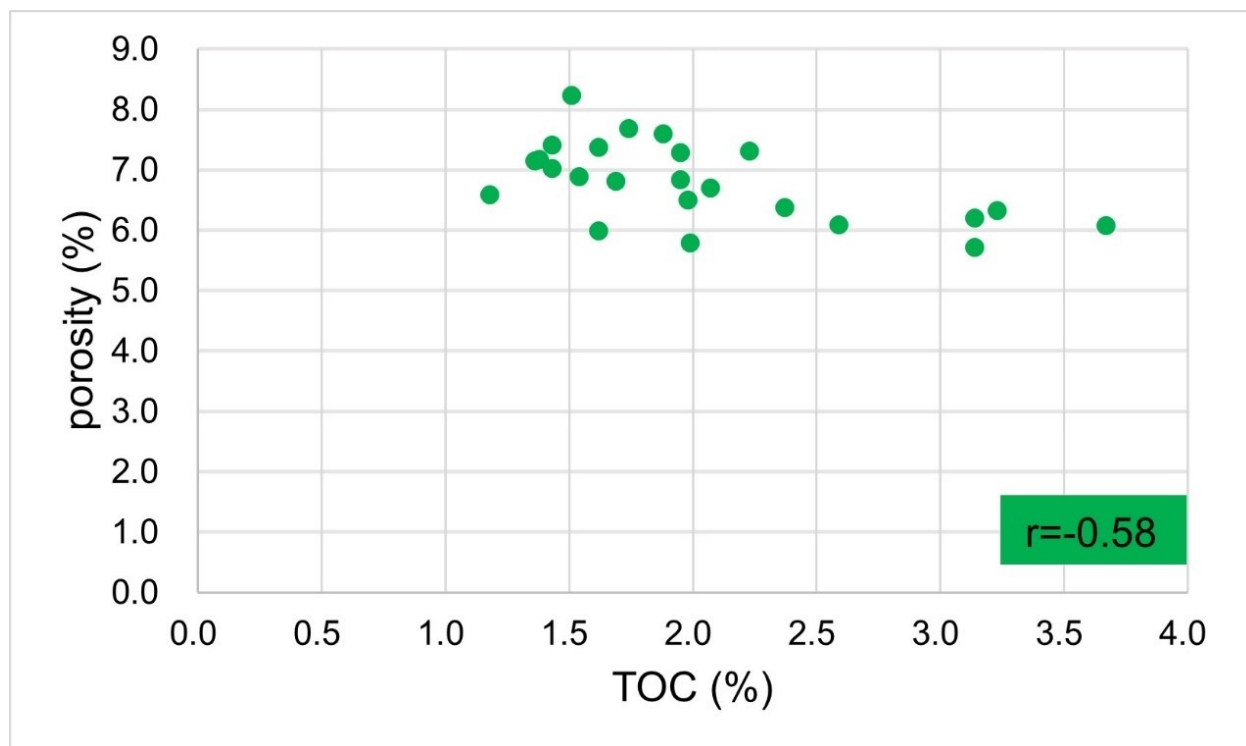
Figure 3.15-Porosity versus TOC of the Shell Monias 4-11-81-21W6 (Pearson correlation coefficient r=-0.58).

DISCUSSION

Sedimentary Processes and Environment

The Montney Formation within the Shell Monias area (UWI 4-11-81-21W6) represents siltstone deposition in a low-gradient, predominantly siliciclastic ramp setting, corresponding to offshore transition to offshore environments (Fig. 3.16). Deposition in the upper ramp (lithofacies 1) is characterized by tempestites and scarce, intercalated thin mudstone turbidites possibly influenced by storm waves (Myrow et al., 2002; Lamb et al., 2008; Stow and Smillie, 2020). It is similar as the Facies 2B to 2C (offshore to offshore transition environment) identified from the Upper Montney by Gegolick (2017). The presence of wavy parallel lamination and hummocky cross-stratification is indicative of elevated environmental energy associated with storm waves in L-1. However, the relatively low abundance of coarser siltstone beds implies that L-1 is distal from

the sediment source and below mean fair wave base. In the lower ramp (lithofacies 2 and 3), where there is minimal evidence of storm disturbance, low-density turbidity currents initiated by mass wasting played a key role in sediment transport and deposition in lithofacies 1. Sediments delivered to the gentle ramp were probably further transported and redistributed within the ramp mostly by the offshore-directed combined flows (storm waves, turbidity currents and geostrophic flows) (Myrow et al., 2002; Lamb et al., 2008). Below mean storm wave base, deposits became oversteepened and increasingly unstable as a result of continuous sediment accumulation, leading to mass wasting downslope (Mulder and Alexander, 2001). In contrast to submarine-fan systems characterized by channel, levee and lobe complexes fed by single point source, the ramp turbidity system herein mainly derived from mass transport processes lacks well-developed channel, levee and overbank elements. Delivery of clastic sediment to the Montney coastline has been interpreted to have occurred via a few large perennial fluvial systems and numerous, small to medium-scale ephemeral fluvial systems along an arid coast (Zonneveld and Moslow, 2014; 2018). Thus, sediment input from the proximal ramp to the distal ramp largely took place from linear sources (Nardin et al., 1979; Reading and Richard, 1994) derived from ephemeral fluvial input to the Montney coast. It is inferred that sheet-like deposits dominated by medium- to coarse-grained siltstone are extensively distributed within the ramp. The thickness varies, mainly depending on the volume of sediment supplies and the distance from the site of mass wasting. Gegolick (2017) identified and described similar facies (Facies 1A to 2A, distal to proximal offshore environment) from the Upper Montney, characterized by pinstripe laminated siltstone. Pinstripe laminae refer to a striped pattern composed of multiple thin, millimeter-scale laminae, which is equivalent to the interlamination of finer-grained siltstone and coarser-grained siltstone in this study. L-3 and F2A represent the most proximal facies, with deposition characterized by higher proportion of coarser siltstone units. In contrast, L-2, F1A, F1B and F1C represent the deposition distal to the sites of mass wasting, dominated by persistent but slow sedimentation from suspended sediment plume associated with low-density turbidity currents.

Fine-grained turbidites of the Upper Montney in this study are comparable with the silt-mud laminated turbidite model of Stow (Stow, 1979; Stow and Shanmugam, 1980; Stow and Smillie, 2020). The standard sequence of the Stow model is composed of nine sub-divisions (T_0-T_9) and exhibits an overall decrease in grain size and the thickness of silt laminae and laminasets upwards (Stow and Shanmugam, 1980). The thick, sharp-based, locally normal-graded, wavy-parallel

bedded or low-angle cross-bedded, coarser siltstone beds commonly shown in the lithofacies 3 are similar to the T_0, reflecting relatively high-energy depositional conditions in regions proximal to the mass wasting sites. The interlamination of finer and coarser siltstone units occasionally showing soft sediment deformation and ripple features in lithofacies 2 broadly corresponds to T_1-T_4, implying the lowered energy conditions within the distal settings.
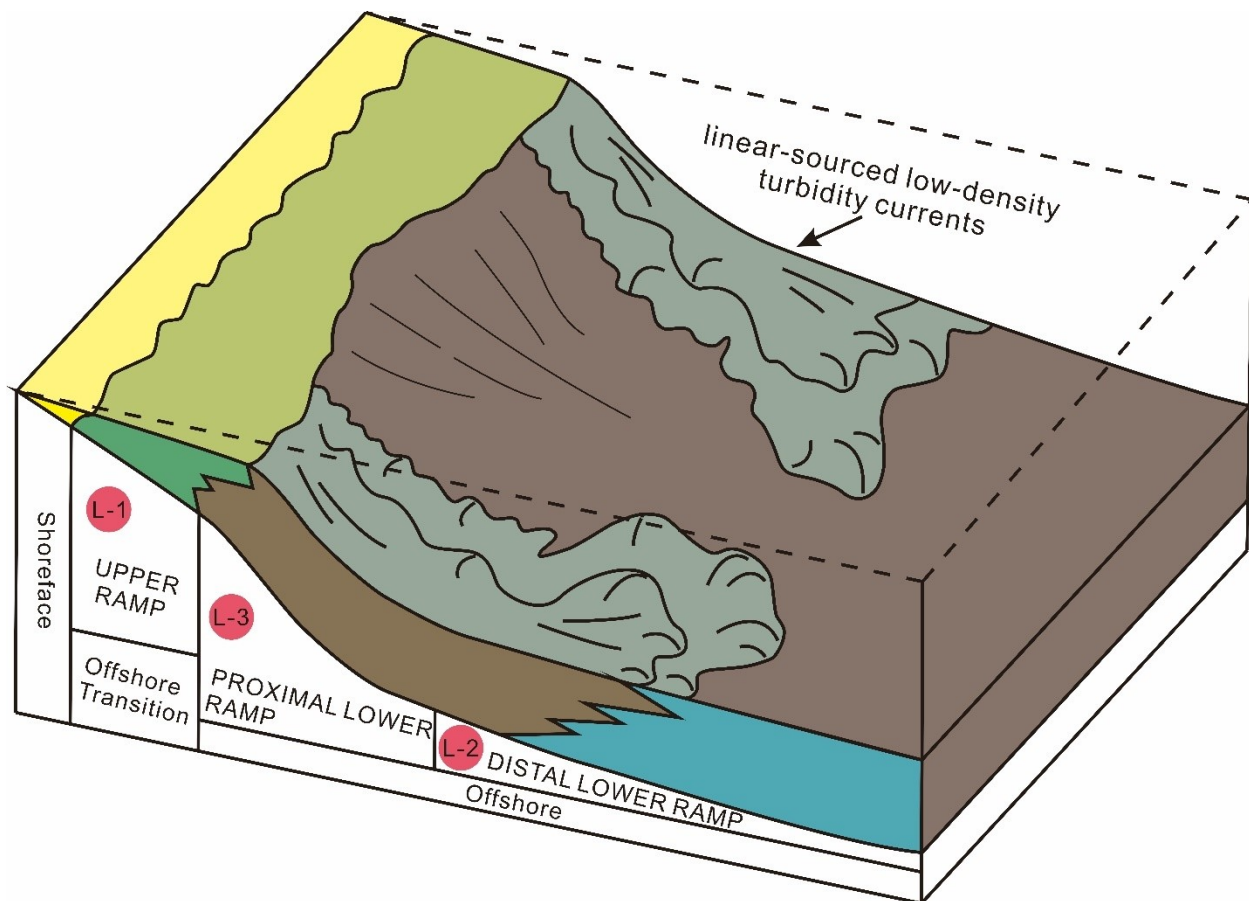
Figure 3.16-Schematic depositional model of a low-gradient, predominantly siliciclastic ramp corresponding to offshore transition and offshore environments. Three lithofacies identified in this study are shown (from Reading and Richards, 1994; Moslow et al., 2018; Prenoslo et al., 2018).

Reservoir Lithologies and Reservoir Quality

The Montney Formation within the study area is considered a tight, gas-producing reservoir composed mainly of dolomitic siltstone. The lithofacies described above have similar lithologies;

75

all samples plot adjacent to the quartz-carbonate line on the ternary diagram owing to the very low amounts of clay present (Fig. 3.7). Detrital grains mainly consist of quartz, calcite, and dolomite (Table 3.3). Other detrital grains include feldspar, muscovite, illite and kaolinite (Table 3.3). Authigenic minerals are predominated by calcite, ferroan calcite, dolomite, ferroan dolomite, pyrite and trace halite (Table 3.3). Feldspar grains are usually plagioclase, however trace amounts of microcline are observed. Muscovite grains are abundant within the siltstone reservoir, suggesting that the sediment was not significantly weathered before deposition, which is evidenced by the overall high feldspar content and very low amounts of clay (Table 3.3). The orientation of muscovite flakes is mostly parallel to the bedding plane, indicating the impact of intense compaction of unconsolidated sediment. Less commonly, unoriented muscovite flakes are observed within fine-grained siltstone lamina (Fig. 3.9E and F) or individual coarse-grained, dolomite-rich siltstone laminae (Fig. 3.11E and F). It is inferred that the unoriented muscovite grains result from detrital dolomite grains and early dolomitic cements reducing the effects of compaction (Schmoker and Halley, 1982; Sun, 1995; Gale et al., 2010).

The lithology of the Montney Formation within this well is characterized by a high amount of carbonate minerals (27.89% on average), especially dolomite (20.17% on average). Authigenic dolomite and calcite occur not only as grain-supporting matrix minerals, but also as replacement minerals. Iron-rich carbonates are abundant (especially ferroan dolomite), primarily occurring as cements in the form of overgrowths on the surface of the dolomite host grains (Fig. 3.9C, 3.10E, 3.11C). Clusters of microcrystalline pyrite framboids are interpreted to represent the replacements of detrital matrix and fill a significant portion of pore spaces (Fig. 3.8C, E, and H). In addition to muscovite, the proportion of clay minerals (mainly illite) is quite small and they are by and large detrital in origin based on morphology studies. As is shown in SEM photographs, detrital clays characterized by atypical crystal morphologies are primarily present as coatings of silt-sized grains and pore-filling matrix (Fig. 3.8B, E, and H). Halite occurs in close association with dolomitic beds or laminae. Their poorly developed crystal habit and irregular crystal boundaries indicate that nearly all halite crystals have experienced partial dissolution. Abundant, well-connected pores were developed because of halite dissolution, with some of them being filled by clay minerals (Fig. 3.8I).

Primary factors that destroy reservoir properties (Table 3.1) in this study include compaction, carbonate cementation, and the presence of detrital clays and microcrystalline pyrite framboids.

Compaction played a significant role in primary porosity reduction because detrital clay minerals occurring as rims and pore-filling matrix prevent the common precipitation of early-stage cement (e.g., quartz overgrowths). Moreover, compaction is further evidenced by tight grain contacts, muscovite flakes arranged parallel to the bedding plane, ductile deformation of clay minerals and local pressure solution. As mentioned above, further compaction was impeded by the formation of rigid carbonate cements, especially those composed of dolomite and Fe-dolomite. However, these cements strongly contributed to the loss of primary porosity. What's more, primary pore spaces were also reduced by illite-rich detrital clay minerals.

The majority of observed pores are classified as intergranular, intragranular and intercrystalline macropores. It is worth emphasizing that halite dissolution in the coarser siltstone beds formed interconnected elliptical to polygonal pores. This may explain why L-3 generally has higher porosity values than that of L-1 or L-2 (Table 3.2). Conversely, the small, elongate to irregular pores of the finer siltstone layers are commonly filled with clay particles, muscovite flakes and microcrystalline pyrite framboids as intercrystalline pores (Fig. 3.8A, C, E, and H). These features have an adverse effect on the preservation of primary pores (intergranular pores). Small pores are also present as intergranular pores at grain boundaries or as intragranular pores inside mineral grains such as quartz, dolomite, and plagioclase (Fig. 3.8B, D, F, and G).

Self-Sourcing Reservoir System and TOC Distribution

Total organic carbon (TOC), represented by weight percent of organic carbon, is a crucial parameter for the evaluation of source rock reservoir quality (Steiner et al., 2016). Previous studies have suggested that the organic matter within the siltstone units of the Montney Formation almost entirely consist of solid bitumen, which is the dominant component of the TOC content (Chalmers and Bustin, 2012; Sanei et al., 2015; Wood et al., 2015; Wood et al., 2018). However, the origin of the solid bitumen is still debatable. Several researchers interpreted the solid bitumen as being derived from hydrocarbon migration and subsequent thermal degradation with increasing burial depth and temperature (Sanei et al., 2015; Wood et al., 2015; Wood et al., 2018). Alternatively, other previous work proposed that the solid bitumen may be altered from primary kerogen deposited *in situ* during the process of thermal maturity. (Jacob, 1989; Chalmers and Bustin, 2012). In this study, it is interpreted that solid bitumen identified within wellbore 4-11-81-21W6 is mostly

converted from kerogen deposited *in situ*, mainly because of the positive correlation (r=0.66) between illite, muscovite content and TOC (Fig. 3.12), and the negative correlation (r=-0.44) between the amount detrital grains (quartz, calcite, and dolomite) and TOC (Fig. 3.13) (Chalmers and Bustin, 2012). Based on lithological analysis, illite is thought to be of detrital origin. Since organic matter is commonly absorbed by clay minerals to form organic matter-clay mineral aggregates in sediments (Arnarson and Keil, 2007; Yu et al., 2009), the strong positive correlation may imply that organic matter was deposited at the same time as the clay minerals. The strong positive correlation (r=0.78) between pyrite and TOC (Fig. 3.14) further indicates that the organic matter (kerogen) weas deposited and then converted to bitumen within the siltstone reservoirs (Chalmers and Bustin, 2012). This is because in normal marine environments, the pyrite formation is inextricably linked to bacteria-associated organic matter decomposition and sulphate reduction under anoxic conditions (Berner and Raiswell, 1983; Berner, 1984; Berner et al., 1985). In addition, it bears noted that an increase in TOC values results in a gradual decrease in porosity (r=-0.58) (Fig. 3.15). If the solid bitumen was degraded from an allochthonous, pore-filling liquid oil phase, a positive correlation between TOC and porosity should be exhibited. This provides further evidence that the organic matter present within the siltstone reservoirs is autochthonous. It can be concluded that the Upper Montney Member within the Shell Monias area is possibly a self-sourcing reservoir system.

Overall, TOC ranges from 0.52% to 3.67% with an average of 1.92% (Table 3.1). Lithofacies 3 displays the highest TOC levels (1.43 to 3.67%, 2.42% on average) (Table 3.2). However, these values are only slightly higher than that of L-2 (0.52-3.14%, 1.99% on average) and L-1 (0.89-1.99%, 1.47% on average) (Table 3.2). The variability in TOC among the three lithofacies is probably attributable to changes in depositional environment (Chalmers and Bustin, 2012; Kennedy et al., 2014). The low TOC levels of L-1, for example, are probably associated with heightened hydraulic energy whereby the offshore transition was intermittently agitated by storm-generated waves that reworked the organic material. In contrast, L-3 exhibits the highest TOC levels. The relatively weak hydraulic energies by which L-3 was deposited favored the accumulation of organic matter. In addition, low-density turbidity currents transported large quantity of organic-rich sediment to the site of deposition. The deposition of L-2 in the offshore setting (distal to the site of mass wasting) suggests that the area was only occasionally influenced by low-density turbidity currents. Thus, L-2 will contain lower amounts of TOC but a higher

proportion of suspended sediment compared to L-3 since it was deposited in a more distal setting. As a result, L-2 has lower amounts of organic matter than that of L-3.

CONCLUSIONS

This study identifies 3 lithofacies from the Upper Montney Member in the Shell Monias area, recording deposition within a low-relief, predominantly siliciclastic ramp setting (ranging from offshore transition to offshore environments). Lithofacies 1 was deposited within the upper ramp, corresponding to the offshore transition setting, with intermittent storm influences, whereas lithofacies 2 and 3 represent the deposition from distal to proximal lower ramp, subject to the low-density turbidity currents under the mean storm wave base. These 3 lithofacies are collectively characterized by abundant carbonate and low amounts of clay minerals. Detrital and authigenic dolomite preserve primary pore space by resisting compaction, whereas dolomite cements significantly reduce pore space. Pore spaces were also reduced by small amounts of illite. Overall, the lithofacies studied have similar reservoir properties.

Pervasive bitumen within this Montney siltstone reservoir is inferred to be sourced from organic matter that accumulated *in situ*. This interpretation is supported by the positive correlation of TOC with illite and muscovite, and its negative correlation with detrital minerals such as quartz, calcite and dolomite. These trends indicate that the accumulation of TOC was associated with the deposition of finer grained sediments. In addition, the co-occurrence of TOC and pyrite suggests that anoxic to dysoxic conditions were present at the water-sediment interface during deposition or early diagenesis. Lastly, TOC and porosity are negatively correlated, suggesting that the bitumen was autochthonous, since allochthonous bitumen is expected to have TOC values that are higher in more porous rocks. These lines of evidence indicate that the Montney reservoir within the Shell Monias area is a self-sourcing reservoir.

CHAPTER 4：ICHNOLOGY OF THE UPPER MONTNEY MEMBER IN WEST-CENTRAL ALBERTA

INTRODUCTION

Bioturbation in the Lower Triassic Montney Formation is highly variable in abundance, diversity and facies selectivity (Davies et al., 2018). Low-diversity suites of diminutive trace fossils attributable to the *Cruziana* ichnofacies are relatively common in the Montney Formation (Davies et al., 2018). Although only a few studies have provided thorough assessments pertaining to the ichnology of the Montney Formation, Zonneveld et al. (2010a, 2010b) provided a comprehensive ichnological analysis of an area within the Montney Formation. On the basis of careful analysis of sedimentological and ichnological features, the Lower Montney Member in the Pedigree-Ring/Border-Kahntah River area was interpreted as a ramp succession deposited under the influence of infrequent and low-intensity storms (Zonneveld et al., 2010b). Compared to the trace-fossil assemblages studied from the Middle and Upper Triassic, trace-fossil occurrences and distributions in the Pedigree-Ring/Border-Kahntah River area are very different (Zonneveld et al., 2001, 2002, 2004, 2010b). In particular, relatively high-diversity ichnofossil assemblages were common in the proximal lower shoreface (Zonneveld et al., 2010b). In contrast, the distal lower shoreface to offshore transition were characterized by trace-fossil assemblages showing lowered diversity dominated by opportunistic trace fossils produced by storm-transported organisms (Zonneveld et al., 2010b). The main environmental stress during deposition was interpreted to be oxygen deficiency, which globally inhibited bioturbation in shallow marine successions during the Early Triassic (Hallam, 1995; Wignall and Twitchett, 2002; Wignall and Newton, 2003; Zonneveld et al., 2010b). The relatively high-diversity trace-fossil assemblages identified locally in the Lower Montney Member were interpreted as being associated with shallow marine refugia where the water was well-oxygenated (Beatty et al., 2008; Zonneveld et al., 2007, 2010a, 2010b; Furlong et al., 2018). There are several other studies discussing the ichnological characteristics of the Montney Formation, which primarily focus on the low- to moderate-diversity assemblages dominated by robust *Lingulichnus* or *Diplocraterion* within the Lower and Middle Montney

(Zonneveld et al., 2007; Davies et al., 2018; Zonneveld and Moslow, 2018). There are few studies on the bioturbation of the Upper Montney.

In fully marine settings with uniform salinities, environmental stresses that influence infaunas mainly include sedimentation rates, substrate cohesion, oxygenation, water turbidity and hydraulic energy (Bromley and Ekdale, 1984; MacEachern and Pemberton, 1992; Mángano and Buatois, 2020). In storm-dominated shorefaces, fluctuations in hydraulic energies and sedimentation rates potentially exert the dominant controls on the preserved sedimentary fabric. Wave influenced sedimentary environments where infaunalization might still commonly occur is mostly restricted to the lower and middle shoreface, ranging from apparently unburrowed hummocky and swaley cross-stratified sandstone beds to heavily bioturbated muddy sandstone beds, depending on the degree of wave influence (MacEachern and Pemberton, 1992; Dumas and Arnott, 2006). In general, storm-affected shorefaces fall into three categories: strongly storm-dominated shorefaces (high hydraulic energy), moderately storm-dominated shorefaces (intermediate hydraulic energy) and fair-weather dominated or weakly storm-affected shorefaces (low hydraulic energy) (MacEachern and Pemberton, 1992).

The aim of this paper is to analyze the ichnological characteristics and investigate the ichnological variability of the shoreface deposits within the Upper Montney Member from core within the eastern parts of the Montney Formation in Alberta.
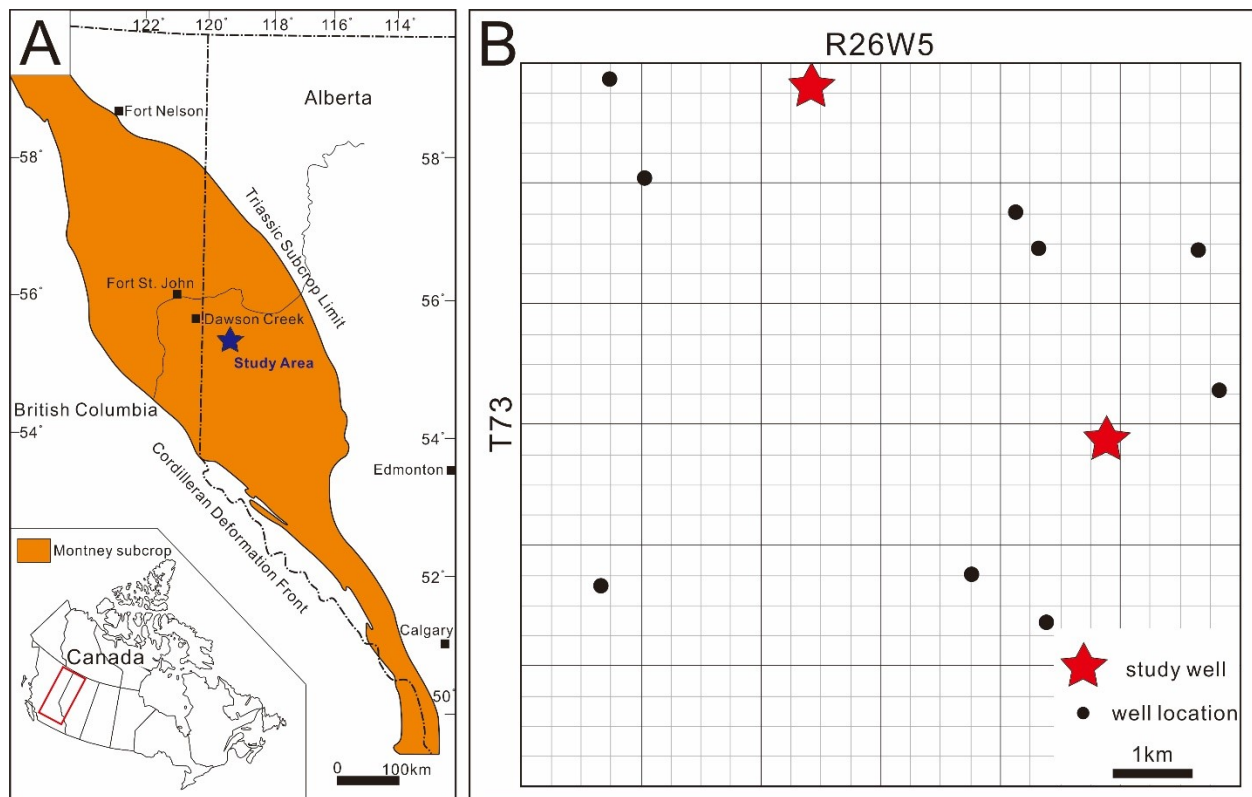
Figure 4.1-Location map of the study area (A) and study wells (B) (after Wood et al., 2018).
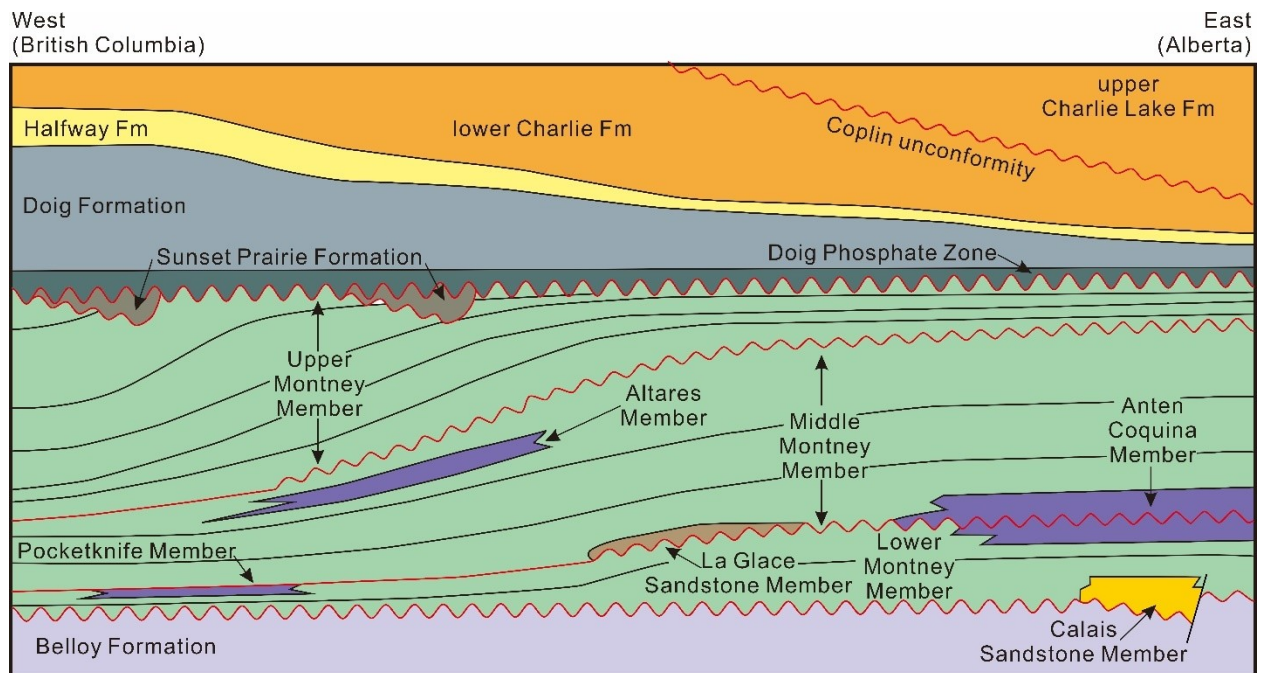
Figure 4.2-Schematic diagram of the Montney stratigraphy, British Columbia to Alberta, exhibiting three unconformity-bounded third-order depositional sequences (Lower, Middle and Upper member) (after Zonneveld and Moslow, 2018).

STUDY AREA AND GEOLOGICAL SETTING

The cores selected for this study are located in west-central Alberta (Dominion Land Survey locations 14-33-73-26W5M and 16-14-73-26W5M) (Fig. 4.1). Since much of the Upper Montney in Alberta has been eroded, it is most commonly described from northeastern British Columbia (Zonneveld and Moslow, 2018). Generally speaking, the Upper Montney unconformably overlies the Altares Member of the Middle Montney, corresponding to the Smithian/Spathian boundary, and is unconformably overlain by the Middle Triassic strata of either the Doig Phosphate Zone or the Sunset Prairie Formation (Furlong et al., 2018; Zonneveld and Moslow, 2018) (Fig. 4.2). Lithologically, the Upper Montney is dominated by the interbedding of bituminous, dolomitic, fine- to coarse-grained siltstone and very fine-grained sandstone, as shown in the established type section within the core c-65-F/94-B-8 (2203-2374.5m) (Zonneveld and Moslow, 2018). Ichnologically, the Upper Montney is characterized by relatively diverse trace-fossil assemblages (Davies et al., 2018; Zonneveld and Moslow, 2018).

METHODOLOGY

Each core was logged using AppleCore© software and divided into facies primarily on the basis of the core observations (e.g., lithology, nature of contacts, physical sedimentary structures, ichnological characteristics).

The cores were logged in detail to determine the ichnogenera that are present and their sedimentological context. Bioturbation Index (BI) was used to record and report the degree of bioturbation, assessed following the schemes of Reineck (1967) and Taylor and Goldring (1993) on a 1.0 m scale of each core, where BI=0 represents unburrowed sediment and BI=6 represents complete homogenization of sediment. Maximum burrow diameter (smallest axis in deformed burrows) and bioturbation diversity were also recorded using 1.0 m bins, meaning the largest diameters of trace fossils and the range of diversities that occur in each meter of core (Botterill et

al., 2015). The size-diversity index (SDI) was obtained to quantitatively illustrate and compare the infaunal communities' responses to the changes in the environmental stresses (Hauck et al., 2009; Botterill et al., 2015; Timmer et al., 2016b). The size-diversity index was calculated by multiplying maximum burrow diameter by the diversity of identified trace-fossil assemblages for each 1.0 m interval. The BI and SDI data of the two cores were plotted against depth from the top of the Upper Montney. Trace fossil assemblages were assigned to Seilacherian ichnofacies and intergradations between archetypal ichnofacies to further aid in the reconstruction of sedimentary environments (Seilacher, 1967 and 1968; MacEachern et al, 2007a, 2007b; Gingras et al., 2011).

RESULTS AND INTERPRETATIONS

Sedimentology

The shoreface strata of the Upper Montney in west-central Alberta are dominated by thinly bedded, wavy-parallel laminated, dolomitic bituminous fine- to coarse-grained siltstone, with subordinate very fine-grained sandstone locally present towards the top of the cored succession (Fig. 4.3). Four facies are proposed on the basis of their sedimentological characteristics. The facies together comprise a conformable, shoaling-upward (coarsening-upward) sequence (Table 4.1).

Facies 1, representing the deposition within the distal lower shoreface, mainly consists of millimeter-scale, sharp-based medium- to coarse-grained siltstone laminae and lenses, commonly interlaminated with bituminous, wavy parallel to planar laminated, fine-grained siltstone. Overall, few coarser siltstone units are the most significant characteristics of Facies 1. Facies 2, interpreted as the deposition within the proximal lower shoreface, is composed of interbedded dolomitic, medium- to coarse-grained siltstone and bituminous, fine-grained siltstone. Coarser siltstone beds (centimeter- to decimeter-scale) are generally sharp-based and display small-scale hummocky cross-stratification, scour and fill structures, laminae truncations, low angle cross-stratification and combined flow ripples. Overall bioturbations of Facies 1 and 2 are very weak and there are only sporadic occurrences of thin (1.7 to 5.4 cm in thick) intensely bioturbated beds. Facies 3 (middle shoreface) is distinguished from Facies 2 by a remarkable increase in dolomitic, medium- to coarse-grained siltstone beds. Its lithology is dominated by decimeter-scale, sharp-based,

84

dolomitic, medium- to coarse-grained siltstone beds, with very few bituminous, fine-grained siltstone laminae or beds. Amalgamated coarser siltstone beds are up to 82 cm in thickness. Physical sedimentary structures are dominated by wavy parallel lamination, low angle cross-stratification, laminae truncations, scour and fill structures. In terms of bioturbation, Facies 3 is characterized by impoverished trace-fossil assemblages. Facies 4 (upper shoreface/foreshore) includes dolomitic, coarse-grained siltstone to very fine-grained sandstone, exhibiting sharp contacts with the underlying Facies 3. It bears noting that Facies 4 (around 0.5 m) is present only at the uppermost part of the well 16-14-73-26W5M. And intensive bioturbation led to poorly defined bedding features and physical sedimentary structures.

In the studied cores, the stacking patterns of these four facies are shown in Figure 4.3 and 4.4. Vertically, the lower part of each core generally exhibits interbedding of Facies 3 (interbedded dolomitic, hummocky cross-stratified medium- to coarse-grained siltstone and bituminous, fine-grained siltstone) and Facies 4 (interlamination of bituminous, wavy parallel to planar laminated, fine-grained siltstone and dolomitic, medium- to coarse-grained siltstone laminae and lenses), accounting for a substantial proportion of the shoreface deposition of the Upper Montney. It is noted that such interbedding is more frequent in the well 16-14-73-26W5M. Conformably overlying the Facies 3 and 4, Facies 2 (dolomitic, low angle cross-stratified to wavy parallel laminated medium- to coarse-grained siltstone) is always present in the upper part of the core. As previously mentioned, Facies 1 (dolomitic, intensively bioturbated coarse-grained siltstone to very fine-grained sandstone) only occurs at the uppermost part of the well 16-14-73-26W5M.
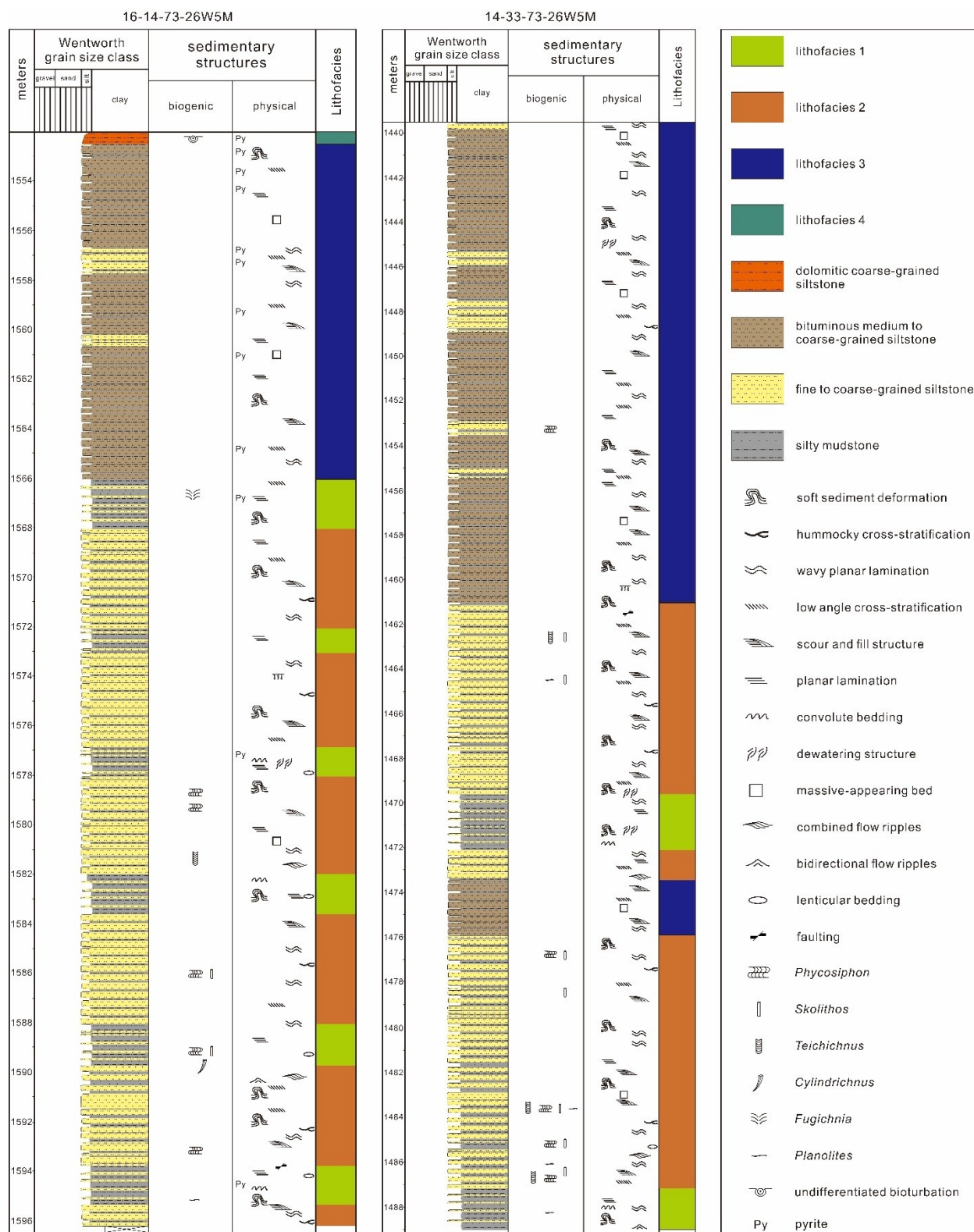
Figure 4.3-Core description for the well 16-14-73-26W5M (1552.01-1596.46 m) and 14-33-73-26W5M (1439.49-1489.49 m).

FACIES	LITHOLOGY	BEDDING	PHYSICAL SEDIMENTARY STRUCTURE	DEP. ENVIRONMENT
1	Interlaminated dolomitic, medium- to coarse-grained siltstone and bituminous, fine-grained siltstone	Sharp based; ungraded; mm-scale beds or laminae associated with storms; In British Columbia, highly deformed intervals are locally common (0.9-11.9 cm in thick)	Wavy parallel lamination; planar lamination; lenticular bedding; load cast; scour and fill structure; current ripples; convolute bedding; soft sediment deformation; microfault; dewatering structure	Distal lower shoreface
2	Interbedded dolomitic, medium- to coarse-grained siltstone and bituminous, fine-grained siltstone	Sharp based; ungraded; cm to dm-scale tempestites; Local, irregularly distributed, thin intensely bioturbated beds dominated by *Phycosiphon* range from 1.7 to 5.4 cm in thick	Hummocky cross-stratification; combined flow ripples; oscillation flow ripples; wavy parallel lamination; low angle cross-stratification; planar-lamination; flame structure; load cast; syneresis crack	Proximal lower shoreface
3	Dolomitic, medium- to coarse-grained siltstone with very few bituminous, fine-grained siltstone laminae or beds	Sharp based; ungraded; amalgamated tempestites (dm-scale) ranging from 18 to 82 cm in thick	Massive bedding; low angle cross-stratification; hummocky cross-stratification; wavy parallel lamination; rippled lamination; planar lamination; load cast; scour and fill structures, truncation	Middle shoreface
4	Dolomitic, coarse-grained siltstone to very fine-grained sandstone	Sharp based; ungraded; 52 cm in thick totally; Bedding features are almost thoroughly destroyed by intense bioturbation	Poorly defined bedding resulted from bioturbation	Upper shoreface/Foreshore

Table 4.1-Summary of sedimentary lithofacies characteristics of the Upper Montney in west-central Alberta.

Sedimentological Interpretation

Based on the presence of common lenticular bedding and abundant wavy parallel interlaminated bituminous, fine-grained siltstone and medium- to coarse-grained siltstone and the absence of hummocky cross-stratification, Facies 1 is interpreted to represent the distal lower shoreface (Reineck and Singh, 1971; Zonneveld et al., 2010a; Basilici et al., 2012). As there are pervasive low angle and hummocky cross-stratified medium- to coarse-grained siltstone interbedded with bituminous, fine-grained siltstone, Facies 2 is interpreted to represent the proximal lower shoreface (Cheel, 1991; Cheel and Leckie, 1993; Plint, 2010). Facies 3 is interpreted to represent the middle shoreface on account of the common presence of amalgamated medium- to coarse-grained siltstone beds displaying low-angle cross-stratification, wavy parallel lamination, laminae truncations, scour and fill structures (Reinson, 1984; MacEachern and Bann, 2008). Because Facies 4 is characterized by intensely bioturbated, coarse-grained siltstone to very fine-grained sandstone, it is interpreted that Facies 4 represents deposition within the upper shoreface/foreshore, specifically, the longshore trough positioned landward of the subaqueous longshore bar (Hunter et al., 1997; Leckie and Walker, 1982; Reading and Collinson, 1996; Herbers et al., 2016).

Taken collectively F1 through F4 form a progradational stacking pattern that is interpreted as Shoreface Facies Association. Within the studied cores, as the dolomitic, medium- to coarse-grained siltstone beds or laminae commonly show load casts, hummocky cross-stratification, wavy parallel lamination, combined flow ripples, rippled lamination, scour and truncation, they are interpreted as tempestites formed by storm waves. While the bituminous, fine-grained siltstone beds or laminae characterized by planar lamination are interpreted to be deposited from suspension under fair-weather conditions. As there are high abundance of thick tempestites in both cores, the Upper Montney in study area are inferred to represent the deposition within the moderately to strongly storm-dominated shoreface settings (MacEachern and Pemberton, 1992), characterized by persistently high hydraulic energies.

Ichnology

In general, the trace fossils within the shoreface successions of the Upper Montney are small in diameter and have a low to moderate diversity. Bioturbation intensities are extremely variable. The most diverse assemblages are associated with Facies 3 (Fig. 4.4). The trace fossils in the studied cores can typically be classified to their ichnogenus, including *Phycosiphon*, *Planolites*, *Teichichnus*, *Cylindrichnus* and *Skolithos* (Table 4.2; Fig. 4.5).
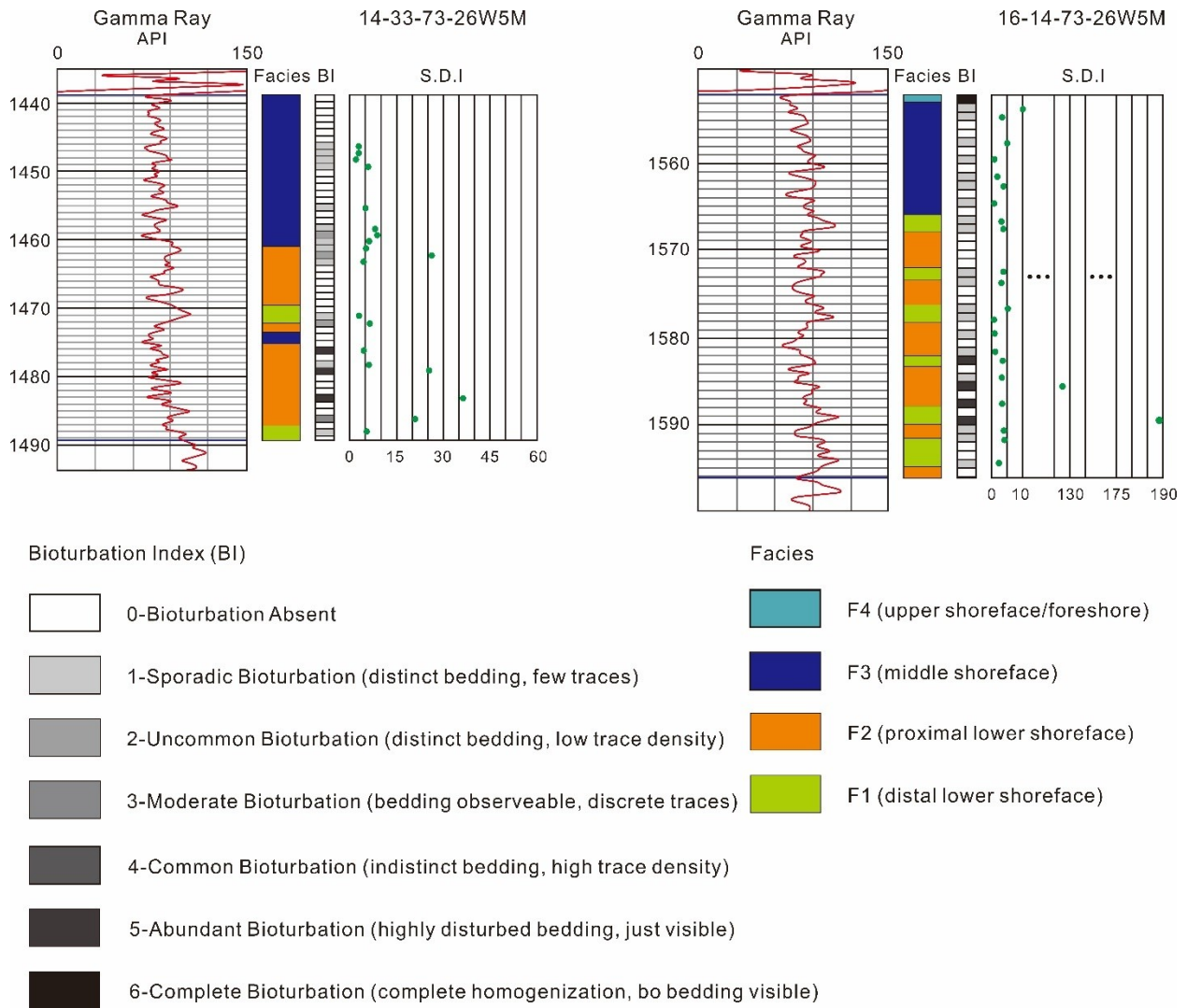
Figure 4.4-Cross-section of the study wells in west-central Alberta summarizing the characteristics and trends in Size-Diversity Index (SDI) and Bioturbation Index (BI).

Table 1

Ichnogenus	Description	Remarks
Phycosiphon (Ph)	• Clusters of marginal, similar-diameter,hook or comma-shaped dots; • Burrows commonly surrounded by very narrow, pale mantles; • Infill contrasts with host sediment; • Locally crosscut or reborrowed by other taxa (e.g., *Teichichnus*); • Burrow diameters are smaller than 1.0 mm on average.	*Phycosiphon* is a common constitute of oxygen-stressed settings, inferred to be constructed by opportunistic deposit-feeding organisms.
Teichichnus (Te)	• Unlined burrows with vertical to inclined, straight to crooked retrusive spreite structures; • Commonly present along with *Phycosiphon*; • Infill contrasts with host sediment, especially within the bituminous finer siltstone beds; • Protrusive and zigzagged spreite are occasionally identified; • Robust in size, up to 42.6 mm in diameter.	*Teichichnus* with retrusive spreite is interpreted to be deposit-feeding burrows. The coexistence of protrusive and retrusive spreite may imply it is a dwelling trace or a combined feeding-dwelling structure.
Cylindrichnus (Cy)	• Inclined and gently curved, tapering-off downward burrow; • Typical clay-rich wall-lining; • Infill is similar to host sediment; • Diminutive in size, 0.9 mm and 11.2 mm in diameter and length.	*Cylindrichnus* is inferred to be a kind of suspension-feeding structures constructed by opportunistic organisms under storm-associated high-energy hydrodynamic conditions.
Skolithos (Sk)	• Straight to slightly curved, vertical to subvertical, similar-diameter, unlined burrows; • Infill is commonly structureless and in contrast with host sediment; • Small burrows ranging from 1.0 to 10.0 mm in diameter and 2.5 to 22.0 mm in length.	In marine settings, *Skolithos* is interpreted as dwelling burrows constructed by suspension-feeding organisms or passive carnivores.
Planolites (Pl)	• Small circular to elliptical unlined burrows; • Structureless infill always contrasts with host sediment; • Rarely reburrowing the pre-existing burrows; • Burrow diameters ranging from 0.1 to 4.1 mm.	*Planolites* is a eurybathic, facies-crossing trace fossil, interpreted as feeding structures constructed by mobile deposit-feeding organisms.

Table 4.2-Summary of ichnological attributes of the Upper Montney in west-central Alberta.
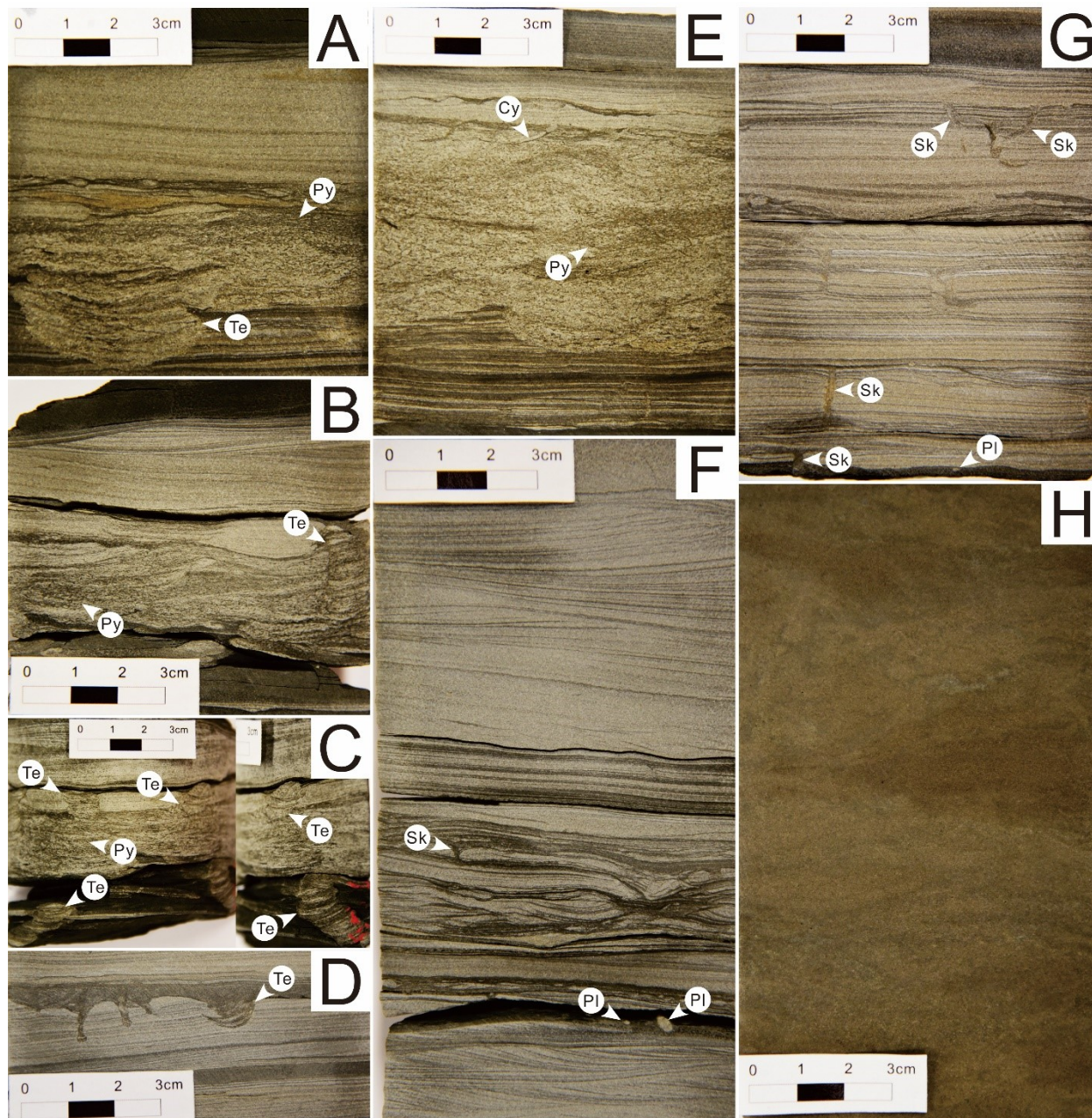
Figure 4.5-Core photographs of ichnofossils within the shoreface successions of the Upper Montney, west-central Alberta. **A.** Facies 2, the lower part of a storm-associated bed was intensely bioturbated by the *Phycosiphon*-dominated trace-fossil assemblages (BI=5-6). The ichnogenera diversity of this thin, intensely bioturbated bed is low, only including *Phycosiphon* and *Teichichnus*. Burrows of *Phycosiphon* are commonly surrounded by very narrow, pale mantles. And locally, the pre-existing *Phycosiphon* were crosscut by the robust *Teichichnus*. The

underlying bed comprising the interlamination of medium- to coarse-grained siltstone and bituminous, fine-grained siltstone is also destroyed locally. 16-14-73-26W5M; 1589.15 m. **B.** Facies 2, thin (2.9 cm), *Phycosiphon*-dominated, intensely bioturbated bed is present at the lower part of a storm bed (BI=5-6), characterized by high in bioturbation intensity but low in diversity. Vertical and slightly crooked *Teichichnus* showing both retrusive and protrusive spreite structures is identified to crosscut the abundant *Phycosiphon*. 14-33-73-26W5M; 1483.44 m. **C.** Facies 2, the opposite side of the core slab shown in the photograph B. More *Teichichnus*, mostly inclined, straight to slightly crooked in morphology, are identified to crosscut the *Phycosiphon* in the intensely bioturbated bed. Isolated *Teichichnus* are also present within the underlying bituminous, fine-grained siltstone bed. 14-33-73-26W5M; 1483.44 m. **D.** Facies 2, small *Teichichnus* showing zigzagged spreite is occasionally present, commonly associated with bituminous, fine-grained siltstone beds or laminae. 14-33-73-26W5M; 1462.66 m. **E.** Facies 1, scarce, diminutive *Cylindrichnus* are present on top of the thin (5.4 cm), *Phycosiphon*-dominated, intensely bioturbated bed (BI=5-6). It seems that almost the whole storm bed has been thoroughly bioturbated, with the underlying layer also seriously impacted. 16-14-73-26W5M; 1589.15 m. **F.** Facies 3, the middle shoreface deposits are characterized by amalgamated, low-angel cross-stratified to wavy parallel laminated, medium- to coarse-grained siltstone beds. The bituminous, fine-grained siltstone beds or laminae are commonly few and thin, occasionally bioturbated by diminutive *Skolithos* and *Planolites* (BI=1). 14-33-73-26W5M; 1459.56 m. **G.** Facies 2, Top-down bioturbation (BI=1) exhibited by the thin, medium- to coarse-grained siltstone beds within the proximal lower shoreface are commonly associated with few diminutive traces of *Skolithos*. 14-33-73-26W5M; 1462.08 m. **H.** Facies 4, the coarse-grained siltstone to very fine-grained sandstone beds representing the deposition of the upper shoreface/foreshore are characterized by homogeneously distributed bioturbation. Trace fossils within these beds are indiscernible. 16-14-73-26W5M; 1552.25 m.

The diversity of trace fossils and bioturbation intensities within the studied cores are very low (Fig. 4.4). Most of the trace fossils are small and lack a discernible lining. The SDI values in two cores are quite low and display numerical stability upwards (Fig. 4.4). The SDI are generally lower than 5.0 in the well 16-14-73-26W5M and < 10.0 in the well 14-33-73-26W5M (Fig. 4.4). Similarly, BI values are also very low, mostly less than 3 in both cores (Fig. 4.4). The occasional

higher SDI and BI values are associated with irregularly distributed, thin, intensely bioturbated beds (1.7-5.4 cm, BI=5-6) identified from Facies 1 and 2. In Facies 2, these beds are closely related to medium- to coarse-grained siltstone tempestites (Fig. 4.5A, B, and C). The intense bioturbation in Facies 1 is commonly observed as bioturbated storm-associated heterolithic interlamination (Fig. 4.5E). The low-diversity trace fossil assemblages within these thin beds are dominated by *Phycosiphon* with subordinate *Teichichnus* and *Cylindrichnus* (Fig. 4.5A, B, C, and E). There are also isolated *Skolithos*, *Planolites* and *Teichichnus* sporadically distributed within the Facies 1 and 2 (Fig. 4.5D and G).

The bioturbation intensity is very low in the amalgamated medium- to coarse-grained siltstone beds of Facies 3 (BI=0-1) (Fig. 4.4). Only scarce and diminutive *Skolithos* and *Planolites* are observed, mostly associated with the bituminous fine-grained siltstone laminae. The coarse-grained siltstone to very fine-grained sandstone beds of Facies 4 exhibit homogeneous distribution of bioturbation (BI=5-6) (Fig. 4.4). The trace fossils are indiscernible because of intense ichnological reworking (Fig. 4.5H), thus the diversity of ichnogenera therein could not be assessed.

Diagnoses of Ichnogenera

Phycosiphon

Description

Phycosiphon is densely distributed in thin, heavily bioturbated beds of Facies 1 and 2, accounting for the majority of the bioturbation in these beds (Fig. 4.5A, B, C, and E). In cross section, they occur as clusters of marginal hook or comma-shaped dots that display a constant diameter (smaller than 1.0 mm on average). The colour of the burrow-fills sharply contrast with the host sediments as they were backfilled with black, fine sediment. Very narrow, pale mantles surround the burrows (Fig. 4.5A and E). Poorly defined meniscae are occasionally observed within the burrows. No spreite are observed.

Remarks

Phycosiphon occur from the Cambrian to the Holocene, occurring widely from continental shelves to submarine fans (Fu, 1991; Goldring et al., 1991; Savrda et al., 2001; Naruse and Nifuku, 2008). It is suggested that *Phycosiphon* were constructed by opportunistic deposit-feeding organisms selectively foraging and ingesting clay-grade material from the sediment, mostly in muddy siltstone and sandstone (Goldring et al., 1991; Wetzel and Uchman, 2001; Naruse and Nifuku, 2008; Bednarz and McIlroy, 2009). *Phycosiphon* has also been associated with oxygen-stressed environments (Gingras et al., 2011). In the thin, heavily bioturbated beds of Facies 1 and 2, *Phycosiphon* are observed to be crosscut or reborrowed by other taxa (e.g., *Teichichnus*). Hence, the trace-makers of *Phycosiphon* are interpreted to be the first organisms colonizing the storm beds shortly after their deposition (Stow and Wetzel, 1990; Wetzel and Balson, 1992; Wetzel and Uchman, 2001). Since the *Phycosiphon* producers did not irrigating their burrows, the rapid colonization is possibly due to increased oxygen availability immediately after storm deposition (Wetzel and Uchman, 2001).

Teichichnus

Description

In comparison to other trace fossils in this dataset, *Teichichnus* (Fig. 4.5A, B, C, and D) is generally robust in size. *Teichichnus* appear in cross section as vertical to inclined, straight to crooked spreiten-bearing structures, comprising tightly packed concave-up (occasionally displaying concave-down), slightly crescentic laminae. They are low in abundance and commonly present along with *Phycosiphon* in the thin, intensely bioturbated, medium- to coarse-grained siltstone beds in Facies 2. *Teichichnus* are also sporadically distributed within the bituminous fine-grained siltstone beds (Fig. 4.5C). As most burrows are passively backfilled by coarser silts, textural and colour contrasts between the host sediment and traces are much sharper in the bituminous finer grained siltstone beds. In addition, there are isolated *Teichichnus* exhibiting zigzagged spreite in Facies 2 (Fig. 4.5D). They are smaller in size and commonly backfilled by bituminous finer grained siltstone.

Remarks

Teichichnus is a characteristically marine ichnogenus and a common constitute of low-energy depositional environments such as the lower shoreface and offshore transition, ranging from the Cambrian to the Holocene (Gingras et al., 2011; Knaust, 2018). In the study area, on basis of the burrow morphology and spreite, *Teichichnus* mainly belong to two ichnospecies: *Teichichnus rectus* (Seilacher, 1955; Gingras et al., 2011) and *Teichichnus zigzag* (Frey and Bromley, 1985; Knaust, 2018). The retrusive spreite is primarily interpreted to represent systematic burrowing for food within the sediment by deposit feeders (Seilacher, 1955; Corner and Fjalstad, 1993; Pemberton et al., 2001; Knaust, 2018). However, in this study, the common occurrence of *Teichichnus* within the coarser siltstone tempestites and the occasional coexistence of protrusive and retrusive spreite within one burrow imply that *Teichichnus* is possibly a dwelling trace or a combined feeding-dwelling structure (Corner and Fjalstad, 1993; Knaust, 2018). Construction of protrusive and retrusive spreite is inferred to respond to erosion and sedimentation processes by trace makers (Gingras et al., 2007; Knaust, 2018).

Cylindrichnus

Description

A few small *Cylindrichnus* (approximately 0.9 mm and 11.2 mm in diameter and length, respectively) are observed on the top of the thin, intensely bioturbated beds in Facies 2 (Fig. 4.5E). In cross-section, the traces are inclined and gently curved, tapering downward. The burrow also has a prominent clay-rich wall-lining (Fig. 4.5E).

Remarks

Cylindrichnus is a common trace fossil in sandy shoreface successions ranging from the lower Carboniferous to the Holocene (Knaust, 2021). They are interpreted as suspension-feeding structures constructed by opportunistic organisms (Ekdale and Harding, 2015), although Gingras and MacEachern (2012) suggested that interface-deposit feeding is a viable interpretation for the structure. The absence of spreite suggests that there were no progressively downward foraging behaviors exhibited by the trace-makers (Ekdale and Harding, 2015). The occurrence of *Cylindrichnus* in the Upper Montney is similar to that in the Upper Cretaceous Rock River Formation, which was deposited in lower shoreface and offshore settings of present-day Wyoming

and Utah and wave-dominated delta deposits of the Cretaceous Dunvegan Formation (Gingras et al., 1998, 1999). Specifically, they occur in hummocky cross-stratified sandstone beds with low-diversity trace fossil assemblages, suggesting the tolerance or even preference of the trace-makers for the storm-associated high-energy hydrodynamic conditions (Frey, 1990; Ekdale and Harding, 2015).

Skolithos

Description

   Skolithos (Fig. 4.5F and G) is characterized by straight to slightly curved, vertical to subvertical, unlined burrows with a constant diameter. The infill is commonly structureless and in contrast with the host sediment. The burrow sizes (1.0-10.0 mm in diameter) are relatively small, and the penetration depths are quite low, ranging from 2.5 to 22.0 mm on average. The majority of *Skolithos* are sporadically distributed within Facies 3, commonly penetrating through the storm-associated interlaminated medium- to coarse-grained siltstone and bituminous, fine-grained siltstone (Fig. 4.5G). Few burrows concordant to the bedding plane are also locally identified. Moreover, there are scarce and diminutive *Skolithos* present within the Facies 1 and 3, mostly within the medium- to coarse-grained siltstone beds.

Remarks

   Skolithos is very widespread in shallow-marine environments from the late Precambrian to recent (Fillion and Pickerill, 1990, Schlirf and Uchman, 2005) and has also been found in non-marine settings (Bromley and Asgaard, 1979; Schlirf et al., 2001). In marine environments, *Skolithos* is interpreted as a dwelling burrow constructed by suspension-feeding organisms or passive carnivores (Schlirf and Uchman, 2005). Zonneveld et al (2010b) reported that *Skolithos* are small and rare in the Montney Formation, mostly identified from the sandstone beds deposited in the upper shoreface or foreshore, which is consistent with the characteristics of the *Skolithos* in the study area.

Planolites

Description

In cross section, *Planolites* (Fig. 4.5F and G) is characterized by unlined, circular to elliptical burrows of different diameter (ranging from 0.1 to 4.1mm). The amount of *Planolites* in the Upper Montney is very low, sporadically distributed within the bituminous, fine-grained siltstone laminae or beds of Facies 1, 2 and 3. The structureless burrow fills are different in lithology (commonly coarser) from the host sediment.

Remarks

Planolites is a eurybathic, facies-crossing trace fossil that occurs in virtually all sedimentary environments from the Cambrian to Holocene (Pemberton and Frey, 1982; Uchman et al., 2005; Shahkarami et al., 2017). It is interpreted to represent a feeding structure constructed by mobile deposit-feeding organisms that actively backfilled the burrows (Pemberton and Frey, 1982; Díez-Canseco et al., 2016).

DISCUSSION

A Shoreface Lifestyle in the Upper Montney

For storm-dominated shoreface settings, the intensity of bioturbation within the storm beds and thickness of the fair-weather deposits reflect a combination of storm severity (i.e., the depth of storm erosion into fair-weather and previous storm deposits), storm frequency (i.e., the thickness of fair-weather deposits allowed to accumulate) and relative water depth (MacEachern and Pemberton, 1992). As storm and fair-weather waves are the predominant physical processes impacting the middle and lower shoreface, the greatest extent of sedimentological and ichnological variability is commonly exhibited by the middle and lower shoreface, which may range from hummocky cross-stratified and swaley cross-stratified sandstones to thoroughly bioturbated muddy sandstones (MacEachern and Pemberton, 1992). Nevertheless, the ichnological characteristics of the amalgamated middle and lower shoreface deposits of the Upper Montney in this study are typified by overall lower bioturbation intensities and sporadically distributed bioturbation. The dominant trace fossils are constructed by opportunistic colonizers, including *Phycosiphon, Skolithos* and *Cylindrichnus* (Fig. 4.5) and considering the sporadic nature of burrow

distribution, essentially all bioturbations may be opportunistic and post-storm. Integrated with the aforementioned sedimentological features, the Upper Montney Memmber in this study is interpreted to represent the deposition within the moderately to strongly storm-dominated shoreface settings.

Specifically, in the middle shoreface, frequent and strong storm activities are inferred to lead to persistently high rates of sedimentation or rapid emplacement of storm beds, which inhibited infaunal colonization (Pemberton and MacEachern, 1997). Elevated sedimentation rates are implied by the presence of massive-appearing bedding, common soft sediment deformation features and small sand dykes. In addition, high intensity storms in the middle shoreface probably contributed to the scarce bioturbation by erosional exhumation of fair-weather and previous storm deposits (MacEachern and Pemberton, 1992; Pemberton et al., 1992; Saunders et al., 1994; Pemberton and MacEachern, 1997): this is supported by the presence of common truncation surfaces, scour and fill structures.

Similarly, the overall minimal bioturbation in the lower shoreface is in part ascribed to persistent and energetic hydrodynamic conditions. Additionally, lowered levels of oxygen at the sediment-water interface likely played a significant role in precluding bioturbation, as trace fossils are almost absent within the relatively abundant and thick fine-grained siltstone beds representing fair-weather deposits. The rare, irregularly distributed, thin beds characterized by high-intensity, but low-diversity bioturbation in the lower shoreface possibly record episodically favourable conditions (e.g., an availability of oxygenated bottom water and lowered hydrodynamic energies) facilitating infaunal colonization during or shortly after storms. This is further evidenced by the cross-cutting relationship identified from these beds between the opportunistic (e.g., *Phycosiphon*) and fair-weather (e.g., robust *Teichichnus*) communities identified from these beds (Fig. 4.5A and B) (MacEachern and Pemberton, 1992), implying a post-storm colonization succession.

Ichnological Variability of the Upper Montney

Compared to some previous Upper Montney Member ichnological studies (e.g., Davies et al., 2018; Zonneveld et al., 2018), trace fossils identified from the Upper Montney in the study area are diminutive and low in abundance and diversity. This dataset is similar to the northern Montney where the Upper Montney Member was interpreted to be deposited within offshore to offshore

transition settings and ichnogenera were characterized by sporadic distributions (BI=0-4), diminutive in size, and low in diversity (Gegolick, 2017). There, the most common ichnogenera included *Teichichnus*, *Scolicia*, *Chondrites*, *Palaeophycus*, *Bergaueria* or *Lockeia*, and *Phycosiphon*, probably representing a distal *Cruziana* Ichnofacies (Gegolick, 2017). Similarly, the paucity of bioturbation within the Upper Montney, recording the deposition from offshore to lower shoreface, was reported by Playter (2013) in the Kobes area of northeastern British Columbia. Overall sporadic and rare trace fossils (e.g., *Planolites*, *Lingulichnus*) were interpreted to represent "doomed pioneers" possibly associated with storm-induced turbidity currents or hyperpycnal flows (Föllmi and Grimm, 1990; Playter, 2013).

It is accepted that trace fossils represent behaviors or responses by *in-situ* organisms to given sets of paleoecological parameters prevailing during deposition (Seilacher, 1964; Pemberton and MacEachern, 1995; Rindsberg, 2012; Furlong et al., 2018). Based on the above comparison, it is clear that the Upper Montney deposited in similar environments from different areas shows remarkable ichnological variability. As with the Lower Montney Member, this range of ichnological expressions is best explained as follows: 1. The more diverse expressions are similar to the relatively high-diversity trace-fossil assemblages identified locally in the Lower Montney Member that were interpreted as extinction refugia (Zonneveld et al., 2010a, 2010b); and, 2. For more restricted trace fossil assemblages, the epifaunal and infaunal communities had not been fully recovered from the end-Permian mass extinction event in Spathian and some of the conditions that led to the Permian extinction lingered into the Upper Montney Member timing of deposition.

CONCLUSIONS

The shoreface strata of the Upper Montney Member primarily consist of a thick succession of dolomitic, sharp-based, medium- to coarse-grained siltstone interbedded with bituminous fine-grained siltstone, presumably deposited under different intensities and frequencies of storm activities. In west-central Alberta, the Upper Montney is characterized by the interbedding of abundant thick, hummocky cross-stratified medium- to coarse-grained siltstone and few thin, planar to wavy-parallel laminated fine-grained siltstone, interpreted to represent the deposition within the moderately to strongly storm-dominated shoreface settings. In contrast, the Upper Montney within northeastern British Columbia displays a higher proportion of thick fine-grained,

planar to wavy-parallel laminated siltstone beds, with relatively fewer and thinner tempestites, suggesting that deposition might be controlled by fair-weather conditions.

The ichnological characteristics of the Upper Montney shoreface deposits exhibit remarkable variability between west-central Alberta and northeastern British Columbia, responding to the distinct hydrodynamic conditions. In west-central Alberta, persistent and strong storm reworking resulted in low intensity and diversity trace-fossil assemblages throughout the successions. Few thin, intensely bioturbated beds sporadically distributed within the lower shoreface mainly include *Phycosiphon*-dominated trace-fossil assemblages constructed by opportunistic organisms. As *Phycosiphon* are locally crosscut by the traces associated with the fair-weather infaunal communities (i.e., *Teichichnus*), it is interpreted that there were occasionally long periods of optimal conditions between storm activities conducive to the bioturbation. In northeastern British Columbia, the low hydrodynamic conditions contributed to relatively high bioturbation intensity and more diverse trace-fossil assemblages within the shoreface deposits. Commonly observed from the proximal lower shoreface, the continuous, thick, intensely bioturbated beds mainly including the elements of *Cruziana* Ichnofacies indicate temporally stable and favorable conditions promoting the flourishing of infaunal communities. In addition, alternating *Skolithos* and *Cruziana* Ichnofacies identified from the proximal lower shoreface also suggest alternations of relatively weak and infrequent storm influences.

In contrast to the hydraulic energy-stressed proximal lower shoreface, the impoverished, diminutive trace fossil assemblages within the distal lower shoreface are likely the result of oxygen deficiency. The distal lower shoreface in northeastern British Columbia are inferred to be more oxygen-stressed because the ichnogenera are much lower in abundance, diversity and smaller in diameter.

CHAPTER 5: INTERPRETING CRYPTIC ICHNOTAXA IN CORE: UPPER MONTNEY MEMBER, NORTHEASTERN BRITISH COLUMBIA

INTRODUCTION

Ichnology integrated with petrologic, sedimentologic and paleontologic data, has been proven to be a useful and necessary tool in formulating interpretations associated with sedimentology, environmental reconstruction, paleoecology and paleontology (Chamberlain, 1978; Ranger and Pemberton, 1991; Pemberton et al., 1992; MacEachern and Pemberton, 1994; Hubbard et al., 1999, 2004; McIlroy, 2004; Caplan et al., 2007; Mackay and Dalrymple, 2011; Knaust and Bromley, 2012; Botterill et al., 2015; Timmer, 2016a, 2016b). Generally, bioturbation is common in Phanerozoic sedimentary rocks, and many core-studies have provided analogues for the identification of ichnogenera, ichnospecies and various ichnofacies and ichnofabrics. Some early papers provide interpretive frameworks for trace fossil identifications in cores (e.g., Chamberlain, 1978; Frey and Pemberton, 1985; Gerard and Bromley, 2008; Knaust, 2017). However, there are still challenges applying ichnotaxonomy to core datasets, as the observation of the overall morphological characteristics are restricted by the 2-D cross-sectional views provided by core.

Abundant work has been done on ichnotaxonomy (e.g., Frey et al., 1978; Pemberton and Frey, 1982; Pickerill, 1994; Bertling, 2007; Gingras et al., 2011; Rindsberg, 2012; Rindsberg, 2018; Knaust, 2021), so that trace fossils can be clearly and repeatedly classified. Ichnotaxonomy mainly includes ichnogenus and ichnospecies as "working units" (Pemberton and Frey, 1982; Frey and Pemberton, 1985). Ichnospecies are erected upon a set of diagnostic morphological features.taphonomy (Bertling et al., 2006; Rindsberg, 2012; Rindsberg, 2018). For each new ichnospecies, at least one type specimen is designated so that it can be used as a basis for other similar trace fossils (Rindsberg, 2012). In contrast, ichnogenera are philosophically founded upon morphological features that are more highly ethologically significant (Pemberton and Frey, 1982; Frey and Pemberton, 1985; Rindsberg, 2012). Therefore, an ichnogenus is an abstraction of a range of ichnospecies (Rindsberg, 2012).

This study focuses on the challenge of ichnotaxonomic assignment and interpretation of trace fossils that are not readily classified to the ichnogenus or ichnospecies levels. Two Upper Montney Member (Montney Formation) cores are presented (4-9-84-22W6M and 16-6-81-17W6M) from northeastern British Columbia. The studied interval is characterized by common bioturbation. Although features such as meniscae or spreite may be locally observed, the overall poorly defined morphologies of the trace fossils make several taxonomic assignments difficult. This provides an opportunity to explore the ichnotaxonomic treatment and best practices for such trace fossils. This study takes the approach of morphologically classifying the ichnofossils and deriving ethological interpretations from the observed physical characteristics. As such, the study shows the potential of studying the distributions of these characteristic ichnofossils / ichnofabrics, even in the absence of a binomial taxonomic assignment.

STUDY AREA AND GEOLOGICAL SETTING

The cores selected for this study are located in northeastern British Columbia (4-9-84-22W6M and 16-6-81-17W6M) (Fig. 5.1). Since much of the Upper Montney in Alberta has been eroded, it is most commonly described from northeastern British Columbia (Zonneveld and Moslow, 2018). Generally speaking, the Upper Montney unconformably overlies the Altares Member of the Middle Montney, corresponding to the Smithian/Spathian boundary, and is unconformably overlain by the Middle Triassic strata of either the Doig Phosphate Zone or the Sunset Prairie Formation (Furlong et al., 2018; Zonneveld and Moslow, 2018) (Fig. 5.2). Lithologically, the Upper Montney is dominated by the interbedding of bituminous, dolomitic, fine- to coarse-grained siltstone and very fine-grained sandstone, as shown in the established type section within the core c-65-F/94-B-8 (2203-2374.5m) (Zonneveld and Moslow, 2018). Ichnologically, the Upper Montney is characterized by relatively diverse trace-fossil assemblages (Davies et al., 2018; Zonneveld and Moslow, 2018).
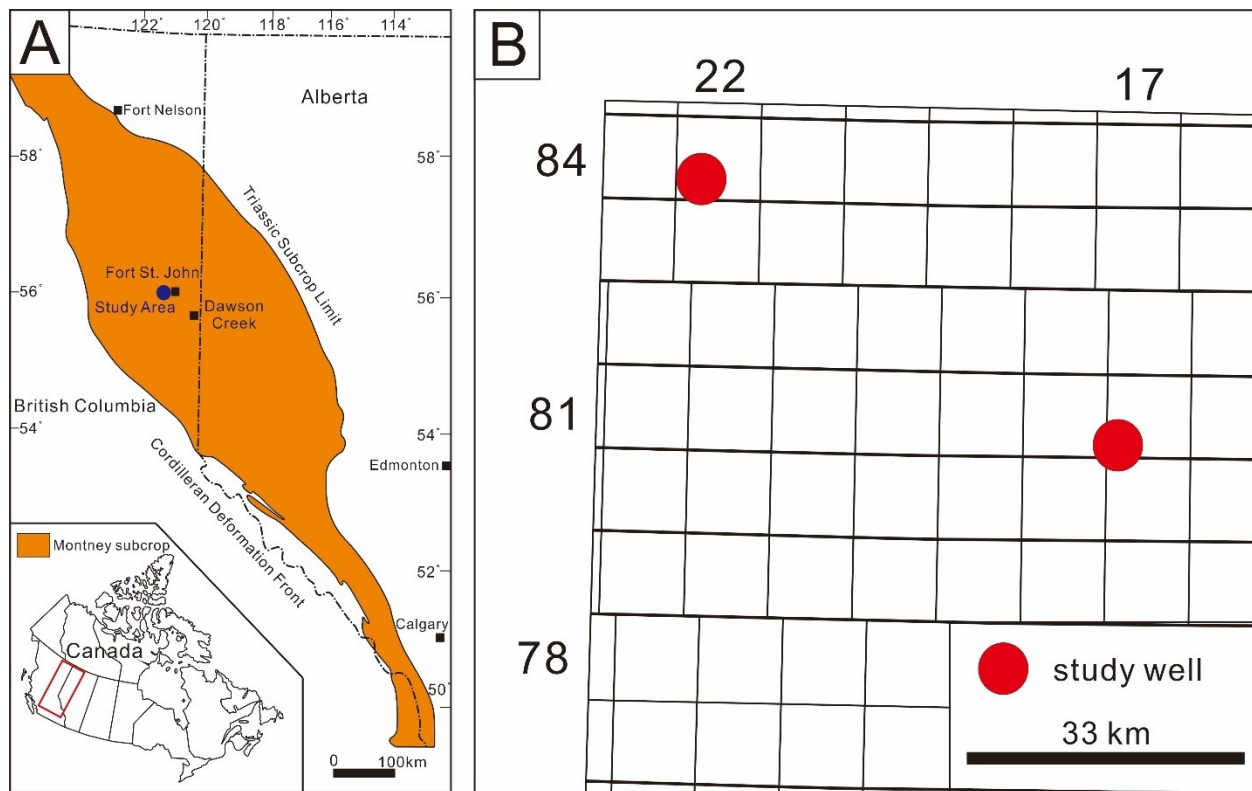
Figure 5.1-Location map of the study area (A) and study wells (B) (after Wood et al., 2018).
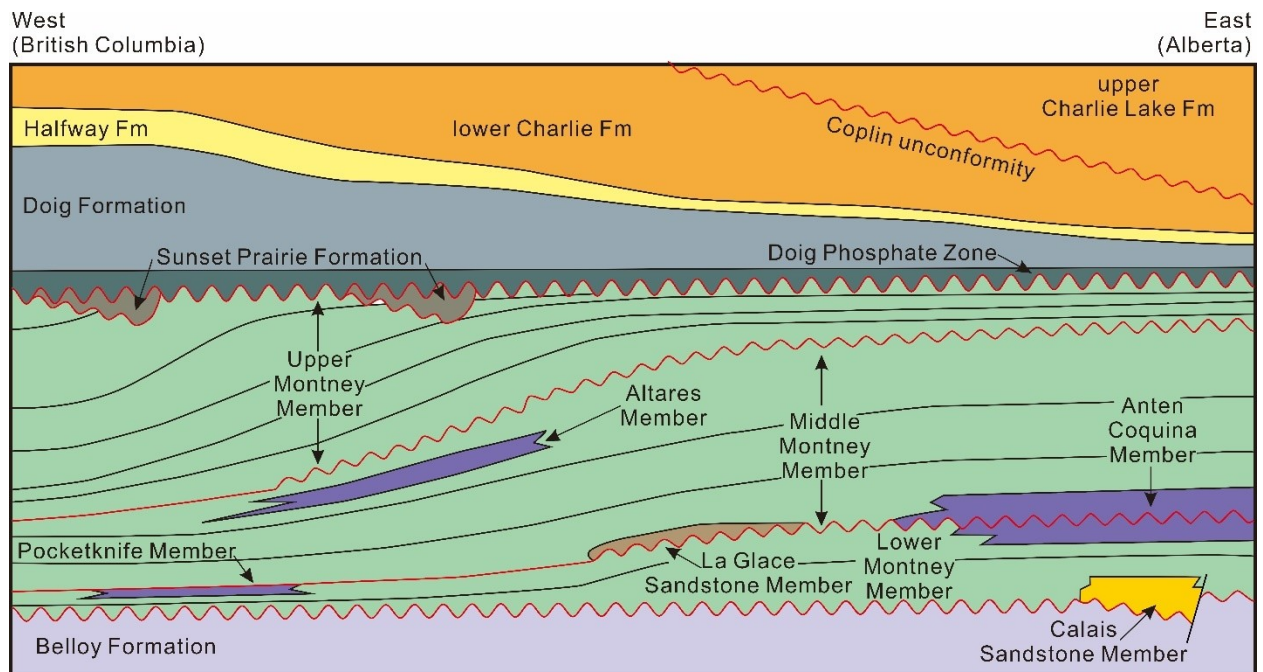
Figure 5.2-Schematic diagram of the Montney stratigraphy, British Columbia to Alberta, exhibiting three unconformity-bounded third-order depositional sequences (Lower, Middle and Upper member) (after Zonneveld and Moslow, 2018).

METHODOLOGY

Each core is logged using AppleCore◦ software and divided into facies primarily on basis of the core observations (e.g., lithology, nature of contacts, physical sedimentary structures, ichnological characteristics).

Bioturbation Index (BI) is used to report the bioturbation intensity, assessed following the schemes of Reineck (1967) and Taylor and Goldring (1993), where BI=0 represents unburrowed sediment and BI=6 represents complete homogenization of sediment. Previous studies have shown that the levels of BI can be used as a proxy for sedimentation rate (Ekdale and Bromley, 1991; Gingras et al., 1999; Taylor et al., 2003; Gingras et al., 2011).

Maximum burrow diameter (smallest axis in deformed burrows) and bioturbation diversity were also recorded for 1.0 m bins (Botterill et al., 2015). The size-diversity index (SDI) was obtained to quantitatively illustrate and compare the infaunal communities' responses to the changes in the environmental stresses (Hauck et al., 2009; Botterill et al., 2015; Timmer et al., 2016b). The size-diversity index was calculated by multiplying maximum burrow diameter by the diversity of identified trace-fossil assemblages for each 1.0 m interval. Burrow diameter and diversity are influenced by the chemical aspects of the sedimentary environment such as salinity and dissolved oxygen (Hauck et al., 2009). The BI and SDI data of the two cores were plotted against depth from the top of the Upper Montney.

The distribution of trace fossils is recorded, which primarily reflects the persistence and stability of environmental conditions in a depositional environment (Gingras et al., 2011). The Seilacherian ichnofacies and intergradations between archetypal ichnofacies further aided in the reconstruction of sedimentary environments (Seilacher, 1967; MacEachern et al, 2007a, 2007b; Gingras et al., 2011).

RESULTS AND INTERPRETATIONS

There are two facies identified from these two cores (Table 5.1). Facies 1 is characterized by highly bioturbated, bituminous, fine- to coarse-grained siltstone. Bioturbation is locally pervasive, and irregularly distributed. As a result of intense bioturbation, bedding features and physical sedimentary structures are commonly poorly defined. Facies 2 is composed of millimeter-scale, sharp-based medium- to coarse-grained siltstone laminae and lenses, which are commonly interlaminated with bituminous, wavy parallel to planar laminated, fine-grained siltstone. Compared with Facies 1, there are fewer thick medium- to coarse-grained siltstone beds (centimeter- to decimeter-scale) within Facies 2. The stacking pattern of the facies is shown in Figure 5.3, 5.4, and 5.5. Vertically, Facies 1 (highly bioturbated, bituminous, fine- to coarse-grained siltstone) is commonly interbedded with Facies 2 (bituminous, wavy parallel to planar laminated, fine-grained siltstone interlaminated with medium- to coarse-grained siltstone laminae and lenses).

FACIES	LITHOLOGY	BEDDING	PHYSICAL SEDIMENTARY STRUCTURE	DEP. ENVIRONMENT
1	Highly bioturbated, bituminous, fine- to coarse-grained siltstone	Sharp based; ungraded; cm to dm-scale tempestites; Bedding or lamination are commonly disturbed by trace fossils; Beds displaying homogeneously distributed bioturbation can be up to 8.7 m in thick	Wavy parallel lamination; combined flow ripples; lenticular bedding; rippled lamination; scour and fill structures; truncation; load cast; soft sediment deformation; dewatering structure	Proximal lower shoreface
2	Interlaminated dolomitic, medium- to coarse-grained siltstone and bituminous, fine-grained siltstone	Sharp based; ungraded; mm-scale beds or laminae associated with storms; In British Columbia, highly deformed intervals are locally common (0.9-11.9 cm in thick)	Wavy parallel lamination; planar lamination; lenticular bedding; load cast; scour and fill structure; current ripples; convolute bedding; soft sediment deformation; microfault; dewatering structure	Distal lower shoreface

Table 5.1-Summary of the facies characteristics of the shoreface successions within the Upper Montney in the northeastern Columbia.
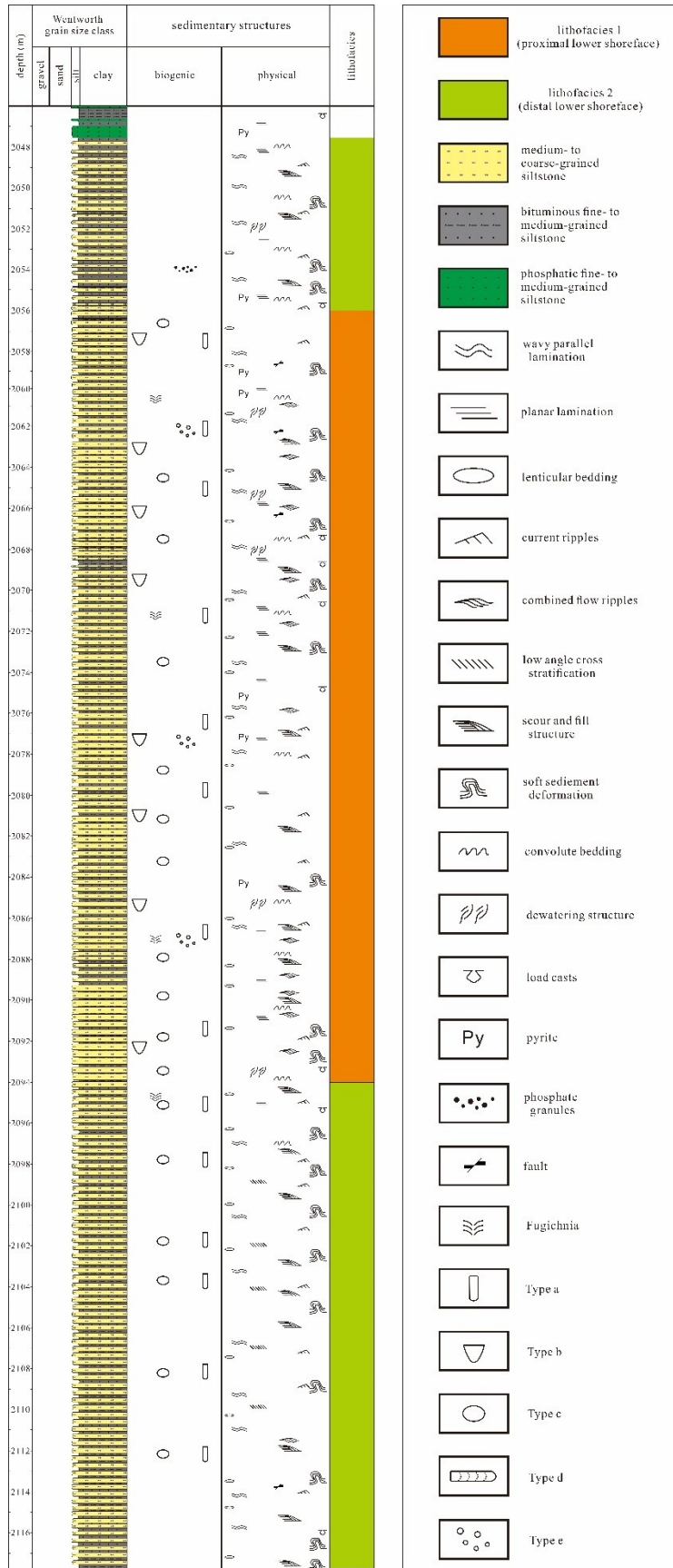
Figure 5.3-Core description for the well 16-6-81-17W6M (2047.66-2117.72 m).
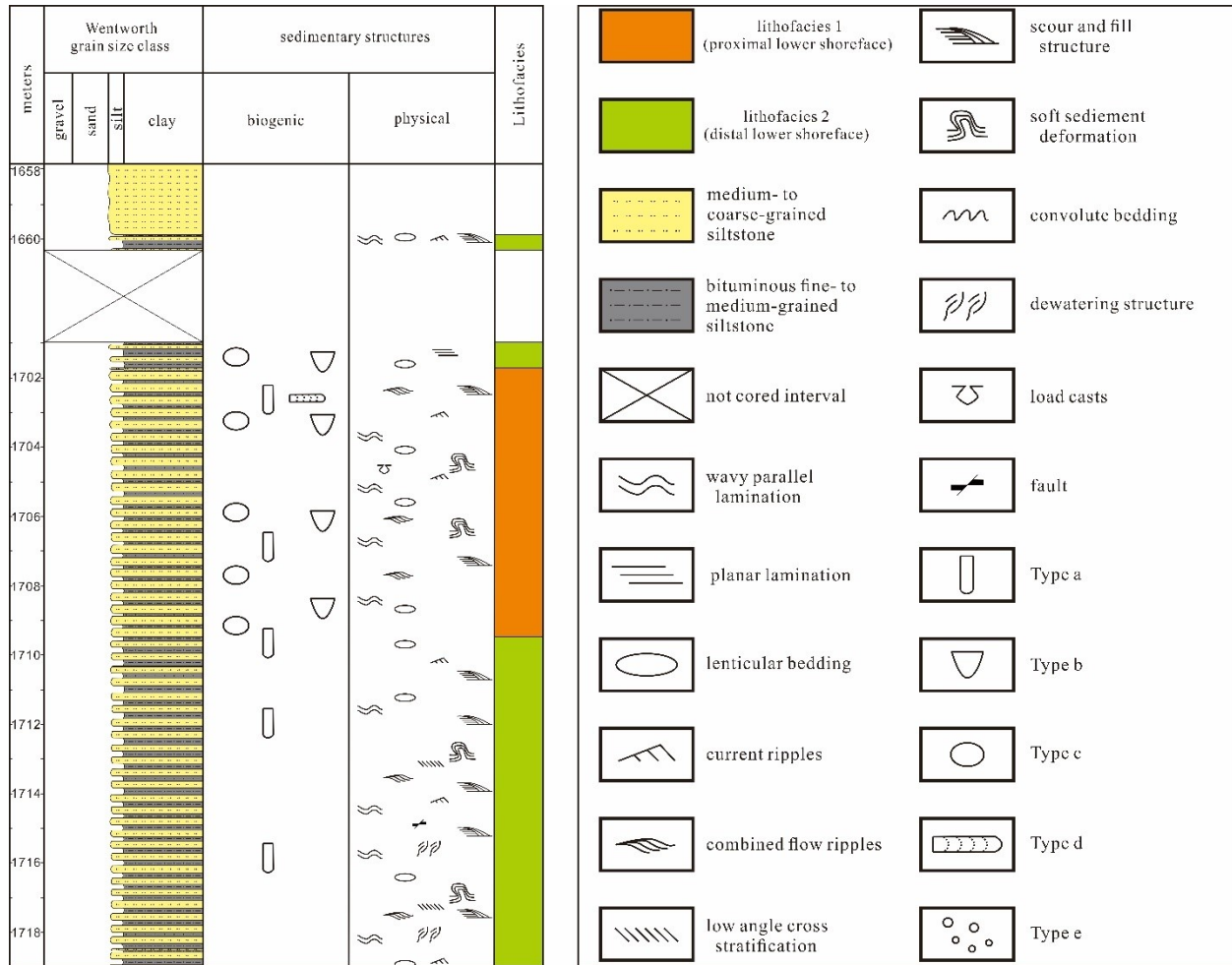
Figure 5.4-Core description for the well 4-9-84-22W6M (1659.84-1660.35 m and 1701.00-1719.00m).
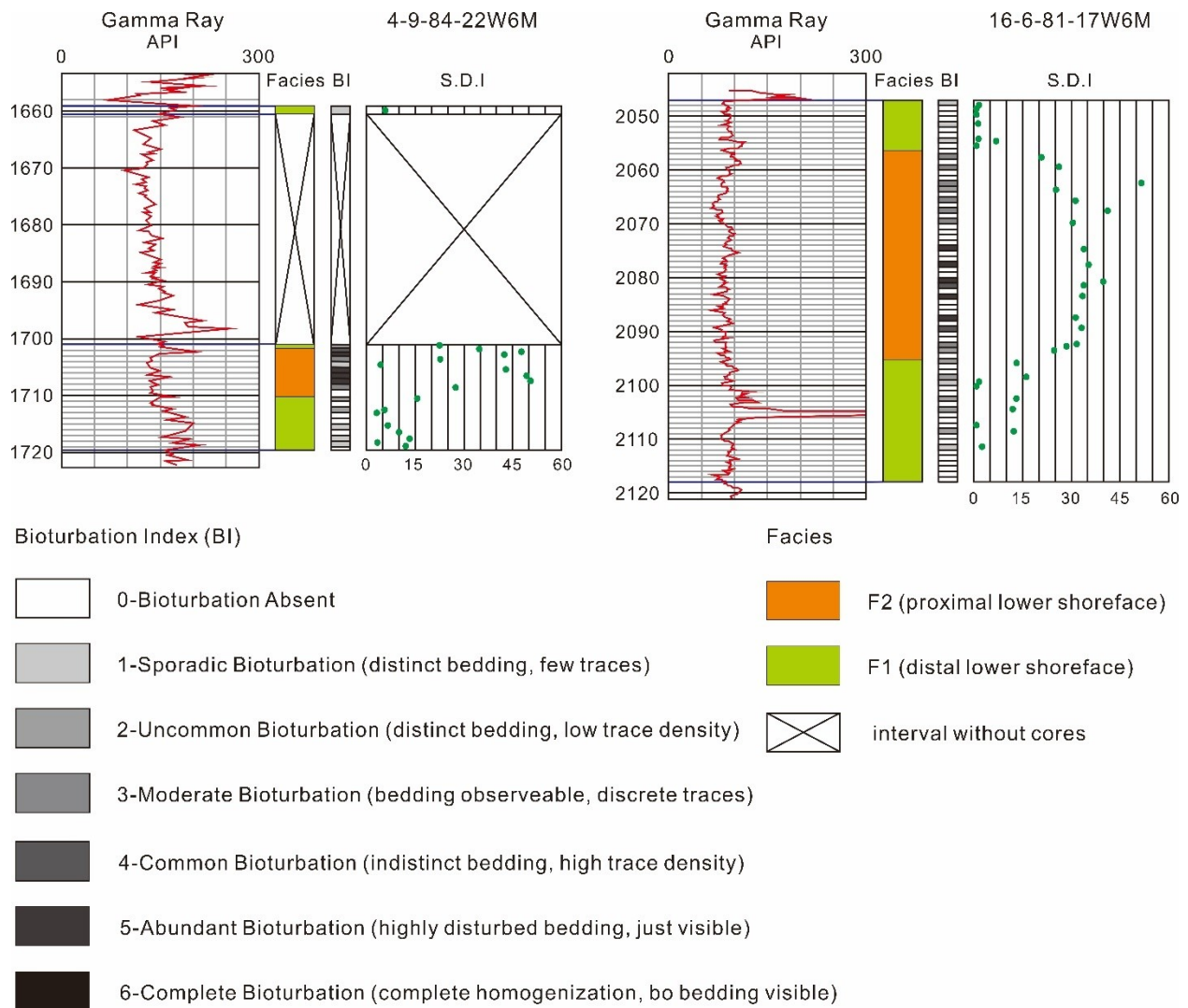
Figure 5.5-Cross-section of the study cores in the northeastern British Columbia summarizing the characteristics and trends in Size-Diversity Index (SDI) and Bioturbation Index (BI).

Sedimentological Interpretation

The interpretation of Facies 1 and 2 is based on the comparison between these two facies. Although most bedding features and physical sedimentary structures of the Facies 1 were destroyed by bioturbation, combined flow ripples, wavy parallel lamination, scour and fill structures, and load casts are commonly identified from the discernible, relatively thick, medium-to coarse-grained siltstone beds (tempestites). So, Facies 1 is interpreted to represent the deposition

within the proximal lower shoreface, under intermittent storm influences. Facies 2 differs from Facies 1 by the dramatic decrease in the thickness and abundance of medium- to coarse-grained siltstone beds (tempestites). In addition, the absence of high-energy sedimentary structures and the pervasive lenticular bedding indicate the deposition was associated with a quiescent environment, possibly around the fair-weather wave base (Zonneveld et al., 2010b). Thus, Facies 2 is interpreted to represent the distal lower shoreface.

As the dolomitic, medium- to coarse-grained siltstone beds or laminae commonly show load casts, hummocky cross-stratification, wavy parallel lamination, combined flow ripples, rippled lamination, scour and truncation, they are interpreted as tempestites formed by storm waves. While the bituminous, fine-grained siltstone beds or laminae characterized by planar lamination are interpreted to be the products of suspension deposition under fair-weather conditions. On the basis of the amount and thickness of the tempestites, the Upper Montney in the studied cores are interpreted to be deposited within the fair-weather dominated shoreface settings (MacEachern and Pemberton, 1992). Fewer and thinner dolomitic coarser siltstone beds imply there were only weak influences of storm waves. Relatively weak hydraulic conditions facilitated the colonization of benthos, which is consistent with the intense bioturbation identified from the cores. It is worth mentioning that in two cores, the black, sharp-based, thin mudstone laminae (ranging from 0.1 to 1.0 cm thick) are locally present within Facies 1, inferred to be deposited by the low-density turbidity currents. The thickest bed (approximately 7cm) concentrated by these mudstone laminae is identified from well 4-9-84-22W6M (Fig. 5.6B). Soft sediment deformation and dewatering structures are quite common in Facies 1 and 2, with contorted to convolute beds up to 16.2 cm thick (Fig. 5.6A and C).
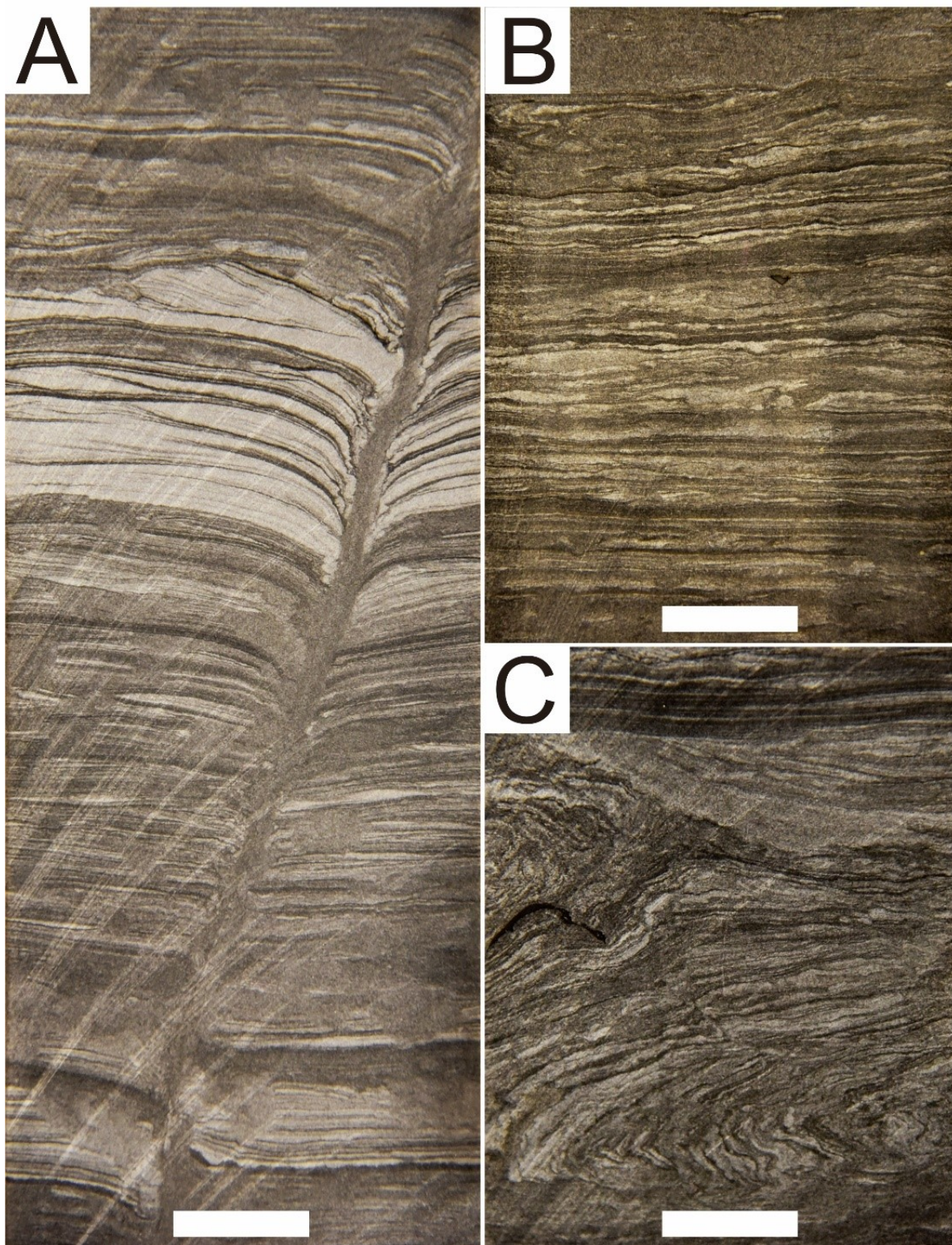
Figure 5.6-Core photographs of locally common dewatering structures, beds frequently interfered by low-density turbidity currents and contorted to convolute beds in Facies 1 and 2, northeastern

British Columbia. Scale bars for core photos = 2 cm. **A.** Facies 1, deformed beds caused by the large dewatering structure and trace fossils become fewer in this bed. 16-6-81-17W6M; 2092.39 m. **B.** Facies 1, abundant thin (ranging from 0.1 to 1.0 cm), grey to black, sharp-based mudstone laminae interpreted as the products of low-density turbidity currents. It is noted that ichnogenera are almost absent within this interval. 4-9-84-22W6M; 1704.60 m. **C.** Facies 2, highly contorted to convolute bed characterized by impoverished bioturbation. 16-6-81-17W6M; 2100.40 m.

Ichnology

Owing in part to a lack of grain-size variability, trace fossils observed in both cores are poorly defined, making it difficult to determine the specific ichnospecies or ichnogenera. An alternative approach to the ichnotaxonomy is used here, which is classifying trace fossils into types primarily based on their discernible orientation and shape. Herein, five types of trace fossils (Type a, b, c, d and e) are recognized (Table 5.2; Fig. 5.7).

Diagnoses of Ichnofossil Types

Type a and b

Description

Type a (Fig. 5.7A, B, C, F, and G) trace fossils are vertical to inclined and club shaped. In Facies 1, burrow diameters are up to 11.1mm, respectively. There is an obvious decrease in the abundance and size of Type a in Facies 2, with the diameter smaller than 4.1 mm. Burrow fills are massive-appearing and there is no observable lining. Type a is generally observed in the medium- to coarse-grained siltstone beds or laminae (tempestites) that show cross-lamination. Isolated occurrences are typical for Type a, although multiple burrows associated with a bedding plane are occasionally observed. Type b structures are dominantly vertical to slightly inclined and funnel shaped. The diameter of the burrows gradually tapers downward. In Facies 1, burrows of Type b are commonly larger in size than Type a, up to 15.5 mm in diameter. The infill is massive appearing and the lining is indiscernible. In terms of distribution, the majority of Type b is present in the coarser siltstone beds or laminae within the Facies 1, with only sporadic small burrows (smaller

than 4.7 mm in diameter) being reported from the Facies 2. Like Type a, Type b generally exhibits top-down bioturbation that commonly penetrates through the bed or lamina where they originate. Burrows of Type b are generally observed individually.

Remarks

Based on the burrow's appearance as passively infilled features descending from the sediment-water interface, these burrows are best considered to be domiciles of filter-feeding or interface-deposit feeding animals. As such, Types a and b belong to the distal *Skolithos* and proximal *Cruziana* Ichnofacies, largely dominated by structures constructed by suspension feeders, passive carnivores and deposit feeders, but also include some feeding and grazing structures (MacEachern et al., 2009). These mixed trace-fossil assemblages commonly correspond to moderate to high energy, sandy settings. The tracemakers penetrate deeply so that they avoid the unfavourable effects brought by the instability of the shifting substrate surface (MacEachern et al., 2009). Trace-fossil assemblages belonging to *Skolithos* Ichnofacies and containing passively infilled domichnia were similarly preserved in the storm-derived "lam-scram" beds of the Upper Cretaceous Cardium Formation of Alberta, Canada (Pemberton and Frey 1984; Vossler and Pemberton 1988; Pemberton and MacEachern 1996).

Type c

Description

Type c (Fig. 5.7A, C, D, E, and F) is a collection of circular to elliptical, unlined burrows that are usually truncated. Individual burrows vary in size, commonly ranging from 5.7 mm to 14.9 mm in diameter. Overall, the burrow fill is apparently structureless, with very few exhibiting vaguely meniscate and meandering infill. A significant difference between Type c and Type a and b is the distribution. Unlike Type a and b, large quantities of Type c are observed in the bituminous fine-grained siltstone layers. In contrast to Type a and b, burrows of Type c occur in greater densities, locally resulting in poorly defined isolated burrows. It is noted that the distribution of Type c tends to be sporadic where the bituminous fine-grained siltstone beds are thinner or where the interlamination of finer and coarser siltstone is well developed. Nevertheless, there are a few

small-sized examples (smaller than 6.8 mm in diameter) of Type c scattered in Facies 2, mostly associated with the bituminous fine-grained siltstone beds.

Remarks

Rare preservation of meniscae in circular to elliptical burrows points towards active backfilling by the tracemaker. Common truncation implies that although infaunal, the burrows occupied a very shallow tier. In some ways, Type c are similar to *Scolicia*, a deposit-feeding structure that is generally included in the *Cruziana* Ichnofacies. Trace fossil assemblages of the archetypal *Cruziana* Ichnofacies generally record activities of mobile deposit feeders and carnivores searching for food and feeding from the relatively nutritious, fine-grained deposits in lowered energy, shallow marine environments (Pemberton and MacEachern 1996; Furlong et al., 2018). Relatively cohesive and organic-rich substrates and reduced energy levels facilitate organisms to burrow horizontally instead of vertically (MacEachern et al., 2009). Zonneveld et al. (2010b) reported the *Cruziana* Ichnofacies within the Lower Montney strata in the Pedigree-Ring/Border-Kahntah River area, Canada. Low-diversity assemblages present in the storm-generated heterolithic succession are dominated by feeding traces and dwelling burrows of indigenous infaunae, mainly including *Planolites*, *Helminthopsis*, *Rhizocorallium* and *Treptichnus* (Zonneveld et al., 2010b). It is highlighted that the ichnogenera of the *Cruziana* Ichnofacies identified from both Upper and Lower Montney are low in diversity, which may be attributed to poorly oxygenated conditions and, to a lesser degree, elevated hydraulic energies (Zonneveld et al., 2010b; Feng et al., 2021). Moreover, it has been suggested that *Scolicia* are closely associated with reduced energy environments, such as the fair-weather periods on the lower shoreface and in the proximal offshore (Fu and Werner, 2000).

Type d

Description

Burrows of Type d (Fig. 5.7D) are elongate, sub-horizontal to horizontal tunnels. The trace fossil mm-scale meniscate. Due to a lack of grain-size variability, the meniscate can be very vaguely defined. The trace fossil is unlined. Type d maybe an elongate view of Type c, although the observed examples of Type d are smaller: burrow diameters are approximately 4.2 mm on

114

average. The orientations of the burrows are oblique to parallel to the bedding. As with Type c, Type d bears some similarities to the ichnogenus *Scolicia*, including the coarse but regular meniscate and the somewhat variable pathway that the burrow takes through the sediment with small and abrupt shifts in direction.

Remarks

As with Type c, Type d burrows are comparable to *Scolicia*, a deposit feeding trace commonly showing meniscate backfills (Hammersburg et al., 2018) (see Remarks Type c).

Type e (*Planolites* isp.)

Description

Burrows of Type e (Fig. 5.7A, B, and E) comprise diminutive, circular/elliptical (in cross-section) to irregular infilled tunnels (approximately 1.1 to 1.4 mm in diameter on average). These structures are rare and sporadically distributed within the medium- to coarse-grained siltstone beds of Facies 1 and 2. Type e trace fossils commonly occur in clusters, occasionally reborrowing pre-existing traces. Structureless burrow fills commonly contrast with the host sediment.

Remarks

As the burrows have unlined walls and the structureless backfills are different from the host matrix in lithology, Type e are referred to the ichnogenus *Planolites* which are interpreted to be constructed by the mobile organisms mainly through deposit-feeding activities (Nicholson 1873; Pemberton and Frey 1982; Shahkarani et al., 2017). Trace-makers of *Planolites* are reported to reborrow many other kinds of traces, probably because the pre-existing burrows provided easier path for new burrowing activities or were enriched with nutrients (e.g., Frey and Chowns 1972; Frey and Seilacher 1980; Pemberton and Frey 1982).

Ichnofossil Type	Description	Remarks (also see Diagnosis)
a	• Vertical to inclined, club shaped, unlined burrows; • Top-down bioturbation; commonly crosscut laminae or beds; • The infill is typically structureless; • Burrow diameters up to 11.1 mm in Facies 1 and smaller than 4.1 mm in Facies 2.	attributable to distal *Skolithos* to proximal *Cruziana* ichnofacies, representing dwelling burrows of suspension-feeding organisms.
b	• Vertical to inclined, funnel shaped, unlined burrows; • Burrows are obviously tapering; • Top-down bioturbation; commonly penetrate through laminae or beds; • The infill is typically structureless; • Burrow diameters up to 15.5 mm in Facies 1 and smaller than 4.7 mm in Facies 2.	attributable to distal *Skolithos* to proximal *Cruziana* ichnofacies, representing dwelling burrows of suspension-feeding organisms.
c	• Circular to elliptical unlined burrows, usually truncated; • The infill is occasionally vaguely meniscal and meandering; • Commonly ranging from 5.7 mm to 14.9 mm in diameter in Facies 1. In Facies 2, burrow diameters are generally smaller than 6.8 mm.	attributable to *Cruziana* ichnofacies, representing feeding burrows of deposit-feeding organisms; may be comparable with the *Scolicia*.
d	• Elongate, subhorizontal to horizontal, unlined burrows; • Meniscate backfills are indistinct; • Burrows are oblique or nearly parallel to the bedding; • Burrow diameters are about 4.2 mm on average.	attributable to *Cruziana* ichnofacies, representing feeding burrows of deposit-feeding organisms; may be comparable with the *Scolicia*.
e	• Appears as diminutive, circular/elliptical to irregular dots; • Infill always contrasts with host sediment; • Occasional reburrowing other burrows; • Approximately 1.1 to 1.4 mm in diameter on average.	*Planolites*-like trace fossils may be interpreted as feeding burrows of deposit feeders.

Table 5.2-Summary of ichnological attributes of the Upper Montney in northeastern British Columbia.
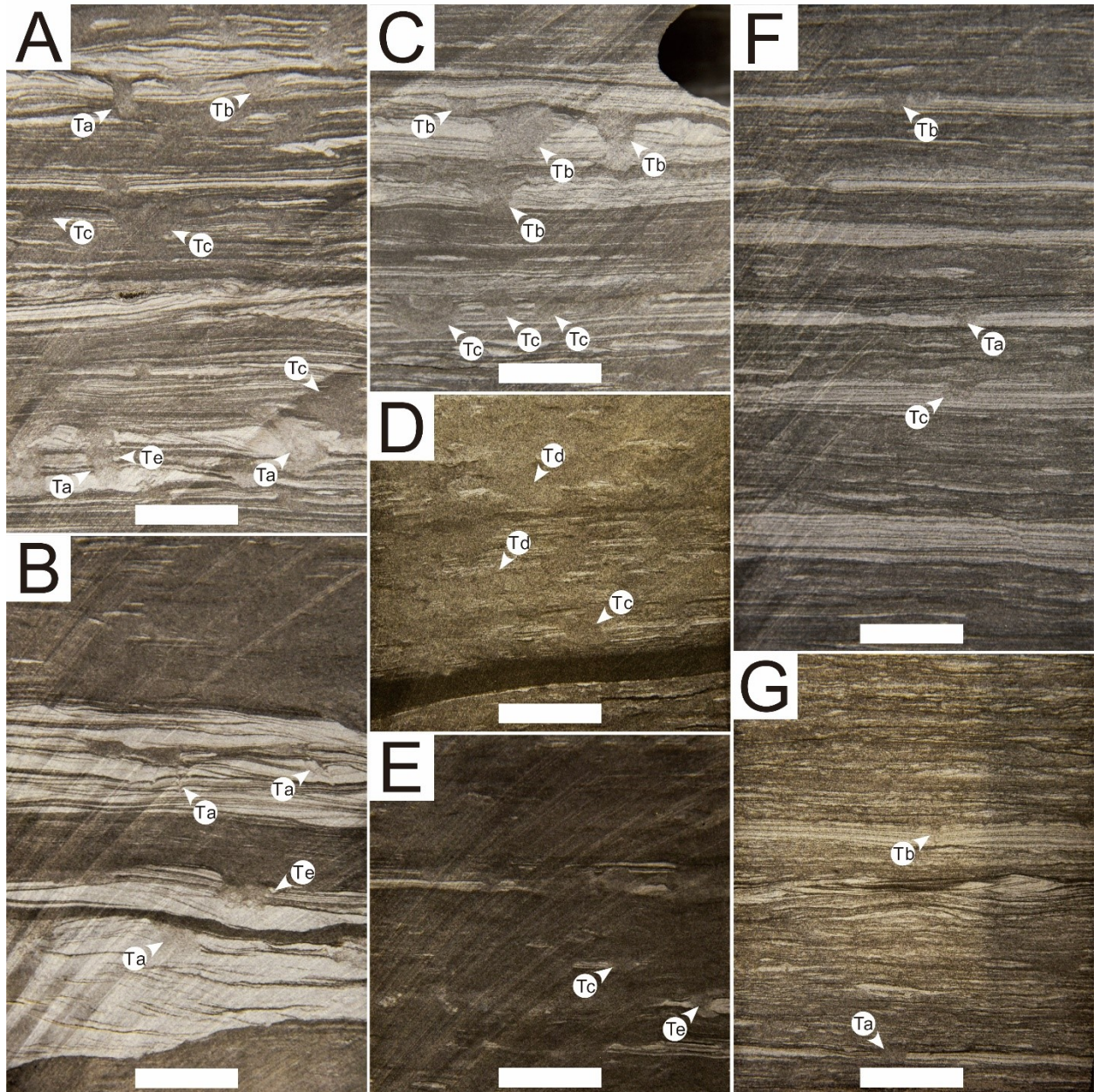
Figure 5.7-Core photographs of trace-fossil types within the shoreface successions of the Upper Montney, northeastern British Columbia. Scale bars for core photos = 2 cm. **A.** Facies 1, sharp-based, wavy parallel laminated medium- to coarse-grained siltstone interbedded with bituminous fine- to coarse-grained siltstone (BI=3). Type a and b always show top-down bioturbation within the coarser siltstone beds and commonly penetrate through these beds. It is noted that one trace of Type a was reborrowed by Type e. Type c are commonly identified within the bituminous finer siltstone beds or laminae. 16-6-81-17W6M; 2062.28 m. **B.** Facies 1, relatively thick medium- to

coarse-grained siltstone beds (BI=1-2) are characterized by combined flow ripples, scour and wavy parallel lamination, including small burrows attributable to Type a. Type e are identified to reborrow the pre-existing trace fossil. The bituminous fine-grained siltstone beds are intensely bioturbated (BI=5-6), with most physical sedimentary structures indiscernible. Specific trace-fossil types are difficult to discern because of the lack of grain-size variability. 16-6-81-17W6M; 2087.25 m. **C.** Facies 1, multiple burrows of Type c apparently truncated are distributed along a certain horizon within the interlamination of medium- to coarse-grained siltstone and bituminous fine-grained siltstone (BI=2-3). Bioturbation in the thicker coarser siltstone beds is dominated by Type b (BI=2). 16-6-81-17W6M; 2067.81 m. **D.** Facies 1, the characteristic intensely bioturbated bed show thorough bioturbation (BI=5-6). Most of the ichnogenera are difficult to determine, except few Types c and d. The thin, sharp-based, black mudstone bed is only slightly bioturbated on the top, presumably representing the deposits of the low-density turbidity currents. 4-9-84-22W6M; 1702.60 m. **E.** Facies 1, intensely bioturbated bed (BI=5-6). The bedding features and physical sedimentary structures are almost completely overprinted due to the homogeneously distributed bioturbation. 16-6-81-17W6M; 2077.81 m. **F.** Facies 2, bioturbation of the interbedding of medium- to coarse-grained siltstone and bituminous fine-grained siltstone is low (BI=1). Only scarce trace fossils, largely Types a, b, and c, are identified from the top of the thin medium- to coarse-grain beds or laminae. And compared to their counterparts in the Facies 3, they are extraordinarily small in diameter. 16-6-81-17W6M; 2104.39 m. **G.** Facies 2, trace fossils are almost absent (BI=1). Top-down bioturbation shown by the thin medium- to coarse-grained siltstone beds are closely associated with few diminutive traces of Type a, b. 4-9-84-22W6M; 1716.32 m.

Trace Fossil Distributions and Size Trends

Generally, all the trace fossil types are unlined. Diversity and the intensity of bioturbation are comparably high and burrow diameters are also quite large, especially in Facies 1. Facies 1 exhibits the highest SDI (23.0-52.0) and BI (greater than 3.0, commonly 4 to 6) values vertically (Fig. 5.5). Besides, in Facies 1, the bioturbation intensity of the bituminous fine-grained siltstone beds is so high (BI=4-6) that most bedding features are indiscernible (Fig. 5.7B). Trace fossils identified are largely Type c (Fig. 5.7A and C). In contrast, medium- to coarse-grained siltstone beds show

relatively weaker bioturbation (BI=2-4), commonly displaying top-down bioturbation assemblages with trace fossils occasionally penetrating through the bed (Fig. 5.7A, B, and C). And the bioturbation is primarily associated with Types a and b, with only a few Type c and e observed. It is highlighted that there are some intervals (about 5.2 m in well 4-9-84-22W6M and 8.7 m in well 16-6-81-17W6M) in Facies 1 displaying homogeneously distributed bioturbation (BI=5-6), with trace-fossil types dominated by Types c, d, and e (Fig. 5.7D and E). In addition, the rare unburrowed beds are closely associated with dewatering structures and thin black mudstone laminae (Fig. 5.6A and B).

Both SDI and BI decrease gradually from Facies 1 to Facies 2 and the SDI and BI of Facies 2 are largely smaller than 15.0 and 3.0, respectively (Fig. 5.5). The distribution of trace fossils within Facies 2 is mostly sporadic, usually showing top-down bioturbation (BI=1-2) in the medium- to coarse-grained siltstone laminae (Fig. 5.7F and G). Commonly, most of the burrows are confined to the upper part of the laminae (Fig. 5.7G). Primary trace fossils include Type a, b, and very few Type c. As a result of weak bioturbation, bedding features and physical sedimentary structures are relatively distinct. It is noted that trace fossils are absent within several heavily contorted to convolute beds (Fig. 5.6C) in Facies 2. What's more, it is inferred that the few trace fossils that occur in the fine-grained siltstone beds are too small to identify.

Ichnological Interpretation

Overall, the sedimentological interpretation, which supports an interpretation of wave-influenced sedimentation in the lower shoreface or distal lower shoreface is collaborated by the trace fossil assemblage. Trace fossil types a through d represent a range of domicile, passive carnivory, suspension- and deposit-feeding associated trace fossils that sit solidly between the *Skolithos* and *Cruziana* Ichnofacies. Pemberton et al. (1992) first dealt with similar mixed assemblages by referring to assemblages where suspension feeding was subordinate and deposit feeding comparably dominant as the proximal *Cruziana* Ichnofacies. Where suspension feeding becomes more conspicuous, it is referred to as the distal *Skolithos* Ichnofacies. In this dataset, the assemblage varies somewhat such that the assemblage wavers between suspension- and deposit-feeding centered, the distal *Skolithos* Ichnofacies would normally be assigned to the middle

shoreface and the proximal lower shoreface (as summarized in MacEachern et al 2012). The proximal *Cruziana* expression suggests a distal lower shoreface to offshore affinity.

In this study, Facies 2 (distal lower shoreface) is comparably impoverished and most of the diverse bioturbation occurs in Facies 1 (proximal lower shoreface). Potentially an oxycline separates the proximal lower shoreface from the distal lower shoreface. Supporting this, in Facies 1 (proximal lower shoreface), burrow diameters (and the Size-Diversity Index) become relatively larger and both diversity and intensity of bioturbation are higher (Fig. 5.5).

DISCUSSION

The Problems with Ichnotaxonomy in these Core

The documented trace fossils do not represent idiomorphic examples of any established ichnogenera. On account of the overall poorly defined morphologies of the trace fossils, the ichnotaxonomy is done largely based on discernible features, that include burrow orientations, burrow shapes, burrow walls and linings, burrow infill, and the presence of indistinct meniscate or spreite. Importantly, the lithology of the Upper Montney in the studied cores is dominated by siltstone, and it is in part the lack of grain-size variability that leads to the vague morphologies of trace fossils.

However, the absence of a taxonomic framework need not hinder ethological interpretations of the trace fossils. In this framework, each trace-fossil type is interpreted to represent a group of biogenic sedimentary structures that share ethological affinities. It bears noting that like specific ichnospecies or ichnogenera, ichnological data can also be gathered from the identified 'types' to interpret the physico-chemical stresses in sedimentary environments, such as size and diversity data as shown in this study. What's more, most of the identified types preferentially occur in either finer or coarser siltstone beds. Thus, these types can potentially be fitted into the Seilacherian ichnofacies or ichnofabric concepts.

The Upper Montney and Post Extinction Conditions

The end-Permian extinction event was inferred to have a profound influence on deposition during the Early Triassic (Isozaki, 1997; Penn et al., 2018; Zonneveld and Moslow, 2018). One of the most significant causes for the extinction is inferred to be the development of globally pervasive shallow-marine anoxic conditions (Hallam, 1991; Wignall and Hallam, 1992; Wignall and Twitchett, 1996, 2002a, 2002b; Hayes et al., 2007). The prolonged anoxic conditions extended into the Middle Triassic in many areas, postponing faunal recovery (Wignall and Twitchett, 1996, 2002a, 2002b; Zonneveld et al., 2010b). However, it is reported that the post-extinction recovery of marine ecosystems in the Early Triassic is recorded starting from the Spathian, mostly under shallow-marine environments with increased oxygen levels (Twitchett et al., 2004). This is in part supported by trace fossil assemblages identified from the Upper Montney in the study area.

On the basis of the aforementioned sedimentological analysis, the deposition of the Upper Montney in the study area was subject to weak and infrequent storm activities (MacEachern and Pemberton, 1992). The proximal lower shoreface is characterized by relatively high bioturbation intensity and diverse trace-fossil assemblages (Fig. 5.5), suggesting lowered environmental stress. The common presence of beds showing homogeneously distributed bioturbation, with most trace fossils attributable to the *Cruziana* Ichnofacies, is further indicative of temporal persistence of stable, optimum conditions, which is consistent with the environments dominated by fair-weather conditions. These intensely bioturbated beds usually grade into interbeds exhibiting overall weaker bioturbation, presumably deposited under relatively strong and frequent storm influences. Within these interbeds, thin tempestites mainly consist of sporadically distributed dwelling burrows and subordinate deposit-feeding structures, assigned as distal *Skolithos* to proximal *Cruziana* Ichnofacies. While the thicker fair-weather beds were heavily bioturbated by deposit feeders, with the predominant trace fossil assemblages attributable to *Cruziana* Ichnofacies. Thus, although there were increased storm influences during the deposition of these weakly bioturbated interbeds, the recurring *Skolithos* and *Cruziana* Ichnofacies, as well as preservation of thick fair-weather deposits still suggest that the overall hydraulic energies are low (MacEachern and Pemberton, 1992; MacEachern et al., 2009).

As the distal lower shoreface was only affected by occasional weak storm waves, the remarkable reduction in bioturbation is primarily attributed to anoxic conditions, which may reflect that in Spathian, locally, oxygen level of distal shoreface settings has not been fully recovered from the anoxic conditions caused by the end-Permian mass extinction. In addition, throughout

121

the shoreface in the study area, bioturbation was locally suppressed by low-density turbidity currents, dewatering processes, and soft-sediment deformation during the deposition of the Upper Montney. Finally, as bioturbation is the most robust within the proximal lower shoreface, it is inferred that there was a spatially limited hospitable habitat where the bottom water was well-oxygenated, and the storm-associated hydraulic energies were low enough for infaunal colonization during deposition in northeastern British Columbia.

CONCLUSIONS

The shoreface strata of the Upper Montney Member primarily consist of a thick succession of dolomitic, sharp-based, medium- to coarse-grained siltstone interbedded with bituminous fine-grained siltstone. The Upper Montney within northeastern British Columbia displays a higher proportion of thick fine-grained, planar to wavy-parallel laminated siltstone beds, with relatively fewer and thinner tempestites, suggesting that deposition might be controlled by fair-weather conditions.

In northeastern British Columbia, the low hydrodynamic conditions contributed to relatively high bioturbation intensity and more diverse trace-fossil assemblages within the shoreface deposits. Commonly observed from the proximal lower shoreface, the continuous, thick, intensely bioturbated beds mainly including the elements of the *Skolithos* and *Cruziana* ichnofacies indicate temporally stable and favorable conditions promoting shoreface-associated infaunal communities. In addition, alternating distal *Skolithos* and proximal *Cruziana* Ichnofacies identified from the proximal lower shoreface also suggest alternations of relatively weak and infrequent storm influences, with much colonization occurring during fair-weather conditions.

In contrast to the hydraulic energy-stressed proximal lower shoreface, the impoverished, diminutive trace fossil assemblages within the distal lower shoreface are likely the result of oxygen deficiency. The distal lower shoreface in northeastern British Columbia are inferred to be more oxygen-stressed because the ichnogenera are much lower in abundance, diversity and smaller in diameter.

CHAPTER 6: CONCLUSIONS

This thesis focusses on shoreface to offshore examples of the Lower Triassic Montney Formation. The goal of this dissertation is three-fold: 1) divide and interpret the lithofacies representing the deposition of the upper shoreface/foreshore, middle shoreface, lower shoreface, offshore transition and offshore settings; 2) establish and compare the reservoir properties and lithofacies between the shoreface and offshore intervals; 3) interpret physico-chemical stresses resulting in the ichnological variability of the shoreface successions within the Upper Montney Member in northeastern British Columbia and west-central Alberta.

Chapter 2 and Chapter 3 suggest that the Montney Formation in the Puskwaskau Field and Shell Monias Field represents deposition on a wave- and storm-dominated, low-gradient, predominantly siliciclastic ramp settings. It is mainly composed of multicyclic, coarsening upwards successions of bituminous fine- to medium-grained siltstone, medium- to coarse-grained siltstone and very fine-grained sandstone. There are totally seven lithofacies identified in the study areas comprising a conformable shoaling-upwards sequence from the lower ramp setting (offshore) to upper shoreface/foreshore. Generally speaking, in the Puskwaskau Field, reservoir quality increases from the distal lower shoreface to middle shoreface because of an increase in grain size and sorting and decrease in the amount of clay, muscovite and microcrystalline pyrite framboids. The reservoir quality of the upper shoreface/foreshore is significantly reduced by authigenic pore-filling dolomite cements. The dolomite is present dominantly within the cleaner, coarser laminae or beds, significantly reducing the porosity. Winland plots are established to correlate the relationship between lithofacies and pore-throat radii, porosity and permeability distributions, demonstrating that lithofacies can be used to reliably estimate pore-throat radii and reservoir properties in the shoreface intervals.

However, on account of lithological similarities (mostly bituminous fine- to medium-grained siltstone interbedded or interlaminated with medium- to coarse-grained siltstone), 3 lithofacies (upper ramp, proximal lower ramp and distal lower ramp) identified from the Upper Montney Member in the Shell Monias area are characterized by similar and remarkably poor reservoir properties. The reasons for the low porosity and permeability are dominated by the pervasive dolomite cementation, with the subordinate factors including compaction, the presence of detrital clays and microcrystalline pyrite framboids. It is summarized that in contrast to the shallow marine

deposits showing strongly lithofacies-dependent reservoir properties, when getting away from the nearshore shoreface environments, overall reservoir properties of the Montney Formation are comparably predictable and less heterogeneous.

Pervasive bitumen within this Montney siltstone reservoir is inferred to be sourced from organic matter that accumulated in situ. This interpretation is supported by the positive correlation of TOC with illite and muscovite, and its negative correlation with detrital minerals such as quartz, calcite and dolomite. These trends indicate that the accumulation of TOC was associated with the deposition of finer grained sediments. In addition, the co-occurrence of TOC and pyrite suggests that anoxic to dysoxic conditions were present at the water-sediment interface during deposition or early diagenesis. Lastly, TOC and porosity are negatively correlated, suggesting that the bitumen was autochthonous, since allochthonous bitumen is expected to have TOC values that are higher in more porous rocks. These lines of evidence indicate that the Montney reservoir within the Shell Monias area is probably a self-sourcing reservoir.

Chapter 4 shows that in west-central Alberta, the shoreface strata of the Upper Montney Member primarily consist of a thick succession of dolomitic, sharp-based, medium- to coarse-grained siltstone interbedded with bituminous fine-grained siltstone, interpreted to represent the deposition within the moderately to strongly storm-dominated shoreface settings. Because of the persistent and energetic hydraulic conditions, the shoreface deposits of the Upper Montney are characterized by overall minimal bioturbation and sporadic distribution of trace fossil assemblages. Bioturbation index (BI) commonly ranges from 0 to 3 and Size-Diversity index (SDI) is generally less than 10, suggesting the intense environmental stresses.

Rare thin, intensely bioturbated beds (BI= 4-6; SDI occasionally higher than 125) within the lower shoreface mainly include *Phycosiphon*-dominant trace-fossil assemblages constructed by the opportunistic organisms. As the *Phycosiphon* are locally crosscut by the traces associated with the fair-weather infaunal communities (i.e., *Teichichnus*), it is interpreted that there were occasionally, relatively longer periods of optimal conditions between storm activities, conducive to the bioturbation. Since the storm influences are commonly lowered when closing to the mean storm wave base, the impoverished, diminutive trace fossil assemblages within the distal lower shoreface are likely the result of oxygen deficiency. So, during the Spathian, in the shallow part of shoreface settings, storm-associated strong hydraulic conditions played a key role in inhibiting the

colonization by organisms, while in the deeper area, the survival of epifauna was probably suppressed by the lowered levels of oxygen around the interface between sea water and sediment.

Chapter 5 indicates that in northeastern British Columbia, the deposition of the Upper Montney shoreface successions was subject to weak and infrequent storm activities. The overall optimal environments, especially the lowered hydraulic conditions contributed to bioturbation. Trace fossil assemblages are characterized by high intensity and diversity. The common presence of beds showing homogeneously distributed bioturbation (BI=5-6), with most trace fossils attributable to the *Cruziana* Ichnofacies, is further indicative of temporal persistence of stable, optimum conditions, which is consistent with the environments dominated by fair-weather conditions. The overall weaker bioturbation in the distal lower shoreface is also inferred to be led by oxygen deficiency.

In addition, a new method on how to work on ichnotaxonomy when morphologies of trace fossils are poorly defined is introduced in Chapter 5. Ichnofossils are classified as "Types" on the basis of their discernible features. And these identified types can also be used to interpret the physico-chemical stresses in sedimentary environments. What's more, most of the identified types preferentially occur in either finer or coarser siltstone beds. Thus, these types can potentially be fitted into the Seilacherian ichnofacies or ichnofabric concepts.

BIBLIOGRAPHY

Ager, D.V. 1973. The nature of the stratigraphical record. Wiley, New York, p. 114.

Aguilera, R. 2002. Incorporating capillary pressure, pore throat aperture radii, height above free-water table, and Winland r35 values on Pickett plots. The American Association of Petroleum Geologists Bulletin, v. 86, p. 605-624.

Aitken, J.D., 1993, Tectonic Framework; Subchapter 2D, in Stott, D.F., and Aitken, J.D., eds., Sedimentary Cover of the Craton in Canada: Geological Survey of Canada, Geology of Canada, v. 5, p. 45-54.

Algeo, T.J., Chen, Z.Q., Fraiser, M.L. and Twitchett, R.J. 2011. Terrestrial-marine teleconnections in the collapse and rebuilding of the Early Triassic marine ecosystem. Palaeogeography, Palaeoclimatology, Palaeoecology, v. 308, p. 1-11.

Al-shaieb, Z. and Shelton, J.W. 1978. Secondary ferroan dolomite rhombs in oil reservoirs, Chadra Sands, Gialo Field, Libya. The American Association of Petroleum Geologists Bulletin, v. 62, p. 463-468.

Alroy, J., Aberhan, M., Bottjer, D.J., Foote, M., Fursich, F.T., Harries, P.J., Hendy, A.J.W., Holland, S.M., Ivany, L.C., Kiessling, W., Kosnik, M.A., Marshall, C.R., McGowan, A.J., Miller, A.I., Olszewski, T.D., Patzkowsky, M.E., Peters, S.E., Villier, L., Wagner, P.J., Bonuso, N., Borkow, P.S., Breneis, B., Clapham, M.E., Fall, L.M., Ferguson, C.A., Hanson, V.L., Krug, A.Z., Layou, K.M., Leckey, E.H., Nurnberg, D., Powers, C.M., Sessa, J.A., Simpson, C., Tomasovych, A. and Visaggi, C.C. 2008. Phanerozoic trends in the global diversity of marine invertebrates. Science, v. 321, p. 97–100.

Armitage, J.H. 1962. Triassic oil and gas occurrences in northwestern British Columbia, Canada. Journal of the Alberta Society of Petroleum Geologists, v. 10, p. 35-56.

Arnarson, T.S. and Keil, R.G. 2007. Changes in organic matter-mineral interactions for marine sediments with varying oxygen exposure times. Geochimica et Cosmochimica Acta, v. 71, p. 3545-3556.

Baas, J.H., Best, J.L. and Peakall, J. 2015. Predicting bedforms and primary current stratification in cohesive mixtures of mud and sand. Journal of the Geological Society, v. 173, p. 12-45.

Barclay, J.E., Krause, F.F., Campbell, R.I. and Utting, J. 1990. Dynamic casting and growth faulting: Dawson Creek Graben Complex, Carbiniferous-Permian Peach River Embayment, Western Canada. Bulletin of Canadian Petroleum Geology, v. 38A, p. 115-145.

Basilici, G., de Luca, P.H.V. and Poiré, D.G. 2012. Hummocky cross-stratification-like structures and combined-flow ripples in the Punta Negra Formation (Lower-Middle Devonian, Argentine Precordillera): a turbiditic deep-water or storm-dominated prodelta inner-shelf system? Sedimentology Geology, v. 267, p. 73-92.

Baucon, A., Ronchi, A., Felletti, F. and De Carvalho, C. N. 2014. Evolution of crustaceans at the edge of the end-Permian crisis: ichnonetwork analysis of the fluvial succession of Nurra (Permian-Triassic, Sardinia, Italy). Palaeogeography, Palaeoclimatology, Palaeoecology, v. 410, p. 74-103.

Beatty, T.W., Zonneveld, J.-P. and Henderson, C.M. 2008. Anomalously diverse Early Triassic ichnofossil assemblages in northwest Pangea: A case for shallow-marine habitable zones. Geology, v. 36, p. 771-774.

Bednarz, M. and McIlroy, Duncan. 2009. Three-dimensional reconstruction of "*Phycosiphoniform*" burrows: Implications for identification of trace fossils in core. Paleontologia Electronica, v. 12, p. 1-15.

Benton, M.J. and Twitchett, R.J. 2003. How to kill (almost) all life: The end-Permian extinction event. Trends in Ecology and Evolution, v. 28, p. 358-365.

Beranek, L.P. and Mortensen, J.K. 2007. Investigating a Triassic overlap assemblage in Yukon: On-going field studies and preliminary detrital-zircon age data. In: Yukon Exploration and Geology 2006, D.S. Emond, L.L. Lewis and L.H. Weston (eds.), Yukon Geological Survey, p. 83-92.

Beranek, L.P., Mortensen, J.K., Lane, L.S., Allen, T.L., Fraser, T.A., Hadlari, T. and Zantvoort, W.G. 2010. Detrital zircon geochronology of the western Ellesmerian clastic wedge, northwestern Canada: Insights on Arctic tectonics and the evolution of the northern Cordilleran miogeocline. Geological Society of America Bulletin, v. 122, p. 1899-1911.

Beranek, L.P. and Mortensen, J.K. 2011. The timing and provenance record of the Lake Permian Klondike orogeny in northwestern Canada and arc-continent collision along western North America. Tectonics, v. 30, p. 1-23.

Bertling, M., Braddy, S.J., Bromley, R.G., Demathieu, G.R., Genise, J., Mikulas, R., Nielsen, J.K., Nielsen, K.S.S., Rindsberg, A.K., Schlirf, M. and Uchman, A. 2006. Names for trace fossils: a uniform approach. Lethaia 39, 265–286.

Bertling, M., 2007. What's in a name? Nomenclature, systematics, ichnotaxonomy. In: Miller III, W. (Ed.), Trace Fossils. Concepts, Problems, Prospects. Elsevier, Amsterdam, p. 92–109.

BC Oil and Gas Commission. 2012. Montney Formation Play Atlas NEBC, p. 19-20.

Botterill, S.E., Campbell, S.G., Pemberton, S.G. and Gingras, M.K. 2015. Process ichnological analysis of the Lower Cretaceous Bluesky Formation, Alberta. Bulletin of Canadian Petroleum Geology, v. 63, p. 123-142.

Bromley, R.G. and Asgaard, U. 1979. Triassic freshwater ichnocoenoses from Carlsberg Fjord, East Greenland. Palaeogeography, Palaeoclimatology, Palaeoecology, v. 28, p. 39-80.

Bromley, R.G. and Ekdale, A.A.1984. Chondrites: a trace fossil indicator of anoxia in sediments. Science, v. 224, p. 872-874.

Buatois, L.A. and Mángano, M.G. 2002. Trace fossils from Carboniferous floodplain deposits in western Argentina: implications for ichnofacies models of continental environments. Palaeogeography, Palaeoclimatology, Palaeoecology, v. 183, p. 71-86.

Buatois, L.A., Santiago, N., Parra, K. and Steel, R. 2008. Animal-substrate interactions in an early Miocene wave-dominated tropical delta: delineating environmental stresses and depositional dynamics (Tacata Field, Eastern Venezuela). Journal of Sedimentary Research, v. 78, p. 458-479.

Canada Energy Regulartor. 2020. Canada's Energy Future 2019 Supplement: Natural Gas Production.

Caplan, M.L., Lamond, B. and Mackay, D. 2007. Reservoir characterization of the Bluesky Formation at Shell Canada's Carmon Creek Thermal Project, northwestern Alberta, Peace River Oil Sands Area: an example of interdisciplinary data integration (abstract). In: Canadian Society of Petroleum Geology, GeoConvention 2007.

Chalmers, G.R.L. and Bustin, R.M. 2012. Geological evaluation of Halfway-Doig-Montney hybrid gas shale-tight gas reservoir, northeastern British Columbia. Marine and Petroleum Geology, v. 38, p. 53-72.

Chamberlain, C.K. 1978. Recognition of trace fossils in cores. In: Basan, P.B. (Ed.), Trace Fossil Concepts. SEPM Short Course 5, p. 119–166.

Chatellier, J.-Y., Simpson, K., Perez, R. and Tribovillard, N. 2018. Geochemically focused integrated approach to reveal reservoir characteristics linked to better Montney productivity potential. Bulletin of Canadian Petroleum Geology, v. 66, p. 516-551.

Cheel, R.J. 1991. Grain fabric in hummocky cross-stratification storm beds: genetic implications. Journal of Sedimentary Petrology, v. 61, p. 102-110.

Cheel, R.J. and Leckie, D.A. 1993. Hummocky cross-stratification. Sedimentology Review No. 1. Oxford, UK, Blackwell Scientific Publications, p. 103-122.

Clarkson, M.O., Kasemann, S.A., Wood, R.A., Lenton, T.M., Daines, S.J., Richoz, S., Ohnemueller, F. and Meixner, A. 2015. Ocean acidification and the Permo-Triassic mass extinction. Science, v. 348, issue, 6231.

Colpron, M., Nelson, J.L. and Murphy, D.C. 2007. Northern Cordilleran terranes and their interactions through time. Geological Society of America, v. 17, p. 4-10.

Coney, P.J., Jones, D.L. and Monger, J.W.H. 1980. Cordilleran suspect terranes. Nature, v. 288, p. 329-333.

Corner, G.D. and Fjalstad, A. 1993. Spreite trace fossils (*Teichichnus*) in a raised Holocene fjord-delta, Breidvikeidet, Norway. Ichnos, v. 2, p. 155-164.

Crombez, V., Rohais, S., Baudin, F. and Euzen, T. 2016. Facies, well-log patterns, geometries and sequence stratigraphy of a wave-dominated margin: insight from the Montney Formation (Alberta, British Columbia, Canada). Bulletin of Canadian Petroleum Geology, v. 45, p. 474-505.

D'Alessandro, A. and Bromley, R.G. 1987. Meniscate trace fossils and the Muensteria–Taenidium problem. Paleontology, v. 30, p. 743-763.

Dalrymple, R.B. 2010. Tidal depositional systems. In: Facies Models 4. James, N.P. and Darlymple, R.B. (eds.). NewFoundland & Labrador, Canada, Geological Association of Canada, p. 207.

Dattilo, B.F., Brett, C.E. and Schramm, T.J. 2012. Tempestites in a teapot? Condensation-generated shell beds in the Upper Ordovician, Cincinnati Arch, USA. Palaeogeography, Palaeoclimatology, Palaeoecology, v. 367-368, p. 44-62.

Davies, G.R. 1997a. The Triassic of the Western Canada Sedimentary Basin: tectonic and stratigraphic framework, palaeogeography, palaeoclimate and biota. Bulletin of Canadian Petroleum Geology, v. 45, p. 434-460.

Davies, G.R., Moslow, T.F. and Sherwin, W.D. 1997b. The Lower Triassic Montney Formation, west-central Alberta. Bulletin of Canadian Petroleum Geology, v. 45, p. 475-505.

Davies, G.R., Waston, N., Moslow, T.F. and MacEachern J.A. 2018. Regional subdivisions, sequences, correlations and facies relationships of the Lower Triassic Montney Formation, west-central Alberta to northeastern British Columbia, Canada-with emphasis on role of paleostructure. Bulletin of Canadian Petroleum Geology, v. 66, p. 23-92.

Deutsch, K.B. 1992. Sedimentology and stratigraphy of the Cretaceous Cardium Formation, Kakwa region, west-central Alberta. M.Sc. Thesis, The University of Calgary, Calgary, Alberta, p. 300.

Dickson, J.A.D. 1966. Carbonate identification and genesis as revealed by staining. Journal of Sedimentary Petrology, v. 36, p. 491-505.

Dickson, W.R. 1977. Paleozoic plate tectonics and the evolution of the Cordilleran continental margin. In: Stewari, J.H., Stevens, C.H. and Fritsche, A. E. (eds.). Paleozoic Palaeogeography of the Western United States: Pacific Section, Society of Economic Paleontologists and Mineralogists Pacific Coast Palaeogeography Symposium 1, p. 137-155.

Díez-Canseco, D., Buatois, L. A., Mángano, M. G., Díaz-Molina, M. and Benito, M. I. 2016. Ichnofauna from coastal meandering channel systems (Upper Cretaceous Tremp Formation, south-central Pyrenees, Spain): Delineating the fluvial-tidal transition. Journal of Paleontology, v. 90, p. 250-268.

Dixon, J. 2009a. The Lower Triassic Shale member of the Monteny Formation in the subsurface of northeast British Columbia. Geological Survey of Canada, Open File 6274, p. 9.

Dixon, J. 2009b. Triassic stratigraphy in the subsurface of the plains area of Dawson Creek (93P) and Charlie Lake map areas (94A), northeast British Columbia. Geological Survey of Canada, Bulletin, v. 595, p. 1-78.

Douglas, R.J.W. 1970. Geology of western Canada. In: Douglas, R.J.W. (ed.). Geology and Economic Minerals of Canada Geological Survey of Canada Economic Geology Report, No. 1, p. 367-488.

Droser, M.L. and Bottjer, D.J. 1986. A semiquantative classification of ichnofabrics. Journal of Sedimentary Petrology, v. 56, p. 558-569.

Dumas, S. and Arnott, R.W.C. 2006. Origin of hummocky and swaley cross-stratification- The controlling influence of unidirectional current strength and aggradation rate. Geology, v. 34, p. 1073-1076.

Dzulynski, S. and Kotlarczyk, J. 1962. On load-casted ripples. Ann. Soc. Géol. Pologne, v. 32, p. 148–159.

Edwards, D.E., Barclay, J.E., Gibson, D.W., Kvill, G.E. and Halton, E. 1994. Triassic strata of the Western Canadian Sedimentary Basin. In: Mossop, G. and Shetsen, I. (eds.). Geological Atlas of the Western Canadian Sedimentary Basin. Canadian Society of Petroleum Geologists and Alberta Research Council, p. 159-275.

Ekdale, A.A. and Bromley, R.G. 1991. Analysis of composite ichnofabrics: an example in uppermost Cretaceous chalk of Denmark. Palaios, v. 6, p. 232–249.

Ekdale, A.A. and Harding, S.C. 2015. *Cylindrichnus* concentricus toots in Howard, 1966 (trace fossil) in its type locality, Upper Cretaceous, Wyoming. Annales Societatis Geologorum Poloniae, v. 85, p. 427-432.

Embry, A. F. 1997. Global sequence boundaries of the Triassic and their identification in the Western Canada Sedimentary Basin. Bulletin of Canadian Petroleum Geology, v. 66, p. 7–22.

Energy Resources Conservation Board (ERCB). 2012. Summary of Alberta's Shale- and Siltstone-Hosted Hydrocarbon Resource Potential. p. 31.

Erwin, D.H. 1994. The Permo-Triassic extinction. Nature, v. 367, p. 231-236.

Feng, C.Y., Melnyk, S., Ross, C., Shanley, K., Zonneveld, J.-P. and Gingras, M.K. 2021. Lithofacies-dependent pore-throat radii and reservoir properties in the Lower Triassic Montney Formation, Puskwaskau Field, Alberta. Marine and Petroleum Geology, v. 131, article, 10517.

Ferri, F. and Zonneveld, J.-P. 2008. Were Triassic rocks of the Western Canada Sedimentary Basin deposited in a foreland. Canadian Society of Petroleum Geologists Reservoir, v. 35, p. 12-14.

Fillion, D. and Pickerill, R. K. 1990. Ichnology of the Upper Cambrian to Lower Ordovician Bell Island and Waban groups of eastern Newfoundland, Canada. Paleontographica Canadiana, v. 7, p. 1-119.

Föllmi, K.B. and Grimm, K.A. 1990. Doomed pioneers: gravity-flow deposition and bioturbation in marine oxygen-deficient environments. Geology, v. 18, p. 1069-1072.

Frey, R.W. and Bromley, R.G. 1985. Ichnology of American chalks: the Selma Group (Upper Cretaceous), western Alabama. Can. J. Earth Sci., v. 22, p. 801-828.

Frey, R.W. and Chowns, T.M. 1972. Trace fossils from the Ringgold road cut (Ordovician and Silurian) Georgia, p. 25-55. In Chowns, T.M. (eds.), Sedimentary Environments in the Paleozoic Rocks of Northwest Georgia. Georgia Geological Survey, Guidebook 11.

Frey, R.W., Howard, J.D. and Pryor, W.A. 1978. *Ophiomorpha*: its morphologic, taxonomic, and environmental significance. Palaeogeography, Palaeoclimatology, Palaeoecology, v. 23, p. 199-229.

Frey, R. W. and Howard, J.D. 1990. Trace fossils and depositional sequences in a clastic shelf setting, Upper Cretaceous of Utah. Journal of Paleontology, v. 64, p. 803-820.

Frey, R.W. and Pemberton, S.G. 1985. Biogenic structures in outcrops and cores; I, approaches to ichnology. Bulletin of Canadian Petroleum Geology, v. 33, p. 72-115.

Frey, R.W. and A. Seilacher. 1980. Uniformity in marine invertebrate ichnology. Lethaia, v. 13, p. 183-207.

Furlong, C.M., Gegolick, A., Gingras, M.K., González, P., Moslow, T.F., Prenoslo, D., Playter, T. and Zonneveld, J.P. 2018. Sedimentology and ichnology of the Middle Triassic (Anisian) Sunset Prairie Formation of the Western Canada Sedimentary Basin. Bulletin of Canadian Petroleum Geology, v. 66, p. 215-236.

Fu, S. and F. Werner. 2000. Distribution, ecology and taphonomy of the organism trace, *Scolicia*, in northeast Atlantic deep-sea sediments. Palaeogeography, Palaeoclimatology, Palaeoecology, v. 156 (3-4), p. 289-300.

Gale, J.F.W., Lander, R.H., Reed, R.M. and Laubach, S.E. 2010. Modeling fracture porosity evolution in dolostone. Journal of Structural Geology, v. 32, p. 1201-1211.

Gegolick, A.E. 2017. Sedimentology, ichnology and biogenic permeability of the upper Montney Formation, northeastern British Columbia. Unpublished M. Sc. Thesis. University of Alberta.

Gerard, J.R.F. and Bromley, R.G. 2008. Ichnofabrics in clastic sediments-application to sedimentological core studies: a practical guide. Jean, R.F. Gerard, Madrid, p. 97.

Gibson, D.W. and Barclay, J.E. 1989. Middle Absaroka Sequence-The Triassic stable craton. In: Ricketts, B.D. (ed.). Western Canada Sedimentary Basin-A Case History. Canadian Society of Petroleum Geologists, Special Publication, v. 30, p. 219-232.

Gibson, D.W. and Edwards, D.E. 1990. An overview of Triassic stratigraphy and depositional environments in the Rocky Mountain Foothills and western Interior Plains, Peace River Arch area, northeastern British Columbia. Bulletin of Canadian Petroleum Geology, v. 38A, p. 146-158.

Gingras, M.K., MacEachern, J.A. and Pemberton, S.G. 1998. A comparative analysis of the ichnology of wave-and river-dominated allomembers of the Upper Cretaceous Dunvegan Formation. Bulletin of Canadian Petroleum Geology, v. 46, p. 51-73.

Gingras, M.K., Pemberton, S.G., Saunders, T. and Clifton, H.E. 1999. The ichnology of brackish water Pleistocene deposits at Willapa Bay, Washington: variability in estuarine settings. Palaios, v. 14, p. 352-374.

Gingras, M.K., Bann, K.L., MacEachern, J.A., Waldron, J. and Pemberton, S.G. 2007. A conceptual framework for the application of trace fossils. In: MacEachern, J.A., Bann, K.L., Gingras, M.K. and Pemberton, S.G. (eds.), Applied Ichnology. SEPM Short Course Notes, v. 52. p. 1-26.

Gingras, M.K., Pemberton, S.G., Henk, F.B., MacEachern, J.A., Mendoza, C., Rostron, B., O'Hare, R., Spila, M. and Konhauser, K. 2009. Applications of ichnology to fluid and gas production in hydrocarbon reservoirs. In: Applied Ichnology (CD Edition). MacEachern, J.A., Bann, K.L., Gingras, M.K. and Pemberton, S.G. (eds.). Tulsa, Oklahoma, U.S.A., Society for Sedimentary Geology, p. 131-145.

Gingras, M.K., MacEachern, J.A. and Dashtgard, S.E. 2011. Process ichnology and the elucidation of physico-chemical stress. Sedimentary Geology, v. 237, p. 115-134.

Gingras, M.K. and MacEachern, J.A. 2012. Tidal ichnology of shallow-water clastic settings. In: Principles of Tidal Sedimentology. Springer, Dordrecht, p. 57-77.

Goldring, R., Pollard, J.E. and Taylor, A. M. 1991. *Anconichnus horizontalis*: a pervasive ichnofabric-forming trace fossil in post-Paleozoic offshore siliciclastic facies. Palaios, v. 6, p. 250-263.

Golding, M.L., Orchard, M.J. and Zonneveld, J.-P. 2014a. A summary of new conodont biostratigraphy and correlation of the Anisian (Middle Triassic) strata in British Columbia, Canada. Albertiana, v. 42, p. 33-40.

Golding, M.L., Orchard, M.J., Zonneveld, J.-P., Henderson, C.M. and Dunn, L. 2014b. An exceptional record of the sedimentology and biostratigraphy of the Montney and Doig formations in British Columbia. Bulletin of Canadian Petroleum Geology, v. 62, p. 157-176.

Golding, M.L., Orchard, M.J., Zonneveld, J.-P. and Wilson, N.S.F. 2015. Determining the age and depositional model of the Doig Phosphate Zone in northeastern British Columbia using conodont biostratigraphy. Bulletin of Canadian Petroleum Geology, v. 63, p. 143-170.

Golding, M.L., Mortensen, F., Ferri, F., Zonneveld, J.-P. and Orchard, M.J. 2016. Determining the provenance of Triassic sedimentary rocks in northeastern British Columbia and western Alberta using detrital zircon geochronology, with implications for regional tectonics. Canadian Journal of Earth Science, v. 53, p. 140-155.

Golonka, J. 2007. Late Triassic and Early Jurassic palaeogeography of the world. Palaeogeography, Palaeoclimatology, Palaeoecology, v. 244, p. 297-307.

Habicht, J.K.A. 1979. Paleoclimate, paleomagnetism, and continental drift. The American Hallam, A. 1995. The earliest Triassic as an anoxic event, and its relationship to the end-Paleozoic mass extinction. Canadian Society of Petroleum Geologists Memoir, v. 17, p. 797-804.

Hallam, A. 1991. Why was there a delayed radiation after the end-Paleozoic extinctions? Historical Biology, v. 5, p. 257-262.

Hamblin, A.P. and Walker, R.G. 1979. Storm-dominated shallow marine deposits: the Fernie-Kootenay (Jurassic) transition, southern Rocky Mountains. Canadian Journal of Earth Sciences, v. 16, p. 1673-1690.

Hammersburg, S.R., Hasiotis, S.T. and Robison, R.A. 2018. Ichnotaxonomy of the Cambrain Spence Shale Member of the Langston Formation, Wellsville Mountains, Northern Utah, USA. Paleontological Contributions, v. 20, p. 1-66.

Harms, J.C. 1979. Primary sedimentary structures. Annual review of Earth and Planetary Science, v. 7, p. 227-248.

Hartmann, D.J. and Coalson, E.B. 1990. Evaluation of the Morrow Sandstone in Sorrento field, Cheyenne Country, Colorado. Rocky Mountain Association of Geologists, p. 91-100.

Hauck, T.E., Dashtgard, S.E. and Gingras, M.K. 2009. Brackish-water ichnological trends in a microtidal barrier island/embayment system, Kouchibouguac National Park, New Brunswick, Canada. Palaios, v. 24, p. 478-496. Association of Petroleum Geologists Studies in Geology, v. 9, p. 1-29.

Hayes, L.E., Beatty, T.W., Henderson, C.M., Love, G.D. and Summons, R.E. 2007. Evidence for photic zone euxinia through the end-Permian mass extinction in the Panthalassic Ocean (Peace River Basin, Western Canada). Palaeoworld, v. 16, p. 39–50.

Henderson, C.M. 1997. Uppermost Permian conodonts and their Permian- Triassic boundary in the Western Canada Sedimentary Basin. Bulletin of Canadian Petroleum Geology, v. 45, p. 693–707.

Henderson, C.M. and Schoepfer, S. 2017. High-resolution biostratigraphic and XRF-geochemical correlation of the Montney Formation, NEBC. CSPG CSEG CWLS Joint Annual Convention, May 15–19 2017, Calgary, AB.

Henderson, C.M., Golding, M.L. and Orchard, M.J. 2018. Conodont sequence biostratigraphy of the Lower Triassic Montney Formation. Bulletin of Canadian Petroleum Geology, v. 66, p. 7-22.

Howard, J.D. and Frey, R.W. 1975. Regional animal-sediment characteristics of Georgia estuaries. Senckenbergiana Maritima, v. 7, p. 33-103.

Henderson, C.M. and Schoepfer, S. 2017. High-resolution biostratigraphic and XRF-geochemical correlation of the Montney Formation, NEBC. GeoConvention 2017 Abstracts. Geological Association of Canada.

Herbers, D.S., MacNaughton, R.B., Timmer, E.R. and Gingras, M.K. 2016. Sedimentology and ichnology of an early-middle Cambrian storm-influenced barred shoreface succession, Colville Hills, Northwest Territories. Bulletin of Canadian Petroleum Geology, v. 64, p. 538-554.

Hubbard, S.M., Gingras, M.K. and Pemberton, S.G. 2004. Palaeoenvironmental implications of trace fossils in estuarine deposits of the Cretaceous Bluesky Formation, Cadotte region, Alberta, Canada. Fossils and Strata, v. 51, p. 1-220.

Hunter, R.E., Clifton, H.E. and Phillips, R.L. 1979. Depositional processes, sedimentary structures and predicted vertical sequences in barred nearshore systems, southern Oregon coast. Journal of Sedimentary Petrology, v. 49, p. 711-726.

Hurd, T.J., Fielding, C.R. and Hutsky, A.J. 2014. Variability in sedimentological and ichnological signatures across a river-dominated delta deposit: Peay Sandstone Member (Cenomanian) of the northern Bighorn Basin, Wyoming, USA. Journal of Sedimentary Research, v. 84, p. 1-18.

Isozaki, Y. 1994. P-T boundary superanoxia and oceanic stratification in Panthalassa. In: Professor H. Igo Commemorative Volume on Geology and Paleontology of Japan and Southeast Asia. H. Noda and K. Sashida (eds.). Gakujutu-Tosho Publication, Tokyo, p. 29-41.

Isozaki, Y. 1997. Permo-Triassic boundary superanoxia and stratified superocean: Records from lost deep sea. Science, v. 276, p. 235-238.

Jansonius, J. 1962. Palynology of Permian and Triassic sediments, Peace River area, Western Canada. Palaeontographica, v. 110 (B), p. 35-98.

Kennedy, M.J., Lohr, S.C., Fraser, S.A. and Baruch, E.T. 2014. Direct evidence for organic carbon preservation as clay-organic nanocomposites in a Devonian black shale; from deposition to diagenesis. Earth and Planetary Science Letters, v. 388, p. 59-70.

Knaust, D. and Bromley, R.G. 2012. Trace Fossils as Indicators of Sedimentary Environments. Elsevier, The Netherlands.

Knaust, D. 2017. Atlas of trace fossils in well core: appearance, taxonomy and interpretation, Springer, Dordrecht.

Knaust, D. 2018. The Ichnogenus *Teichichnus* Seilacher,1955. Earth-Science Reviews, v. 177, p. 386-403.

Knaust, D. 2021. Rosselichnidae ifam. nov.: Burrows with concentric, spiral or eccentric lamination. Papers in Paleontology, p. 1-29.

Knoll, A.H., Bambach, R.K., Payne, J.L., Pruss, S. and Ficher, W.W. 2007. Paleophysiology and end-Permian mass extinction. Earth and Planetary Science Letters, v. 256, p. 295-313.

Kolodzie, S. 1980. The analysis of pore throat size and the use of the Waxman-Smits equation to determine OOIP in Spindle field, Colorado. Society of Petroleum Engineers, 55th Annual Fall Technical Conference, SPE paper 9382, p. 2-4.

Lamb, M.P., Myrow, P.M., Lukens, C., Houck, K. and Strauss, J. 2008. Deposits from wave-influenced turbidity currents: Pennsylvanian Minturn Formation, Colorado, U.S.A. Journal of Sedimentary Research, v. 78, p. 480-498.

Leckie, D.A. and Walker, R.G. 1982. Storm- and tide-dominated shoreline in Cretaceous Moosebar-Lower Gates interval-outcrop equivalents of Deep Basin gas trap in western Canada. The American Association of Petroleum Geologists Bulletin, v. 66, p. 138-157.

MacEachern, J.A. and Pemberton, S.G. 1992. Ichnological aspects of Cretaceous shoreface successions and shoreface variability in the Western Interior Seaway of North America. In:

Applications of Ichnology to Petroleum Exploration. S.G. Pemberton (ed.). SEPM Core Workshop Notes 17, p. 57-84.

MacEachern, J.A., Pemberton, S.G., Bann, K.L. and Gingras, M.K. 2007a. Departures from the archetypal ichnofacies: effective recognition of physico-chemical stresses in the rock record, in J.A. MacEachern, K.L. Bann, M.K. Gingras, S.G. Pemberton (eds.). Applied Ichnology: SEPM Short Course Notes, v. 52, p. 65-93.

MacEachern, J.A., Pemberton, S.G., Gingras, M.K. and Bann, K.L. 2007b. The ichnofacies concept: a fifty-year retrospective. In: Miller III, W. (ed.), Trace Fossils: Concepts, Problems, Prospects. Elsevier, p. 50-75.

MacEachern, J.A. and Bann, K.L. 2008. The role of ichnology in refining shallow marine facies models. Society for Sedimentary Geology, v. 90, p. 73-116.

MacEachern, J.A., Bann, K.L., Pemberton, S.G. and Gingras, M.K. 2009a. The ichnofacies paradigm: High-resolution paleoenvironmental interpretation of the rock record. In: Applied Ichnology (CD Edition). MacEachern, J.A., Bann, K.L., Gingras, M.K. and Pemberton, S.G. (eds.). Tulsa, Oklahoma, U.S.A., Society for Sedimentary Geology, p. 27-64.

MacEachern, J.A., Pemberton, S.G., Bann, K.L. and Gingras, M.K. 2009b. Departures from the archetypal ichnofacies: Effective recognition of physico-chemical stress in the rock record. In: Applied Ichnology (CD Edition). MacEachern, J.A., Bann, K.L., Gingras, M.K. and Pemberton, S.G. (eds.). Tulsa, Oklahoma, U.S.A., Society for Sedimentary Geology, p. 65-93.

MacEachern, J.A., Bann, K.L., Gingras, M.K., Zonneveld, J.P., Dashtgard, S.E. and Pemberton, S.G., 2012. The ichnofacies paradigm. In: Developments in sedimentology. Elsevier, v. 64, p. 103-138.

Mackay, D.A. and Dalrymple, R.W. 2011. Dynamic mud deposition in a tidal environment: the record of fluid-mud deposition in the Cretaceous Bluesky Formation, Alberta Canada. Journal of Sedimentary Research, v. 81, p. 901-920.

Markhasin, B. 1997. Sedimentology and stratigraphy of the Lower Triassic Montney Formation, subsurface of northwestern Alberta. Unpublished M.Sc. Thesis, University of Calgary, Alberta, p. 212.

Matin, A.J., Solomon, S.T. and Hartmann, D.J. 1997. Characterization of petrophysical flow units in carbonate reservoirs. The American Association of Petroleum Geologists Bulletin, v. 81, No. 5, p. 734-759.

McIlroy, D. 2004. The application of ichnology to palaeoenvironmental and stratigraphic analysis; introduction: Geological Society, London, Special Publications, v. 228, p. 1-2.

Mederos, S. 1995. Sedimentology and sequence stratigraphy of the Montney Formation in the Sturgeon Lake A and B pool. Unpublished M.Sc. Thesis, University of Alberta, Edmonton, p. 229.

Miall, A.D. and Blakey, R.C. 2008. The Phanerozoic tectonic and sedimentary evolution of North America. In: Miall, A.D. (ed.). Sedimentary Basins of United States and Canada. Elsevier, Amsterdam, p. 1-29.

Monger, J.W.H. and Price, R.A. 1979. Geodynamic evolution of the Canadian Cordillera-progress and problems. Canadian Journal of Earth Sciences, v. 16, p. 770-791.

Morris N.J., Gardner, D. and Glemser C. 2014. Upper Montney geochemistry: Insights into sedimentary provenance. GeoConvention 2014 Abstracts, Geological Association of Canada.

Moslow, T. F. and Pemberton, S.G. 1988. An integrated approach to the sedimentological analysis of some Lower Cretaceous shoreface and delta front sandstone sequences. In: Sequences, Stratigraphy, Sedimentology: Surface and Subsurface. D.P James and D.A. Leckie (eds.). Canadian Society of Petroleum Geologists, Memoir 15, p. 373-386.

Moslow, T.F. 2000. Reservoir architecture of a fine-grained turbidite system: Lower Triassic Montney Formation, Western Canada Sedimentary Basin. In: Deep-water Reservoirs of the World. P. Weimer, R.M. Slatt, J. Coleman, N.C. Rosen, H. Nelson, A.H. Bouma, M.J. Styzen and D.T. Lawrence (eds.).

Moslow, T.F., Haverslew, B. and Pelletier, H. 2014. Fabric selective impacts on reservoir quality and permeability anisotropy in sedimentary facies of the Montney Formation, northeast British Columbia. CSPG, CSEG CWLS Geoconvention 2014, Calgary, Alberta.

Moslow, T.F., Adams, M. and Terzuoli, A. 2016. Bioclastic reservoirs of the distal Montney "shale" play. The American Association of Petroleum Geologists Annual Conference and Exhibition.

Moslow, T.F., Haverslew, B. and Henderson, C.M. 2018. Sedimentary facies, petrology, reservoir characteristics, conodont biostratigraphy and sequence stratigraphic framework of a continuous (395 m) full diameter core of the Lower Triassic Montney Fm, northeastern British Columbia. Bulletin of Canadian Petroleum Geology, v. 66, p. 259–287.

Mulder, T. and Alexander, J. 2001. The physical character of subaqueous sedimentary density flows and their deposits. Sedimentology, v. 48, p. 269-299.

Myrow, P.M., Fischer, W. and Goodge, J.W. 2002. Wave-modified turbidites: combined-flow shoreline and shelf deposits, Cambrian, Antarctica. Journal of Sedimentary Research, v. 72, p. 641-656.

Nardin, T.R., Hein, F.J., Gorsline, D.S. and Edwards, B.D. 1979. A review of mass movement processes, sediment and acoustic characteristics, and contrasts in slope and base-of-slope systems versus canyon-fan-basin floor systems. In: Geology of Continental Slopes. Doyle, L.J. and Pilkey, O.H. (eds.). Tulsa, Oklahoma, USA, Society of Economic Paleontologists and Mineralogists, p. 61-73.

Naruse, H. and Nifuku, K. 2008. Three-dimensional morphology of the ichnofossil *Phycosiphon Incertum* and its implication for paleoslope inclination. Palaios, v. 23, p. 270-279.

National Energy Board (NEB), 2013. Energy Briefing Note. The ultimate potential for unconventional petroleum from the Montney Formation of British Columbia and Alberta.

Nicholson, H. A. 1873. Contributions to the study of the errant annelides of the older Palaeozoic rocks. Royal Society of London Proceedings, v. 21, p. 288-290.

Nickling, W.G. and Neumann, C.M. 2009. Aeolian Sediment Transport in Geomorphology of desert environments. A.J. Parsons and A.D. Abrahams (eds.), p. 517-555.

O'Connell, S.C., Dix, G.R. and Barclay, J.E. 1990. The origin, history and regional structural development of the Peace River Arch, Western Canada. Bulletin of Canadian Petroleum Geology, v. 34, p. 4-24.

Orchard, M.J. and Tozer, E.T. 1997. Triassic conodont biochronology, its calibration with the ammonoid standard, and a biostratigraphic summary for the Western Canada Sedimentary Basin. Bulletin of Canadian Petroleum Geologists, v. 45, p. 675-692.

Orchard, M.J. and Zonneveld, J.-P. 2009. The Lower Triassic Sulphur Mountain Formation in the Wapiti Lake area: lithostratigraphy, conodont biostratigraphy and a new biozonation of the lower Olenekian (Smithian). Canadian Journal of Earth Science, v. 46, p. 757-790.

Pemberton, S.G. and Frey, R.W. 1982. Trace fossil nomenclature and the *Planolites–Palaeophycus* dilemma. Journal of Paleontology, v. 56, p. 843-881.

Pemberton, S.G. and R.W. Frey. 1984. Ichnology of storm-influenced shallow marine sequence: Cardium Formation (Upper Cretaceous) at Seebe, Alberta. In Stott, D.F. and D.J. Glass, (eds.), The Mesozoic of Middle North America, Canadian Society of Petroleum Geologists Memoir 9: 281-304.

Pemberton S.G., Frey, R.W., Ranger, M.J. and MacEachern, J.A. 1992. The conceptual framework of ichnology. In: Applications of lchnology to Petroleum Exploration, A Core Workshop. SEPM core workshop no. 17. S.G. Pemberton, (ed.). p. 1-32.

Pemberton, S.G. and MacEachern, J.A. 1995. The sequence stratigraphic significance of trace fossils: examples from the Cretaceous Foreland Basin of Alberta, Canada, in Van Wagoner, J.C. and Bertram, G.T. (eds.), Sequence Stratigraphy of Foreland Basins: American Association of Petroleum Geologists Memoir v. 64, p. 429-475.

Pemberton, S.G. and MacEachern, J.A. 1996, The ichnological signature of storm deposits: The use of trace fossils in event stratigraphy. In: Brett, C.E. and Baird, G.C. (eds.), Paleontological Events: Stratigraphic, Ecological and Evolutionary Implications: Columbia University Press, New York, p. 73-109.

Pemberton, S.G. and MacEachern, J.A. 1997. The ichnological signature of storm deposits: the use of trace fossils in event stratigraphy. In: Brett, C.E. and Baird, G.C. (eds.), Paleontological Events: Stratigraphic, Ecological and Evolutionary Implications: Columbia University Press, New York, p. 73-109.

Pemberton, S.G., Spila, M.V., Pulham, A.J., Saunders, T., MacEachern, J.A., Robbins, D. and Sinclair, I.K. 2001. Ichnology and sedimentology of shallow to marginal-marine Systems. In: Ben Nevis and Avalon Reservoirs, Jeanne d'Arc Basin. Geological Association of Canada, Short Course Notes 15, p. 343.

Penn, J.L., Deutsch, C., Payne, J.L. and Sperling, E.A. 2018. Temperature-dependent hypoxia explains biogeography and severity of end-Permian marine mass extinction. Science, v. 362, issue, 6419.

Pittman, E.D. 1989. Nature of the Terry Sandstone reservoir, Spindle Field, Colorado, in E.B. Coalson, ed., Petrogenesis and Petrophysics of Selected Sandstone Reservoirs of the Rocky Mountain Region. Rocky Mountain Association of Geologists, p. 245-254.

Pittman, E.D. 1992. Relationship of porosity and permeability to various parameters derived from mercury injection-capillary pressure curves for sandstone. The American Association of Petroleum Geologists Bulletin, v. 76, p. 191-198.

Playter, T.L. 2013. Petrographic and X-ray microtomographic analysis of the Upper Montney Formation, northeastern British Columbia, Canada. Unpublished M. Sc. Thesis. University of Alberta.

Plint, A.G. 2010. Wave- and storm-dominated shoreline and shallow -marine systems. In: Facies Models 4. James, N.P. and Darlymple, R.B. (eds.). NewFoundland & Labrador, Canada, Geological Association of Canada, p. 181.

Prenoslo, D., Furlong, C.M., Gingras, M.K., Playter, T. and Zonneveld, J.P. 2018. The sedimentology, stratigraphy and reservoir characteristics of the Montney D1 and D2 horizons in the Greater Pouce Coupe area. Bulletin of Canadian Petroleum Geology, v. 66, p. 338-358.

Price, R. A. 1994. Cordilleran tectonics and the evolution of the Western Canadian Sedimentary Basin. In: Mossop, G. and Shetsen, I. (eds.). Geological Atlas of the Western Canadian Sedimentary Basin. Canadian Society of Petroleum Geologists and Alberta Research Council, p. 13-24.

Proverbs, I.P., Bann, K.L., Fratton, C.M., Frostad, C.J. and Juska, A. 2018. Facies architecture and sequence stratigraphy of the Lower Triassic Montney Formation, NE British Columbia: Fundamental controls on the distribution of 'sweet spots' in a world-class unconventional reservoir. Bulletin of Canadian Petroleum Geology, v. 66, p. 237-258.

Rampino, M.R. and Caldeira, K. 2005. Major perturbation of ocean chemistry and a "Strangelove Ocean" after the end-Permian mass extinction. Terra Nova, v. 17, p. 554-559.

Ranger, M.J. and Pemberton, S.G. 1991. Multivariate analysis of ichnofossil associations in the subsurface Bluesky Formation (Albain, Alberta, Cananda). Palaeogeography, Palaeoclimatology, Palaeoecology, v. 85, p. 169-187.

Reading, H.G. and Richards, M. 1994. Turbidite systems in deep-water basin margins classified by grain size and feeder system. The American Association of Petroleum Geologists Bulletin, v. 78, p. 792-822.

Reading, H.G. and Collinson, J.D. 1996. Clastic coasts, in Reading, H.G., ed., Sedimentary Environments: Processes, Facies and Stratigraphy. Oxford, UK, Blackwell Science, p. 154-231.

Reineck, H.E. 1963. Sedimentgefüge im Bereich der südlichen Nordsee. Abhandlungen de Senckenbergischen Naturforschenden Gesellschaft, v. 505, p. 1-138.

Reineck, H.E., Gutmann, W.F., Hertweck, G., 1967. Das Schlickgebiet südlich Helgoland als Beispiel rezenter Schelfablagerungen. Senckenbergiana Lethaea, v. 48, p. 219-275.

Reineck, H.E. and Wunderlich, F. 1968. Classification and origin of flaser and lenticular bedding. Sedimentology, v.11, p. 99-104.

Reineck, H.E. and Singh, I.B. 1971. Genesis of laminated sand and graded rhythmites in storm-sand layers of shelf mud. Sedimentology, v. 18, p. 123-128.

Reinson, G.E. 1984. Barrier-island and associated strand-plain systems. In: Walker, R.G. (ed.). Facies Models. Geoscience Canada, Reprint Series 1. Geol. Ass. Can., St. John's, p. 119-140.

Rindsberg, A.K. 2012. Ichnotaxonomy: finding patterns in a welter of information. In: Knaust, D. and Bromley, R.G. (eds). Trace Fossils as Indicators of Sedimentary Environments. Development in Sedimentology. Elsevier, Amsterdam, v. 64, p. 43-78.

Rindsberg, A.K. 2018. Ichnotaxonomy as a science. Annales Societatis Geologorum Poloniae. V. 88, p. 91-100.

Rohais, S., Crombez, V., Euzen, T. and Baudin, F. 2016. The Montney- Doig-Halfway Formations from Western Canadian Sedimentary Basin (WCSB): passive margin, back-arc or fore-arc geodynamic setting? Abstract, Canadian Society of Petroleum Geology Geoconvention 2016.

Rohais, S., Crombez, V., Euzen, T. and Zonneveld, J.-P. 2018. Subsidence dynamics of the Montney Formation (Early Triassic, Western Canada Sedimentary Basin): Insights for its geodynamic setting and wider implications. Bulletin of Canadian Petroleum Geology, v. 66, p. 128-160.

Ross, G.M., Gehrels, G.E. and Patchett, P.J. 1997. Provenance of Triassic strata in the Cordilleran miogeocline, Western Canada. Bulletin of Canadian Petroleum Geology, v. 45, p. 461-473.

Rouquérol, J., Avnir, D., Fairbridge, C.W., Everett, D.H., Haynes, J.M., Pernicone, N., Ramsay, J., Sing, K.S.W. and Ünger, K.K. 1994. Recommendations for the characterization of porous solids. Pure Appl. Chem, v. 66, p. 1739-1758.

Sanders, S., Etienne, C., Gegolick, A., Kelly, D. and Zonneveld, J.-P. 2018. The Middle Montney Altares Member: lithology, depositional setting and significance for horizontal drilling and completion in the Altares Field, British Columbia. Bulletin of Canadian Petroleum Geology, v. 66, p. 318-337.

Sanei, H., Wood, J.M., Ardakani, O.H., Clarkson, C.R. and Jiang, C.Q. 2015. Characterization of organic matter fractions in an unconventional tight gas siltstone reservoir. International Journal of Coal Geology, v. 150-151, p. 296-305.

Savrda, C.E., Krawinkel, H., McCarthy, F.M.G., McHugh, C.M.G., Olson, H.C. and Mountain, G. 2001. Ichnofabrics of a Pleistocene slope succession, New Jersy margin: Relations to climate

and sea-level dynamics. Palaeogeography, Palaeoclimatology, Palaeoecology, v. 171, p. 41-61.

Saunders, T.D.A., MacEachern, J.A. and Pemberton, S.G. 1994. Cadotte Member sandstone: Progradation in a boreal basin prone to winter storms: in Pemberton, S.G., James, D.P, and Wightman, D.M., ed., CSPG Mannville Core Conference: Canadian Society of Petroleum Geologists, Exploration Update, p. 331-349.

Schiarizza, P. 2013. The Wineglass assemblage, lower Chilcotin River, south-central British Columbia: Late Permian volcanic and plutonic rocks that correlate with the Kutcho assemblage of north British Columbia. In: Geological Fieldwork, 2012, British Columbia Ministry of Energy, Mines and Natural Gas, British Columbia Geological Survey Paper 2013-1, p. 53-70.

Schlirf, M., Uchman, A. and Kummel, M. 2001. Upper Triassic (Keuper) non-marine trace fossils from the Haßberge area (Franconia, south-eastern Germany). Paläontologische Zeitschrift, v. 75, p. 71-96.

Schlirf, M. and Uchman, A. 2005. Revision of the Ichnogenus *Sabellarifex* Richter, 1921 and its relationship to *Skolithos* Haldeman, 1840 and *Polykladichnus* Fursich, 1981. Journal of Systematic Paleontology, v. 3, p. 115-131.

Schmoker, J.W. and Halley, R.B. 1982. Carbonate porosity versus depth: a predictable relation for south Florida. The American Association of Petroleum Geologists Bulletin, v. 66, p. 2561-2570.

Seilacher, A. 1955. Spuren und Fazies im Unterkambrium. In: Schindewolf, O.H. and Seilacher, A. (Eds.), Beiträge zur Kenntnis des Kambriums in der Salt Range (Pakistan). Akademie der Wissenschaften und der Literatur zu Mainz, Mathematisch-nat-urwissenschaftliche Klasse, Abhandlungen, v. 10, p. 11-143.

Seilacher, A. 1967. Bathymetry of trace fossils. Marine Geology, v. 5, p. 413-428.

Seilacher, A. 1978. Use of trace fossil assemblages for recognizing depositional environments. In: Basan, B. (eds.), Trace Fossil Concepts: Society of Economic Paleontologists and Mineralogists: Short Course, v. 5, p. 167-181.

Shahkarami, S., Mángano, M.G. and Buatois, L.A. 2017. Discriminating ecological and evolutionary controls during the Ediacaran-Cambrian transition: Trace fossils from the

Soltanieh Formation of northern Iran. Palaeogeography, Palaeoclimatology, Palaeoecology, v. 476, p. 15-27.

Steiner, S., Ahsan, S.A., Raina, I., Dasgupta, S. and Lis, G.P. 2016. Interpreting total organic carbon TOC in source rock oil plays. Abu Dhabi International Petroleum Exhibition & Conference, 7-10 November 2016, Abu Dhabi, UAE.

Stow, D. 1979. Distinguishing between fine-grained turbidites and contourites on the Nova Scotian deep water margin. Sedimentology, v. 26, p. 371-387.

Stow, D. and Shanmugam, G. 1980. Sequence of structures in fine-grained turbidites: comparison of recent deep-sea and ancient flysch sediments. Sedimentary Geology, v. 25, p. 23-42.

Stow, D. and Wetzel, A. 1990. Hemiturbidite: a new type of deep-water sediment. In: Cochran, J.R., Stow, D.A.V., et al. (eds.), Proceedings of the Ocean Drilling Project. Scientific Results, v. 116, p. 25-34.

Stow, D. and Smillie, Z. 2020. Distinguishing between deep-water sediment facies: turbidites, contourites and hemipelagites. Geosciences, v. 10.

Sturrock, D.L. and Dawson, S.W. 1991. Ring/Border Field: A significant gas discovery in the Triassic Montney Formation. Canadian Society of Petroleum Geologists Reservoir, v. 18, p. 1-2.

Swanson, B.F. 1977. Visualizing pores and non-wetting phase in porous rocks. Society of Petroleum Engineers, Annual Fall Technical Conference, SPE Paper 6857, p. 10.

Swanson, B.F. 1981. A simple correlation between permeabilities and mercury capillary pressures. Journal of Petroleum Technology, Dec., p. 2488-2504.

Swift, D.J.P., Han, G. and Vincent, C.E. 1986. Fluid processes and sea-floor response on a modern storm-dominated shelf: Middle Atlantic shelf of North America. Part 1: the storm-current regime. In: Knight, R.J. and Mclean, J.R. (eds.). Shelf Sands and Sandstones: Canadian Society of Petroleum Geologists, Memoir 11, p. 99-119.

Sun, S.Q. 1995. Dolomite reservoirs: porosity evolution and reservoir characteristics. The American Association of Petroleum Geologists Bulletin, v. 79, p. 186-204.

Taylor, A.M. and Goldring, R., 1993. Description and analysis of bioturbation and ichnofabric; organisms and sediments; relationships and applications. Journal of the Geological Society of London, v. 150, p. 141-148.

Taylor, A., Goldring, R. and Gowland, S. 2003. Analysis and application of ichnofabrics. Earth Science Reviews, v. 60, p. 227-259.

Timmer, E.R., Botterill, S.E., Gingras, M.K. and Zonneveld, J.-P. 2016a. Visualizing a process ichnology dataset, Lower Cretaceous McMurray Formation, NE Alberta, Canada. Bulletin of Canadian Petroleum Geology, v. 64, p. 251-265.

Timmer, E.R., Gingras, M.K. and Zonneveld, J.-P. 2016b. Spatial and temporal significance of process ichnology data from silty-mudstone beds of inclined heterolithic stratification, Lower Cretaceous McMurray Formation, NE Alberta, Canada. Palaios, v. 31, p. 533-548.

Tucker, M.E. 2001. Sedimentary Petrology: An Introduction to the Origin of Sedimentary Rocks. Oxford, UK, Blackwell Science, p. 20-21.

Twitchett, R.J., Krystyn, L., Baud, A., Wheeley, J.R. and Richoz, S. 2004. Rapid marine recovery after the end-Permian mass-extinction event in the absence of marine anoxia. Geology, v. 32, p. 805-808.

Uchman, A. 1995. Taxonomy and paleoecology of flysch trace fossils: The Marnoso-Arenacea Formation and associated facies (Miocene, Northern Apennines, Italy). Beringeria, v. 15, p. 3-115.

Uchman, A., Hanken, N.-M. and Binns, R. 2005. Ordovician bathyal trace fossils from metasiliciclastics in central Norway and their sedimentological and palaeogeographical implications. Ichnos, v. 12, p. 105-133.

Utting, J., Zonneveld, J.-P., MacNaughton, R.B. and Falls, K.M. 2005. Palynostratigraphy, lithostratigraphy and thermal maturity of the Lower Triassic Toad and Greyling, and Montney formations of Western Canada and comparisons with coeval rocks of the Sverdrup Basin, Nunavut. Bulletin of Canadian Petroleum Geology, v. 53, p. 5-24.

Van Loon, A.J. and Wiggers, A.J. 1976. Primary and secondary synsedimentary structures in the lagoonal Almere Member (Groningen Formation, the Netherlands). Sedimentary Geology, v. 16, p. 89-97.

Vossler, S.M. and Pemberton, S.G. 1988. Ichnology of the Cardium Formation (Pembina oilfield): Implications for depositional and sequence stratigraphic interpretations. In: James, D.P. and Leckie, D.A. (eds.), Sequences, Stratigraphy, Sedimentology: Surface and Subsurface: Canadian Society of Petroleum Geologists Memoir, v. 15, p. 237-253.

Vossler, S.M. and Pemberton, S.G. 1989. Ichnology and paleoecology of offshore siliciclastic deposits in the Cardium Formation (Turonian, Alberta, Canada). Palaeogeography, Palaeoclimatology, Palaeoecology, v. 74, p. 217-239.

Wesolowski, L.J.N., Buatois, L.A., Mángano, M.G., Ponce, J.J. and Carmona, N.B. 2018. Trace fossils, sedimentary facies and parasequence architecture from the Lower Cretaceous Mulichinco Formation of Argentina: The role of fair-weather waves in shoreface deposits. Sedimentary Geology, v. 367, p. 146-163.

Wetzel, A. and Balson, P. 1992. Sedimentology of fine-grained turbidites inferred from continuously recorded physical properties data. Marine Geology, v. 104, p. 165-178.

Wetzel, A. and Uchman, A. 2001. Sequential colonization of muddy turbidites in the Eocene Beloveza Formation, Carpathians, Poland. Palaeogeography, Palaeoclimatology, Palaeoecology, v. 168, p. 178-202.

Wignall, P.B. and Hallam, A. 1992, Anoxia as a cause of the Permian/Triassic mass extinction: Facies evidence from northern Italy and the western United States. Palaeogeography, Palaeoclimatology, Palaeoecology, v. 93, p. 21-46.

Wignall, P.B., Kozur, H. and Hallam, A. 1996. On the timing of paleoenvironmental changes at the Permo-Triassic (P-Tr) boundary using conodont biostratigraphy. Historical Biology, v. 12, p. 39-62.

Wignall, P.B. and Newton, R. 2003. Contrasting deep-water records from the Upper Permian and Lower Triassic of South Tibet and British Columbia: Evidence for a diachronous mass extinction. Palaios, v. 18, p. 153-167.

Wignall, P.B. and Twitchett, R.J. 1996. Trace fossils and the aftermath of the Permo-Triassic mass extinction: evidence from northern Italy: Palaeogeography, Palaeoclimatology, Palaeoecology, v. 124, p. 137-151.

Wignall, P.B. and Twitchett, R.J. 2002a, Oceanic anoxia and the end Permian mass extinction: Science, v. 272, p. 1155–1158.

Wignall, P.B. and Twitchett, R.J. 2002b. Extent, duration, and nature of the Permian-Triassic superanoxic event. Geological Society of America Special Paper 356, p. 395-413.

Wilson, K.M., Hay, W.W. and Wold, C.N. 1991. Mesozoic evolution of exotic terranes and marginal seas, western North-America. Marine Geology, v. 102, p. 311-361.

Wilson, N., Zonneveld, J.-P. and Orchard, M. 2012. Biostratigraphy of the Montney Formation: From the Alberta and British Columbia subsurface, to the outcrop. GeoConvention 2012, Vision, p. 1-4.

Wood, J.M., Sanei, H., Curtis, M.E. and Clarkson, C.R. 2015. Solid bitumen as a determinant of reservoir quality in an unconventional tight gas siltstone play. International Journal of Coal Geology, v. 150-151, p. 287-295.

Wood. J.M., Sanei, H., Haeri-Ardakani, O., Curtis, M.E. and Akai, T. 2018. Organic petrography and scanning electron microscopy imaging of a thermal maturity series from the Montney tight-gas and hydrocarbon liquids fairway. Bulletin of Canadian Petroleum Geology, v. 66, p. 499-515.

Woods, A.D. and Bottjer, D.J. 2000. Distribution of ammonoids in the Lower Triassic Union Wash Formation during the recovery from the end-Permian mass extinction. Palaios, v. 15, p. 535–545.

Wust, R.A.J., Tu, S., Nassichuk, B., Bozarth, T., Tucker, J. and Cui, A. 2018. Chemostratigraphy, petrography, and SEM investigations of the Lower Triassic Montney Formation in Alberta: Implications for a new and revised diagenetic and depositional model. Bulletin of Canadian Petroleum Geology, v. 66, p. 436-471.

Xu, Y.F., Wang, Y., Yuan, H.F., Zhang, D.M., Agostini, F. and Skoczylas, F. 2018. Pore structure characterization of tight sandstone from Sbaa Basin, Algeria: Investigations using multiple fluid invasion methods. Journal of Natural Gas Science and Engineering, v. 59, p. 414-426.

Yao, L., Aretz, M., Li, Y. and Wang, X.D. 2016. Gigantoproductid brachiopod storm shell beds in the Mississippian of South China: Implications for their paleoenvironmental and palaeogeographical significances. Geological Belgica, v. 19, p. 57–67.

Yu, B.S., Dong, H.L., Jiang, H.C., Lv, G., Eberl, D., Li, S.Y. and Kim, J.W. 2009. The role of clay minerals in the preservation of organic matter in sediments of Qinghai Lake, NW China. Clays and Clay Minerals, v. 57, p. 213-226.

Zonneveld, J.-P. 1999. Sedimentology and sequence biostratigraphic framework of a mixed siliciclastic-carbonate depositional system, Middle Triassic, northeastern British Columbia. Ph. D Dissertation, University of Alberta.

Zonneveld, J.-P., Gingras, M.K. and Pemberton, S.G. 2001. Trace fossil assemblages in a Middle Triassic mixed siliciclastic-carbonate marginal marine depositional system, British Columbia. Palaeogeography, Palaeoclimatology, Palaeoecology, v. 166, p. 249-276.

Zonneveld, J.-P., Pemberton, S.G., Saunders, T.D.A. and Pickerill, R. 2002. Large, robust *Cruziana* from the Middle Triassic of northeastern British Columbia: ethologic, biostratigraphic and paleobiologic significance. Palaios, v. 17, p. 435-448.

Zonneveld, J.-P., Carrelli, G.G. and Riediger, C. 2004. Sedimentology of the Upper Triassic Charlie Lake, Baldonnel and Pardonet Formations, Northeastern British Columbia. In: Central Foreland NATMAP; Stratigraphic and Structural Evolution of the Cordilleran Foreland. L.S. Lane (ed.). Bulletin of Canadian Petroleum Geology, v. 52, p. 277-301.

Zonneveld, J-P., Beatty, T.B. and Pemberton, S.G. 2007. Lingulide brachiopods and the trace fossil *Lingulichnus* from the Triassic of Western Canada: Implications for faunal recovery after the end-Permian mass extinction. Palaios, v. 22, p. 74-97.

Zonneveld, J.-P., MacNaughton, R.B., Utting, J., Beatty, T.W., Pemberton, S.G. and Henderson, C.M. 2010a. Sedimentology and ichnology of the Lower Triassic Montney Formation in the Pedigree-Ring/Border Kahntah River area, northwestern Alberta and northeastern British Columbia. Bulletin of Canadian Petroleum Geology, v. 58, p. 115-140.

Zonneveld, J.-P., Gingras, M.K. and Beatty, T.W. 2010b. Diverse Ichnofossil Assemblages Following the P-T Mass Extinction, Lower Triassic, Alberta and British Columbia, Canada: Evidence for Shallow Marine Refugia on the Northwestern Coast of Pangaea. PALAIOS, v. 25, p. 368-392.

Zonneveld, J.-P., Golding, M., Moslow, T.F., Orchard, M.J., Playter, T. and Wilson, N. 2011. Depositional framework of the Lower Triassic Montney Formation, West-central Alberta and Northeastern British Columbia. 2011 CSPG CSEO CWLS Convention, Recovery, p. 1-4.

Zonneveld, J.-P. and Moslow, T.F. 2014. Perennial River Deltas of the Montney Formation: Alberta and British Columbia Subcrop Edge. GeoConvention 2014 Abstract. Geological Association of Canada.

Zonneveld, J.-P. and Moslow, T.F. 2018. Paleogeographic setting, lithostratigraphy, and sedimentary framework of the Lower Triassic Montney Formation of western Alberta and northeastern British Columbia. Bulletin of Canadian Petroleum Geology, v. 66, p. 93-127.